Exploring Regulators of Anti-Tumor Immunity:

Chorionic Gonadotropin Beta & Major Vault Protein

Siegen McKellar

A dissertation

submitted in partial fulfillment of the

requirements for the degree of

Doctor of Philosophy

University of Washington

2025

Reading Committee:

Robert Bradley

Edith Wang

Marshall Horwitz

Program Authorized to Offer Degree:

Molecular and Cellular Biology

University of Washington

Abstract

Checkpoint immunotherapy has become a pillar of cancer treatment over the past decade. Immune checkpoint inhibitors (ICIs) have been highly efficacious for many patients, but ultimately many patients do not achieve durable responses and response rates remain variable across cancers and indications. These remain significant challenges in the field, as the patterns of response and resistance and the factors that influence them remain incompletely understood. Here I describe two proteins associated with tumor-immune interactions and response to ICIs. I identify that chorionic gonadotropin beta 7 (CGB7) is expressed widely across cancers and is associated with hallmarks of immune evasion and decreased survival probability in advanced urothelial carcinoma patients undergoing treatment with ICIs. Random survival forest modeling reveals that CGB7 is predictive of decreased survival probability in the context of ICI treatment. This supports the clinical value of CGB7 as a biomarker of immune evasion and resistance to checkpoint immunotherapy. I also describe associations between Major Vault Protein (MVP) and increased response to ICIs in melanoma. In an immunocompetent model, MVP expression in both the host and in the tumor increases survival probability in vivo. Tumoral expression of MVP influences survival in an immune-dependent manner. Single cell RNA-sequencing of tumors from an immunocompetent model reveals that tumor MVP expression is associated with increased abundance of effector CD8+ T cells expressing hallmarks of exhaustion, suggesting a potential mechanism for MVP in protecting effector CD8+ T cells against dysfunction. Taken together, this work identifies both CGB7 and MVP as valuable biomarkers and/or therapeutic targets associated with blunted or augmented anti-tumor immunity in cancer, respectively.

Exploring Regulators of Anti-Tumor Immunity:

Chorionic Gonadotropin Beta & Major Vault Protein

Siegen McKellar

Chair of the Supervisory Committee:

Robert Bradley

Herbold Computational Biology Program

Public Health Sciences Division, Fred Hutch

Basic Sciences Division, Fred Hutch

Acknowledgments

First and foremost, I would like to thank the funding sources that made the work described in these thesis possible: the UW MSTP (T32 GM 007266) and the ARCS foundation.

I would like to extend a sincere thank you to the directors of the MSTP, who provided guidance and perspective throughout grad school: Dr. Marshall Horwitz, Dr. Stephen Tapscott, Dr. Mary Claire King, and Dr. Heather Cheng. In the same vein, I would also like to thank the directors of the MCB program for their support: Dr. Nina Salama, Dr. Celeste Berg, and Dr. Julian Simon.

Thank you to my committee members for four years of thoughtful comments and questions on this work: Dr. Marshall Horwitz, Dr. Edith Wang, Dr. Evan Newell, Dr. Alice Berger, and Dr. Melody Campbell. Thank you for so greatly influencing my development as a scientist and for making this work stronger with your input.

I would like to thank my collaborators at Fred Hutch from the Setty and Newell labs. Thank you Dr. Manu Setty, Tracy Yang, and Dr. Dominik Otto– it has been such a pleasure to work with you on the analysis of our single cell RNA-sequencing data. Thank you Dr. Evan Newell and Dr. Amy Codd– I am grateful for the opportunity to learn about T cell biology and cytometry by time-of-flight (CyTOF) from you both. I would also like to thank my collaborators at Stanford– Dr. Sydney Lu and Rohan Lattupally. Thank you for your contributions and Dr. Lu in particular for his guidance that extended beyond the project that we collaborated on together. Thank you too to Dr. Susan De Wolf for her consultation and input on immune cell annotations.

Next, I would like to thank the Bradley Lab and specifically my colleagues who contributed greatly to this work: Dr. Jose Pineda, who contributed to the work described in chapter two of this thesis, and Dr. Andrea Belleville, who contributed to the work described in

chapter three. I am grateful to have worked alongside you in the Bradley Lab as both lab mates and MSTP colleagues, which is very special. Thank you to Dr. Robert Bradley for supporting this work, for providing guidance when needed, and ultimately for the opportunity to stretch myself farther than I thought possible.

Thank you to my past mentors Dr. Craig Miller and Dr. Nick Ellis from my time as an undergraduate at UC Berkeley for taking a chance on me and for giving me the opportunity to fall in love with the scientific process at the bench. Thank you to the Oro Lab and Dr. Anthony Oro at Stanford for epitomizing the kind of mentor, leader, and true physician-scientist in every sense of the word that I only hope that I can one day aspire to. Thank you to Dr. Amar Mirza, who I was fortunate to have worked closely with and credit for so much of my development as a scientist and perspective on science. I am grateful to have you as a role model, mentor, and friend. I am so fortunate to have gotten to work alongside friends and Dr. Catherine Yao and Dr. Nicole Urman. You three inspire me as scientists and people.

Thank you to my wonderful friends near and far who have kept me grounded, including dear friends from high school, college, and this Seattle chapter of my life. Thank you to my Aunt Jean, who believed in my pursuit of becoming a physician scientist for many years. Though she is no longer with me, she has been a huge part of my motivation for this path in cancer research. Thank you to my grandpa for giving me his love of medicine and the outdoors, and for never failing to cheer me on through every milestone. And thank you most of all to my parents, who have been unwavering in their support of me throughout the greatest challenges I've faced not only in grad school, but in every phase of life. This is something I have never taken for granted and it has made all the difference for me in my pursuit of challenging things.

This work was possible because all of my mentors and advisors past and present, colleagues, friends, and family believed in and invested in me. I stand on the shoulders of giants.

Dedication

This thesis is dedicated to my parents. This would not have been possible without them.

Table of Contents

Table of Figures

Chapter 1 Introduction

Figure 1-1 is reprinted with permission from AACR: License Number 5994060350022. Figure 1-2 is reprinted from Elsevier publisher with License Number: 5994031180057. These figures are reprinted with permission as it was originally licensed under a Creative Commons Attribution 4.0 International License, which permits unrestricted use, distribution, and reproduction in any medium, provided the original author and source are credited.

1.1 Hallmarks of cancer: immune evasion

Cancer, or the uncontrolled growth of cells, is driven by diverse but unifying mechanisms. First proposed in 2000, Hanahan and Weinberg described six core mechanisms of tumorigenesis that have been since updated and amended in 2011 and 2022: evading growth suppressors, enabling replicative immortality, tumor promoting inflammation, avoiding invasion and metastasis, inducing or accessing vasculature, genome instability and mutation, resisting cell death, sustaining proliferative signaling, deregulating cellular metabolism, and avoiding immune destruction (1, 2) . As such, the ability of cancer cells to evade immune detection is a relatively recently recognized hallmark of cancer. Emerging hallmarks added in 2022 include phenotypic plasticity, epigenetic reprogramming, senescence, and the microbiome (2).

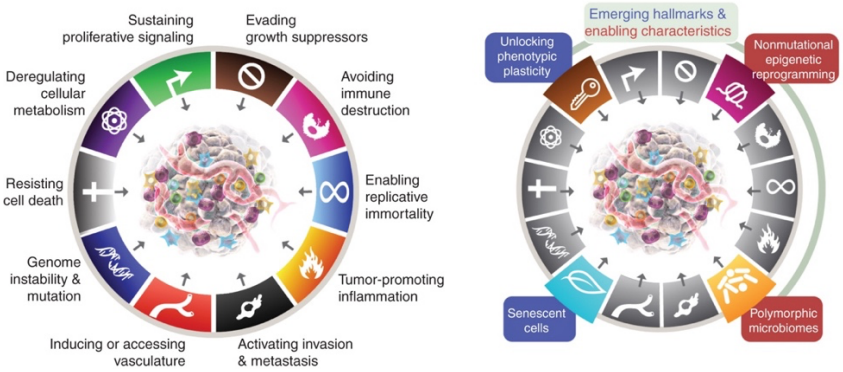

Figure 1-1. Hallmarks of cancer updated in 2022 From Hanahan D. Hallmarks of Cancer: New Dimensions. *Cancer Discovery*. 2022 Jan;12(1):31-46. doi: 10.1158/2159-8290.CD-21-1059. PMID: 35022204.

Initial control of tumorigenesis is cell-intrinsic, where cells contain many protective mechanisms against uncontrolled growth, including growth checkpoints to carefully regulate cell proliferation (3), damage-induced apoptosis (4), and sensitive machinery to detect replication errors in DNA (5), erroneously mis-spliced mRNAs (6), and misfolded proteins (7).

Immune cells can identify and eradicate cancer cells in a process referred to as immune surveillance. Immune surveillance is an important cell-extrinsic secondary line of defense against tumorigenesis. Early evidence of immune surveillance of tumors came from immunodeficient murine models that spontaneously developed tumors and developed tumors in response to carcinogens at higher rates than immunocompetent counterparts (9). Higher rates of malignancy are consistently observed in humans with immunodeficiency as well (8, 10, 11). Immune effector cells eliminate detectable cancer cells, though in the process, this targeting of detectable tumor cells can select for cells that are able to evade detection or immune-mediated killing by a process referred to as "immunoediting" (12). These cells ultimately expand, uninhibited by anti-tumor immune responses. This outgrowth can lead to progression, recurrence, and/or therapeutic resistance.

There are many mechanisms through which cancer can ultimately escape immune surveillance at multiple stages of tumor recognition, activation of immune effectors, and initiation of tumor killing. Cancer cells can acquire the ability to shield themselves to evade immune detection, actively inhibit immune anti-tumor activity, and/or can protect themselves against anti-tumor activity. A common mechanism by which cancer cells can evade immune detection is loss of class 1 major histocompatibility complex molecules (MHC-I) on their surface. These MHC-I molecules display antigens to infiltrating immune cells such as effector

CD8+ T cells, and their loss enables evasion from detection. Loss of MHC-I can occur through regulation of pathways that induce MHC-I expression, such as IFNg, through epigenetic silencing of MHC-I genes, or through structural deletions of MHC-I genes (12, 13). Once detected by CD8+ and CD4+ T cells, cancer cells can inhibit anti-tumor killing. A notable example is through the upregulation and display of immune checkpoints (14). Targeting these immune checkpoints on tumor cells, CD8+ T cells, or CD4+ T cells is the foundation of the most widely utilized immunotherapy in cancer: checkpoint immunotherapy. As a final resort, some cancers have acquired the ability to shield themselves from cytolytic activity. This may manifest through modifications to the cancer cell membrane to make the membrane less permeable to perforin, disabling cellular entry of cytolytic granzymes (15, 16), or the expression of proteases to inhibit and degrade granzymes once inside the cell (17).

1.2 Mechanisms of checkpoint immunotherapy response and resistance

Immune checkpoint inhibition (ICI) has revolutionized the treatment of cancers. By restoring anti-tumor activity to T cell lymphocytes, over the past decade ICI has dramatically extended overall and progression-free survival for many advanced cancers that previously lacked treatment options. ICI has become the standard of care for increasing indications, including use as a first line agent in advanced disease, and is approved in some cancers for neoadjuvant treatment, adjuvant treatment, and as a single agent or combination therapy with chemotherapy, targeted therapy, or a complementary checkpoint inhibitor (18,19).

While ICIs have been highly efficacious for many patients, approximately half, or more, of patients do not achieve durable responses, and as such, response rates remain variable across indications. This remains a significant challenge in the field. Tumors that typically respond well

to immunotherapy are more immunogenic, with higher neoantigen burdens, greater infiltration of pro-inflammatory immune cells such as effector CD8+ T cells, and decreased infiltration of anti-inflammatory immune cells such as T regulatory cells. Three biomarkers of ICI response are FDA-approved and utilized widely in clinical settings: tumor mutational burden (TMB), microsatellite instability/defective mismatch repair (MSI/dMMR), and expression of an immune checkpoint ligand: programmed death ligand 1 (PD-L1), which binds to programmed death 1 (PD1) (20). Together, PD1 and PD-L1 constitute an immune checkpoint axis. Immune checkpoints are a part of healthy immune responses, and functionally damped T cell activation (21). The two most clinically notable immune checkpoints, programmed death 1 (PD1) and cytotoxic T-lymphocyte antigen-4 (CTLA-4), were discovered in 1992 by Tasuku Honjo (22) and in 1995 by James Allison, respectively (23). Both investigators have since received the Nobel Prize for these discoveries. Since these seminal discoveries, many more immune checkpoints have been characterized, including LAG-3 (24), TIGIT (25), and TIM-3 (26). Therapeutic antibodies have been developed against many immune checkpoint axes, with the most commonly clinically utilized antibodies targeting three immune checkpoint proteins: anti-CTLA-4 (Ipilimumab), anti-PD-1 (Nivolumab, Pembrolizumab, Cemiplimab) and anti-PDL-1 (Atezolizumab, Avelumab, Durvalumab), and most recently, anti-LAG-3 (Relatlimab) (18, 19).

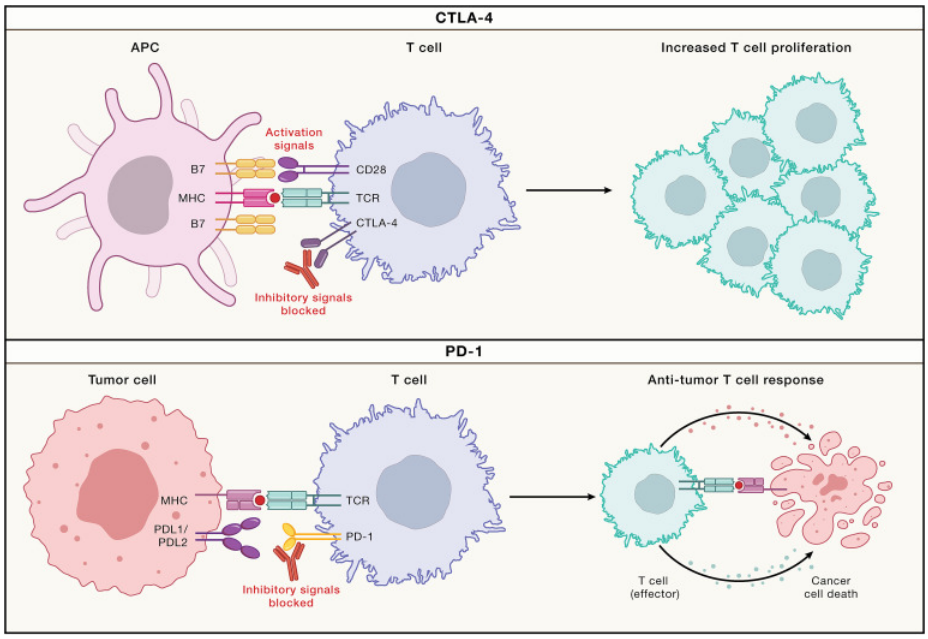

Figure 1-2 Mechanism of immune checkpoints and ICIs. Checkpoint inhibitors are monoclonal antibodies (shown in red) that target, bind, and block immune checkpoints such as CTLA-4 on T cells, PD-1 on T cells (shown in red), or PD-L1 on tumor cells (not shown). From Sharma P, Goswami S, Raychaudhuri D, Siddiqui BA, Singh P, Nagarajan A, Liu J, Subudhi SK, Poon C, Gant KL, Herbrich SM, Anandhan S, Islam S, Amit M, Anandappa G, Allison JP. Immune checkpoint therapy-current perspectives and future directions. *Cell*. 2023 Apr 13;186(8):1652-1669. doi: 10.1016/j.cell.2023.03.006. PMID: 37059068.

CTLA-4 is induced on the surface of CD4+ T cells in response to engagement of the TCR and costimulatory receptor B7-1 (CD80) or B7-2 (CD86) by MHC-II and CD28 on antigen presenting cells. CTLA-4 then competes with CD28 for binding to B7-1 and B7-2 and inhibits activation, ultimately "putting the brakes" on CD4+ T cell function **(Figure 1-2).** Targeting the CTLA-4/CD80 axis with an antibody against CTLA-4 disrupts this inhibitory signal, restoring costimulation to CD4+ T cells to facilitate the activity of the main anti-tumor effectors: CD8+ T cells (27). Ipilimumab was first approved in metastatic melanoma, where patients achieve a 5-year overall survival of 26% (28).

Multiple therapeutic antibodies have been developed against the programmed death 1 (PD-1)/ programmed death ligand 1 (PD-L1) checkpoint axis. Engagement of the TCR with antigens presented by MHC-I on the surface of tumor cells leads to CD8+ T cell activation and

subsequent upregulation of PD-L1. As a consequence of this antigen exposure and activation, inhibitory receptor PD-1 is induced on the surface of CD8+ T cells. In the context of cancer, this normal upregulation of PD-1 can be sustained chronically. In parallel, a particularly common mechanism of tumor immune evasion in tumors is the induction of inhibitory surface molecules such as PD-L1, the ligand for the PD-1 receptor, on the surface of tumors **(Figure 1-2)**. There are many mechanisms that lead to PD-L1 surface expression on tumor cells, including transcriptional regulation by multiple signaling pathways, post-translational regulation, and genomic alterations (33). Engagement of PD-1 with PD-L1 on tumors inhibits CD8+ anti-tumor effector capacity. Targeting this axis with antibodies against PD-1 or PD-L1 restores tumor-killing effector function.

Several clinical trials have investigated and compared the efficacy of CTLA-4 and PD-1 therapeutic antibodies in late-stage melanoma. In the CheckMate 066 randomized phase three trial, nivolumab exhibited a 1-year survival rate of 72.9% with an objective response rate of 40%. A follow up revealed a 3-year overall survival rate of 51.2% (34, 35). The KEYNOTE-006 phase III study enrolled patients with stage IV and unresectable stage III melanoma and compared response rates to pembrolizumab (11.9%) and ipilimumab (33.7%) (36). A two year follow-up reported an overall response rate of 55% for pembrolizumab and 43% for ipilimumab (37). In addition to PD-1 antibodies exhibiting greater response and survival rates, it is meaningful to observe reduced incidence of severe immune-related adverse events (irAEs) in these patients (38). A 10-year follow up nivolumab monotherapy, ipilimumab monotherapy, and combination nivolumab and ipilimumab revealed similar trends, as well as improved overall survival over monotherapy with combination therapy. Here, the median overall survival was 71.9

months with nivolumab plus ipilimumab, 36.9 months with nivolumab, and 19.9 months with ipilimumab (38).

Atezolizumab, an example of a therapeutic antibody against PD-L1, was first approved for metastatic melanoma, where overall survival ranges from about 11%- 25% at three years (29, 30).

Though melanoma is the first approved indication for checkpoint immunotherapy, and exhibits one of the highest response rates, checkpoint inhibitors are also efficacious in other cancers. In renal cell carcinoma, a heterogeneous group of kidney cancers, the Checkmate 025 phase-III clinical trial evaluated the benefit of nivolumab in patients with a treatment history. Here, nivolumab was associated with an objective response rate of 25% (39) . In the phase-III CheckMate 214 trial, with extended follow up, combination therapy of nivolumab plus ipilimumab exhibited greater survival than sunitinib (a tyrosine kinase inhibitor) (41). Combination nivolumab and ipilimumab therapy resulted in an objective response rate of 42% vs 29% with sunitinib treatment (40, 41). These trials demonstrate that checkpoint immunotherapy outperforms standard of care therapeutics in RCC, and again shows improved response rate with combination checkpoint immunotherapy.

In advanced urothelial carcinoma, the IMvigor210 and IMvigor211 clinical trials found that patients treated with Atezolizumab versus chemotherapy displayed similar differences in objective response rates: 23% objective response in the atezolizumab group compared with 22% in the chemotherapy group, though atezolizumab was better tolerated, in line with other clinical trials demonstrating that checkpoint inhibitors targeting the PD-1/PD-L1 axis are generally well tolerated (42, 43). Despite the fact that atezolizumab did not demonstrate improvement in overall survival when compared with chemotherapy, other applications of checkpoint inhibitors did

demonstrate benefit in urothelial carcinoma. For example, avelumab, a therapeutic antibody against PD-L1, did extend overall survival for a subset of patients as a maintenance therapy. The JAVELIN Bladder 100 phase-II clinical trial reported that, for patients with unresectable locally advanced or metastatic urothelial cancer without disease progression and after first-line chemotherapy, avelumab maintenance therapy extended overall survival at 1 year (71.3% versus 58.4%) (44).

Taken together, the advent and clinical implementation of ICIs has transformed the landscape of cancer care and extended the overall survival of substantial percentages of patients, particularly with respect to advanced cancers that previously had minimal treatment options. However, even in cancers that exhibit higher rates of response to checkpoint inhibitors such as melanoma, approximately half of patients do not respond to treatment.

Ultimately, the main contributors to a strong T cell-mediated anti-tumor immune response, and thus response to checkpoint immunotherapy, has been associated with several factors: the mutational burden of the tumor (TMB), and similarly, the status of microsatellite instability (MSI) and mismatch repair deficiency (MMR-D), which leads to increased diversity of neoantigens, PD-L1 expression level in some cancers, integrity of interferon gamma signaling response, degree of pre-treatment T cell infiltration in the tumor, baseline expression on immunosuppressive signaling, intestinal microbiome composition, presence of HLA molecules on the cell surface, and epigenetic modifications in the tumor (45-49).

Tumors that do not respond to checkpoint immunotherapy may present with primary resistance while other tumors may initially respond, but eventually acquire resistance. Often, resistance is conferred through multiple, sometimes overlapping, mechanisms. Mechanisms that drive resistance to checkpoint immunotherapy can be tumor-intrinsic or tumor-extrinsic. Tumors

may possess defects in antigen production and presentation, express factors that facilitate exclusion of lymphocytes, or dysregulated signaling pathways rendering cells insensitive to infiltrating lymphocytes, including defects in interferon gamma signaling. Extrinsic factors arise from cells in the tumor microenvironment, and may manifest from a lack of tumor-antigen specific T cells, or T cells with increased expression of alternative immune checkpoints (such as *HAVCR2*, *LAG-3*, etc.), or an abundance of immunosuppressive immune cells such as immunosuppressive tumor-associated macrophages (TAMs) or T regulatory cells (T-regs) that secrete anti-inflammatory factors into the TME (46).

Thus, while checkpoint immunotherapy has revolutionized and become a pillar of modern cancer care, improving survival for approximately 20-50% of eligible patients that otherwise would have access to minimal therapeutic options, achieving durable responses and overcoming the rates of resistance to checkpoint immunotherapy remains a substantial challenge in the field. Thus continued identification of patterns of response, discovery of factors that influence response, characterization of mechanisms of resistance, and elucidation of novel therapeutic targets is imperative.

1.3 Oncofetal antigens are cancer biomarkers and potential therapeutic antigens

The identification of targetable tumor antigens remains critical for the development of cancer-specific immunotherapies and establishment of cancer-specific biomarkers. Classes of targetable antigens include tumor-specific antigens, tumor-associated antigens, and oncofetal or cancer/testis antigens (CTAs). Oncofetal and cancer/testis antigens are typically expressed in germline cells and/or during development and become re-expressed in some adult cancers (51).

Oncofetal antigens have been studied for decades as cancer biomarkers and potential therapeutic targets or potential antigens for cancer vaccines (50).

Two common and FDA-approved clinical-grade oncofetal biomarkers are carcinoembryonic antigen (CEA), alpha-fetoprotein (AFP), and human chorionic gonadotropin (hCG) (52-54). CEA is used as a main biomarker for colorectal cancer, as well as for lung, breast, ovarian, and prostate cancers (55). AFP is a biomarker for diagnosis and prognosis of hepatocellular carcinoma (56). hCG is a biomarker for germ cell tumors and trophoblastic disease (54).

Several cancer/testis antigens have been explored as targets for cancer vaccines with limited success, including WT1 (Wilms tumor 1) and New York-esophageal cancer 1 (NY-ESO-1) (57). Modern cancer vaccine development efforts have largely been unsuccessful, despite some vaccines showing limited benefit in some contexts, in part due to size limitations of clinical trial studies and due to other cancer immunotherapy approaches such as checkpoint inhibitors being significantly more successful. Despite many failed cancer vaccine attempts, interest in cancer vaccines has recently been renewed for their potential as combination therapies with checkpoint inhibitors to boost T cell priming (57). As such, how the efficacy of cancer vaccines is measured is shifting, with growing interest in exploring and revisiting potential vaccine antigens.

CTAs and oncofetal antigens are also being utilized as targets for cell therapies. An example of this is MAGE-A4-directed autologous T cell immunotherapy, which was recently approved for unresectable or metastatic MAGE-4A expressing synovial sarcoma that meets several treatment criteria (58).

Ultimately, oncofetal and cancer-testis antigens exhibit predominantly cancer-specific expression profiles, making them clinically valuable as disease biomarkers, as well as promising antigens for cancer vaccine development and targets for cell therapies.

Chapter 2 Chorionic Gonadotropin Beta 7 is a marker of immune evasion in cancer

This chapter is currently in the process of initial submission to a peer reviewed journal. I am grateful for the contributions of Dr. Jose Mario Bello Pineda on the generation of a random survival forest model assessing predicative value of *CGB7* (Plots in Figure 2-5 and Figure S2-5 are credited to Jose), editing of the manuscript, and input on computational methodology. Thank you to Rohan Lattupally[6] and Amy S. Codd for their contributions to mechanistic exploration experiments (data not shown), and for the contributions of Evan W. Newell, Sydney X. Lu, and of course Robert K. Bradley for their input on this project.

2.1 Abstract

Human chorionic gonadotropin beta (beta-hCG) is an oncofetal antigen expressed by trophoblast cells of the placenta, with minimal expression in adult somatic tissues. Numerous studies have demonstrated that genes encoding beta-hCG are expressed in various cancers, but expression of these genes (*CGB3*, *CGB5*, *CGB7*, and *CGB8*) across diverse cancers has not been systematically evaluated. Here we report that beta-hCG-encoding genes are more widely expressed across diverse cancer types than previously appreciated. In particular, genes encoding beta-hCG proteins are expressed in the majority of urothelial bladder cancers, with *CGB7* most frequently expressed. *CGB7* expression is significantly associated with hallmarks of an immunosuppressed tumor microenvironment, including decreased CD8+ T cell infiltration.

Multiple CGB genes are associated with failure to respond to immune checkpoint inhibitor (ICI) therapy, and *CGB7* is particularly strongly predictive of poor prognosis. Overall, our findings indicate that beta-hCG may constitute a clinically useful biomarker for tumorigenesis and ICI response.

2.2 Introduction

Oncofetal antigens, or proteins that are canonically expressed in immune-permissive developmental contexts and are re-expressed in cancer, have garnered interest for decades as both tumor-specific biomarkers and attractive targets for anti-cancer therapeutics. Notable examples of clinically utilized oncofetal proteins include carcinoembryonic antigen (CEA) and alpha-fetoprotein (AFP). CEA is elevated in multiple malignancies and is commonly used as a biomarker of colorectal cancer, while AFP is a diagnostic marker of testicular cancer and hepatocellular carcinoma (59, 60). Due to the tumor specificity of these markers, they are both being actively investigated as a target antigen for cell therapies such as AFP-targeted CAR-T cell therapies (61, 62).

Human Chorionic Gonadotropin Beta (beta-hCG), the beta subunit of essential heterodimeric developmental glycohormone human Chorionic Gonadotropin (hCG), is an oncofetal antigen expressed primarily in trophoblast cells during embryogenesis and reexpressed in multiple cancer types (63-65). Detection of beta-hCG immunoreactivity by enzyme linked immunosorbent assay (ELISA) is the basis of modern clinical tests for pregnancy and trophoblastic disease. Elevated beta-hCG has also been observed in both trophoblastic and non-trophoblastic cancers including germ cell tumors such as choriocarcinoma, urothelial bladder cancer, lung cancer, head and neck cancer, breast cancer, cervical cancer, ovarian cancer, colorectal cancer, endometrial cancer, renal cancer, prostate cancer, and pancreatic cancer (64, 65). Highlighting the extensive and cancer-specific expression pattern of genes encoding beta-

hCG, Chew et al. developed a cancer-specificity scoring metric to screen for cancer-specific genes expressed across multiple cancer types and identified *CGB5,* one of the genes encoding beta-hCG proteins, as the gene exhibiting the strongest pan-cancer signal (66).

Beta-hCG expression and the presence of trophoblast-like cells on histology are hallmarks of aberrant trophoblastic differentiation, which can occur in non-choriocarcinomas such as urothelial bladder cancer. Trophoblastic differentiation is associated with poor prognosis and therapeutic resistance (67,68). beta-hCG expression alone in many cancer types is associated with poor prognosis (65).

hCG is a hormone composed of an alpha subunit encoded by *CGA* and a beta subunit encoded by one of four highly homologous genes: *CGB3* (also known as *CGB*), *CGB5*, *CGB7*, and *CGB8*. Functioning at the maternal-fetal interface, it is essential in decidualization and the maintenance of early pregnancy via both endocrine and paracrine signaling mechanisms. hCG carries out endocrine effects as a driver of progesterone production and exerts paracrine effects that facilitate invasion (69, 70), angiogenesis (71-73), and maternal immunotolerance (73-78). hCG belongs to the gonadotropin family of hormones, which includes thyroid stimulating hormone (TSH), follicle stimulating hormone (FSH), and luteinizing hormone (LH). This hormone family shares a common alpha subunit, CGA. hCG, TSH, FSH, and LH have essential, but distinct, functions in pregnancy, metabolism, and in development and fertility respectively, with functional specificity conferred by unique beta subunits that possess varying degrees of homology. It is intriguing that upregulation of these specificity-conferring genes encoding beta-hCG proteins is observed in cancer.

Beta-hCG proteins are encoded by four highly homologous primate-specific coding genes arranged in tandem on chromosome 19: *CGB3, CGB5*, *CGB7*, and *CGB8*. This is in contrast

with *CGB1* and *CGB2*, which have historically been classified as pseudogenes due to the presence of frameshifts that disrupt their open reading frames. *CGB3*, *CGB5*, and *CGB8* encode identical proteins classified as type 2 CGB proteins. The CGB7 protein differs by three amino acids and encodes a type 1 CGB protein. *CGB7* expression is also observed in some extra-trophoblast tissues and is uniquely regulated (79-81). We refer to this collection of genes as CGB genes.

As detection and level of CGB protein is currently clinically utilized for pregnancy testing and as a clinical-grade biomarker of trophoblastic disease and germ cell tumors, we sought to explore the potential of CGB proteins as cancer biomarkers. While numerous reports suggest that expression of CGB genes may be valuable cancer biomarkers and prognostic factors, the extent to which each CGB gene is expressed in diverse cancers has not yet been systematically evaluated using the large cohorts of cancer patients available today. Furthermore, the quantitative prognostic utility of CGB expression and the specific cancer phenotypes with which CGB expression is associated remain incompletely understood, particularly across diverse cancer types.

Here, we systematically assess expression of CGB genes across diverse cancer types and reveal that all CGB genes are pervasively expressed across many cancer types, including urothelial cancer, with *CGB7* most frequently expressed. We confirm that CGB genes are transcribed and proteins are detectable as secreted proteins from cancer cells by isoform-specific qRT-PCR and bulk CGB ELISA. We determine that *CGB7* expression is strongly associated with hallmarks of an immunosuppressed tumor microenvironment by re-analyzing RNA-sequencing data, CD8+ T cell infiltration data as measured by immunohistochemistry (IHC), and tumor subtyping data from a cohort of advanced urothelial carcinoma patients. Kaplan-Meier

survival analyses elucidate an association between *CGB7* expression and decreased survival probability in a cohort of advanced urothelial carcinoma patients treated with PD-L1 inhibition immunotherapy, which is supported by an association between *CGB7* expression and progressive disease in this cohort. Finally, we propose *CGB7* as a prognostic marker with strong predictive value for response to immune checkpoint inhibition via a random survival forest machine learning model of patient survival.

2.3 CGB genes are expressed in multiple cancer types

We sought to systematically evaluate the expression patterns of each functional CGB gene (*CGB3, CGB5, CGB7,* and *CGB8*) across 20 distinct cancer types utilizing gene expression data from The Cancer Genome Atlas (TCGA) **(Figure 2-1A)**. We confined this analysis to the 20 tumor types with at least one peritumoral control tissue sample in order to be able to accurately assess cancer specificity of CGB expression. Comparing expression of each CGB gene in tumor and matched normal peritumoral tissues across these datasets elucidated extensive cancer-specific expression of *CGB3, CGB5, CGB7,* and *CGB8* across cancer types **(Figure 2-1B, 2-1C, Figure S2-1D – 2-1K)**.

Our results both confirm and notably extend previous reports of CGB expression in cancers as well as identify CGB expression in tumor types in which it has not been previously reported. For example, Cook et al. reports mRNA expression of CGB genes in 30% (n=70) of bladder cancers (84). Hotakainen et al. reports mRNA expression of CGB genes in 50% (n=84) of the transitional cell carcinoma cases and in none of the healthy controls assayed (n=15) (82). Our new analyses reveal that nearly 68% of such tumors express one or more CGB genes at the mRNA level, while our analyses also reveal common CGB expression in tumor types such as

thymoma, which has not been previously reported to our knowledge. Conversely, though *CGA* is expressed across numerous cancers, it is also expressed more frequently in numerous normal tissues, and thus expression of *CGA* does not share a cancer specific expression profile **(Figure S2-1A – S2-1B)**. This is consistent with the pleiotropy of *CGA*, where CGA is a subunit of all gonadotropin hormones, including thyroid stimulating hormone (TSH), follicle stimulating hormone (FSH), and luteinizing hormone (LH), which are expressed outside of development in healthy somatic tissues. Together, these data highlight the specific upregulation of CGB genes in cancer. We conclude that CGB genes are specifically and pervasively expressed in cancers and hypothesize that this specific upregulation reflects a potential novel function of CGB proteins in cancer.

We next identified cancer types that exhibited particularly high frequencies of expression of at least one CGB gene. The three cancer types with highest expression of any CGB are thymoma, pancreatic adenocarcinoma, and urothelial carcinoma **(Figure 2-1D)**. Trophoblastic differentiation and beta-hCG expression in urothelial cancer have been recognized for decades (86-88). As urothelial cancer exhibits low frequency of *CGA* expression in our analyses despite the high frequency of expression of CGB genes–highlighting the specificity of CGB gene expression in this cancer type–we selected urothelial cancer as a model to further explore the effects of CGB expression on cancer **(Figure 2-1D, S2-1A)**.

Of the four CGB genes, *CGB7* is expressed most frequently across cancer types and in urothelial cancer **(Figure S2-2, Figure S2-1J, Figure S2-1K, Figure S2-1L, Figure S2-1M)**. We therefore sought to further explore the expression pattern of CGB7 in urothelial carcinoma. We first wondered how frequently *CGB7* is coexpressed with *CGB3*, *CGB5*, *CGB8*, and *CGA* in urothelial carcinoma. Further evaluation of expression of these genes in the TCGA urothelial

carcinoma cohort revealed that while tumors tend to co-express *CGB3*, *CGB5*, and *CGB8, CGB7*-expressing tumors cluster independently, suggesting that *CGB7* is less frequently co-expressed with *CGB3, CGB5,* and *CGB8* **(Figure 2-1E)**. We conclude that *CGB7* exhibits a unique expression pattern in urothelial cancer and is expressed more frequently than *CGB3, CGB5,* and *CGB8* in this dataset **(Figure 2-1E)**. This is consistent with a previous report of type-I CGBs being the predominantly expressed type at the mRNA level in renal cell carcinoma samples (86). Furthermore, *CGB7* is frequently expressed independently of *CGA*, suggesting a potential beta-subunit specific effect independent of the hCG heterodimer **(Figure 2-1E)**. These findings regarding the unique expression pattern of *CGB7* are particularly notable as *CGB7* differs from *CGB3, CGB5,* and *CGB8* in sequence, tissue expression profile, and the sequences of its untranslated regulatory regions (79-81).

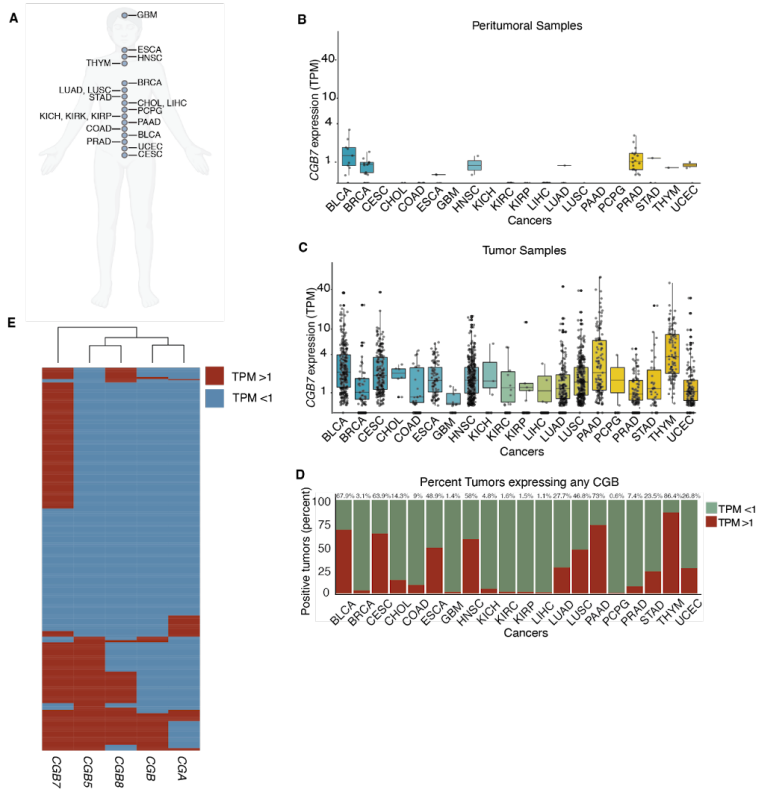

Figure 2-1. CGB is expressed in multiple cancer types TPM = transcripts per million. Data re-analyzed from the TCGA. (A) selection of 20 unique cancer mRNA sequencing datasets from The Cancer Genome Atlas (TCGA). CGB7 mRNA expression in healthy peritumoral tissue samples (B), and matched tumor tissue samples (C) across 20 cancer types. Cancer type reflects the site of the primary tumor. (D) Fraction of tumors across 20 cancer types expressing at least one CGB gene with TPM >1. Percent positive is annotated above each cancer type. (E) Expression status of CGB3, CGB5, CGB7, CGB8, and CGA in tumors from the TCGA bladder cancer (BLCA) dataset. Expressed genes are defined as TPM > 1, non-expressed genes are defined as TPM < 1.

2.4 CGB proteins are secreted by urothelial cancer cells

The comprehensive RNA-seq data provided by the TCGA allows for systematic analysis of CGB gene expression, but these data do not directly address the question of whether expressed CGB mRNA is translated into protein. We therefore directly tested whether CGB protein is produced and secreted by urothelial cancer. We focused on urothelial cancer given the particularly high and frequent expression of CGB that we observed in this tumor type.

We first sought to validate that CGB genes are expressed in human urothelial cancer cells with an orthogonal assay and confirmed that this expression can be reversed by gene silencing. We utilized gene expression data from the Cancer Cell Line Encyclopedia (CCLE) to stratify human urothelial cancer cell lines by CGB expression **(Supplemental Table 2-1)**. As in human tumor samples, urothelial cancer cell lines exhibit a range of expression of CGB genes **(Table 2-1).** Interestingly, *CGB3*, *CGB5,* and *CGB8* frequently exhibited markedly higher expression than did *CGB7* in these cell lines – in contrast to the primary tumor mRNA expression data from the TCGA, where all CGB genes were expressed at a similar level (**Table 2-1**). However, this observation is consistent with prior findings that type II CGBs (CGB3, CGB5, and CGB8) exhibited higher expression than type I CGBs (CGB7) in urothelial cancer (86). *CGA* expression was low or absent from the majority of these cell lines (**Table 2-1**).

We selected seven urothelial cancer cell lines with high summed CGB expression and one cell line with undetectable CGB expression as examples of CGB-positive and CGB-negative tumors to validate CGB gene expression and protein levels *in vitro*. All cell lines selected are negative

for *CGA* expression at the mRNA level. We observed expression of *CGB3, CGB5,* and *CGB8* across the seven positive cell lines surveyed, but not in the negative cell line **(Figure 2-2A)**. Treatment of J82 cells with a pan-CGB targeting siRNA pool depleted signal from the CGB3/5/8-specific probe in J82 cells **(Figure 2-2B)**, confirming that the detected mRNA signal arises from expression of CGB genes. We observed clear but low *CGB7* expression in one of the seven assayed cell lines (SCaBER cells; **Figure 2-2C**). *CGB7* expression is too low to be reliably detected in the remaining cell lines not shown. This is supported by the lower expression of *CGB7* relative to other CGB genes that we observed in gene expression data from CCLE data **(Table 1)**.

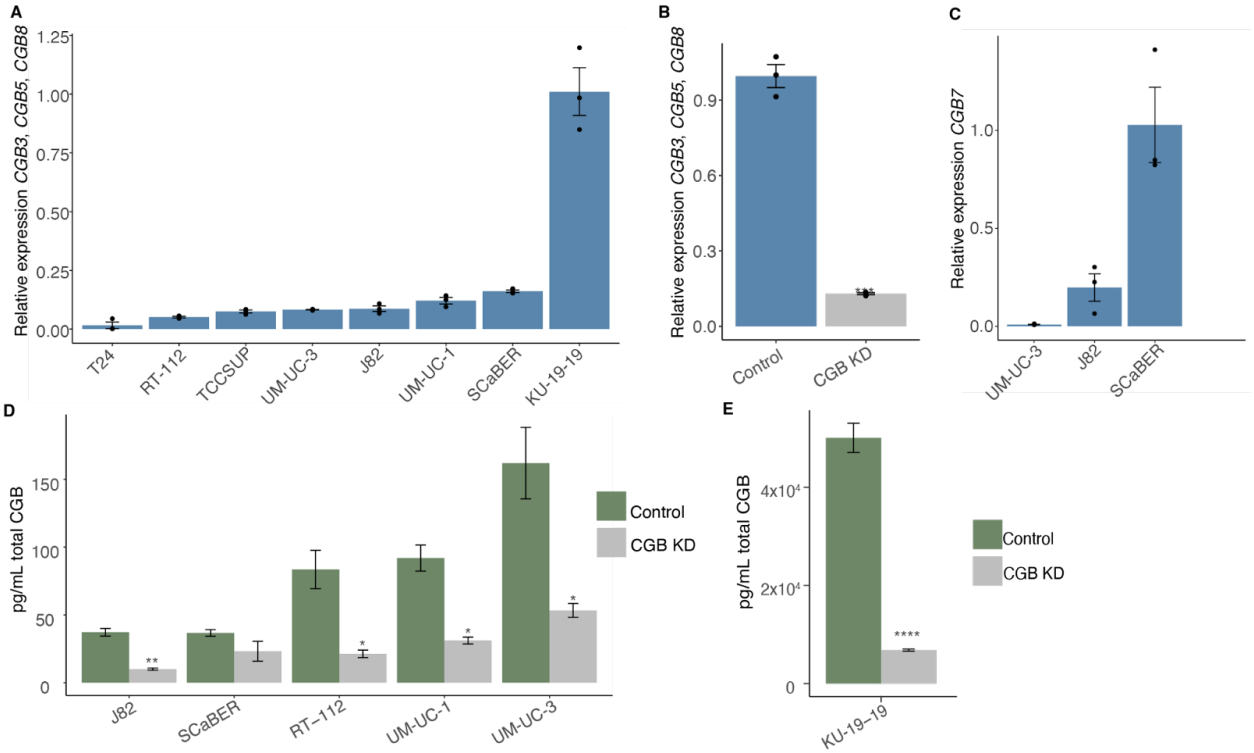

Figure 2-2. CGB is expressed in multiple human urothelial carcinoma cell lines. All experiments run in biological and technical triplicate; all error bars represent SE; *p < 0.5; **p < 0.01; ****p < 0.0001. (**A**) Expression of bulk CGB3, CGB5, and CGB8 mRNA normalized to GAPDH quantified by RT-qPCR in human urothelial carcinoma cell lines. Expression is relative to the cell line with the highest expression. Data in Figure 2A–Source Data 2A file. (**B**) Expression of CGB3, CGB5, and CGB8 mRNA normalized to GAPDH quantified by RT-qPCR in J82 cells treated with a non-targeting siRNA pool or an siRNA pool targeting all CGB genes. Expression is relative to the cell line with the highest expression. P-value calculated via welch two sample t-test. Data in Figure 2B–Source Data 2B file. (**C**) Expression of CGB7 mRNA normalized to GAPDH quantified by RT-qPCR in human urothelial carcinoma cell lines. Expression is relative to the cell line with the highest expression. (**D**) Secretion of total CGB protein quantified by ELISA in human urothelial carcinoma cell lines treated with a non-targeting siRNA

pool or an siRNA pool targeting all CGB genes. pg/mL CGB protein shown per 10,000 cells. P-value calculated via welch two sample t-test. Data in Figure 2D–Source Data 2D file. (**E**) Secretion of total CGB protein quantified by ELISA in KU-19-19 cells treated with a non-targeting siRNA pool or an siRNA pool targeting all CGB genes. pg/mL CGB protein shown per 10,000 cells. P-value calculated via welch two sample t-test.

We next validated that CGB proteins are translated and secreted as free beta subunits and that the signal arises from CGB mRNA. Previously, secretion of CGB proteins from several urothelial cancer cell lines was shown (90). Iles et al. did not confirm reversibility of signal with knockdown of CGB genes, so we sought to confirm specificity of detection with pan-CGB gene knockdown. We selected J82, SCaBER, RT-112, UM-UC-1, UM-UC-3, and KU-19-19 cells given both their high expression of CGB genes and absent *CGA* expression by mRNA analysis and performed ELISA to detect total CGB protein from supernatant **(Figure 2-2D, 2-2E)**. These data confirmed that CGB protein is readily produced and detectable as a secreted protein from all cell lines, with KU-19-19 cells producing particularly notable amounts. As *CGA* is not appreciably expressed in these cell lines **(Table 2-1)**, we infer that CGB proteins are stable and secreted unbound to CGA. Specificity of the assay was further supported by targeted knock down of bulk CGB genes, resulting in a significant decrease in detected CGB protein **(Figure 2-2D, 2-2E)**.

We conclude that both type-I-encoding (*CGB7*) and type-II-encoding (*CGB3, CGB5,* and *CGB8*) CGB genes are expressed in human urothelial cancer cells and that CGB proteins are stable as free beta subunits and are secreted from cancer cells.

Table 1. Expression of Chorionic Gonadotropin genes in cell lines from the Cancer Cell Line Encyclopedia

Cell Line	*CGB3*	*CGB5*	*CGB7*	*CGB8*	*CGA*	Sum of CGB genes
KU-19-19	0.56	229.23	2.45	14.12	0.00	246.35
J82	2.50	25.04	4.17	36.35	0.75	68.06
UM-UC-3	0.36	0.71	0.41	28.27	0.00	29.76
SCaBER	1.42	2.63	2.20	16.69	0.45	22.93
RT-112	0.28	3.11	3.79	10.81	0.33	18.00
UM-UC-1	0.25	2.19	1.81	11.97	0.42	16.22
639-V	0.75	7.79	1.66	3.78	0.26	13.98
VM-CUBl	0.50	3.23	7.22	1.81	0.00	12.75
JMSU-1	0.14	1.36	1.33	4.37	0.23	7.19
5637	0.11	1.41	2.10	2.63	0.39	6.25
HT-1197	0.62	0.45	2.45	1.98	1.06	5.50
SW-1710	0.12	0.15	1.95	2.74	0.32	4.96
KMBC-2	0.10	1.56	1.93	1.35	0.76	4.95
647-V	0.11	1.22	0.37	1.89	0.00	3.59
CAL-29	0.18	1.29	1.04	0.64	0.42	3.14
HT-1376	0.38	0.74	1.00	0.29	9.73	2.41
RT4	0.08	0.33	1.91	0.05	0.22	2.38
BFTC-905	0.10	0.41	1.46	0.14	0.32	2.11
BC-3C	0.11	0.21	0.11	0.79	0.34	1.22
T24	0.05	0.09	0.53	0.05	0.00	0.72
TCCSUP	0.06	0.08	0.39	0.08	0.27	0.62

Values in Transcripts
Per Million (TPM).

2.5 CGB7 expression is associated with reduced anti-tumor immune activity

As *CGB7* is the most frequently expressed of the CGB genes in our analyses of the TCGA urothelial carcinoma cohort, we elected to focus on *CGB7*. To interrogate the possible functional effects of *CGB7* expression in cancer, we re-analyzed RNA-sequencing data from the TCGA primary urothelial carcinoma cohort by comparing the gene expression profiles of *CGB7*-

positive and *CGB7*-negative tumors. Gene Ontology (GO) enrichment analysis revealed that downregulated genes in *CGB7*-positive tumors are enriched for diverse biological processes **(Figure S2-3A)**. Interestingly, one of the highest-ranked enriched GO terms was related to immune response, which we found to be particularly intriguing given previous literature demonstrating a functional role for hCG in immune tolerance in pregnancy (74-78). Further probing of associated GO terms revealed that *CGB7* expression was specifically associated with downregulation of genes involved in the adaptive immune response, lymphocyte activation, and positive immune system regulation, indicating that *CGB7* expression is inversely associated with inflammation **(Figure 2-3A)** in a manner reminiscent of hCG's documented role in maternal immunotolerance.

To confirm this finding in an orthogonal dataset, we analyzed mRNA-sequencing data from the IMVigor 210 multicenter, single-arm, phase II clinical trial (94). This cohort is composed of patients with advanced urothelial carcinoma that received Atezolizumab, an anti-PD-L1 checkpoint inhibitor, and is ideally suited for our investigation given that pre-treatment samples were characterized by both RNA-seq and immunohistochemistry (94). We again found that genes downregulated with *CGB7* expression were strongly associated with inflammatory processes **(Figure 2-3A)**. Notably, in genes that are downregulated in *CGB7*-positive tumors, at least 17 of the 20 highest ranked enriched GO terms are robustly associated with inflammation and immunity, reinforcing a negative association between *CGB7* and inflammation **(Figure S2-3B)**. The association between *CGB7* expression and regulation of immune response in this dataset is further supported by pronounced downregulation of genes involved in interferon gamma response in *CGB7*+ tumors identified by gene set enrichment analysis via GSEA software (82). **(Figure 2-3B)**.

Interferon gamma signaling is strongly associated with response to immune checkpoint inhibition, and indeed, disruption of interferon gamma signaling remains a mechanism of resistance to ICI (47, 95). Exploring this *CGB7*-associated downregulation of interferon gamma response genes in both the IMVigor210 cohort dataset and in the TCGA urothelial carcinoma cohort dataset reveals downregulation of numerous genes encoding inflammatory cytokines and chemokines, immune checkpoints such as PD-L1, and HLA proteins involved in antigen presentation; all features of immune evasion in cancer **(Figure 2-3C, 2-3D)**. As hCG is well-established as a facilitator of maternal immunosuppression (74-78), we hypothesize that *CGB7* may similarly exhibit immunosuppressive functions that ultimately promote immune escape of tumors.

As interferon gamma facilitates tumor infiltration of CD8+ T cells and is ultimately a marker of CD8+ T cell activity, we next investigated whether *CGB7* expression affects CD8+ T cell infiltration using immune phenotype classification data for tumor samples from the IMVigor 210 cohort. Here, immunophenotype is determined by CD8a IHC staining of FFPE tumor sections (94). Tumors were scored on the basis of CD8a staining frequency and pattern as exhibiting an immune infiltrated, immune excluded, or immune desert phenotype (94). We stratified tumors by *CGB7* expression and binned samples according to negative-low (<25%), moderate (25%-75%), or high (>75%) *CGB7* expression. Comparing the distribution of immunophenotypes between *CGB7*-low and *CGB7*-high tumors elucidates a significantly distinct distribution of inflamed tumors ($p=6.89x10^{-5}$) **(Figure 2-3E)**. We observed no statistically significant differences in the distributions of immune excluded or immune desert phenotypes between *CGB7*-low and *CGB7*-high tumors, though there is a trend toward higher incidence of immune exclusion in *CGB7*-high tumors ($p= 0.062$, $p= 0.32$). These findings that

CGB7-high tumors exhibit decreased immune infiltration is consistent with our findings that *CGB7* expression is associated with downregulated IFNg signaling, as IFNg is predominantly secreted by activated lymphocytes, promotes tumor infiltration of immune cells such as CD8+ T cells, and is a marker of ICI response (47).

Furthermore, when we compare *CGA*-low and *CGA*-high tumors, there is no significant difference in the distribution of inflamed tumors (p=0.35), supporting a possible *CGB7*-specific effect on CD8+ T cell exclusion **(Figure 2-3F)**.

Additionally, when we explored associations between *CGB7* expression and subtype as scored by Mariathasan et al. according to the Lund classification system, an established system for urothelial cancer classification (96,97), we observe a significantly decreased fraction of immune-infiltrated tumors in *CGB7*-high tumors compared with *CGB7*-low tumors ($p=2.65x10^{-8}$) **(Figure 2-3G)**. This infiltrated class of tumors is described as enriched for immune system processes and lymphocyte activation, including an enrichment of activated T cell markers and cytotoxic T cell effector genes (96). There was no association between the immune infiltrated subtype and *CGA* expression, further supporting an association between *CGB7* expression and reduced immune infiltration (p=0.53) **(Figure 2-3H)**.

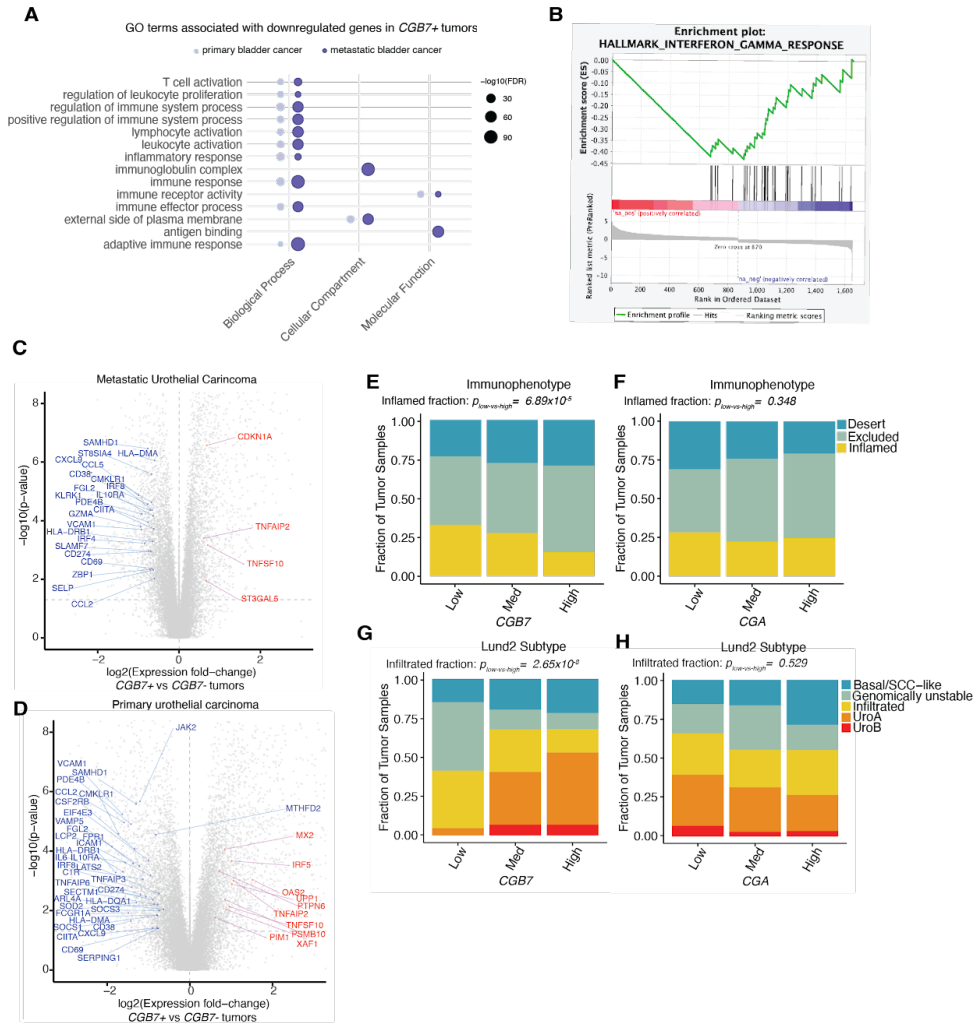

Figure 2-3. CGB expression correlates with altered immune infiltrate. Med = medium. (**A**) Immune-associated Gene Ontology terms associated with genes downregulated in CGB7+ tumors in metastatic urothelial cancer (data re-analyzed from Mariathasan et al., 2018) and in primary urothelial cancer (data re-analyzed from TCGA BLCA cohort). CGB7+: >1 TPM. CGB7-: <0.25 TPM. (**B**) Interferon Gamma response genes are negatively correlated with CGB7 expression in metastatic urothelial tumors (data re-analyzed from Mariathasan et al., 2018). GSEA normalized Enrichment Score (NES): -2.20. FWER p-Value: 0.004. (**C**) Differentially expressed genes in CGB7+ vs CGB7- metastatic urothelial tumors (data re-analyzed from Mariathasan et al., 2018) as determined by Mann-Whitney U Test. Interferon gamma response genes that are significantly differentially expressed are in red (upregulated) or blue (downregulated) and reach p-value < 0.05 and log fold change > 1.5. CGB7+: >1 TPM. CGB7-: <0.25 TPM. (**D**) Differentially expressed genes in CGB7+ vs CGB7- primary urothelial tumors (data re-analyzed from TCGA) as determined by Mann-Whitney U Test. Interferon gamma response genes that are significantly differentially expressed are in red (upregulated) or blue (downregulated) and reach p-value < 0.05 and log fold change > 1.5. CGB7+: >1 TPM. CGB7-: <0.25 TPM. (**E**) Immunophenotype data in tumors stratified by CGB7 expression: immune desert, immune excluded, or inflamed. P-values determined by proportions test with continuity correction. Chi-squared = 15.84, p-value = 6.89×10^{-5}. (**F**) As in (**E**), but stratified by CGA expression. Chi-squared = 0.88, p-value = 0.35. (**G**) Tumor subtype data in tumors stratified by CGB7 expression: basal/SCC-like, genomically unstable, immune infiltrated, urothelial type A, or urothelial type B. P-values determined by proportions test with continuity correction. Chi-squared = 30.95, p-value = 2.65×10^{-8}. (**H**) As in (**G**), but stratified by CGA expression. Chi-squared = 0.40, p-value = 0.53.

We focused these and prior analyses on *CGB7* because *CGB7* is more commonly expressed than other CGB genes in this cancer type **(Figure 2-1E)**. Because some CGB-positive samples express only genes encoding type I CGBs (*CGB7*), others express only genes encoding type II CGBs *(CGB3, CGB5,* and *CGB8*), and others both type I and type II, we sought to test whether the functional association between CGB gene expression and immunophenotypes was likely driven by genes encoding type I or type II CGBs (or both). We used a patient stratification approach to address this question.

We first tested whether the associations between *CGB7* and CD8+ T cell infiltration and tumor subtype are upheld independently of *CGB3, CGB5,* and *CGB8* expression. We selected samples negative for *CGB3, CGB5,* and *CGB8* expression, and to ensure sufficient samples for analysis, we lowered the threshold for negative expression from 0.25 to 1 TPM to increase sample size. We then stratified samples by negative-low, moderate, or high *CGB7* expression as described. Consistent with our prior findings, *CGB7*-high tumors exhibit significantly decreased CD8+ T cell infiltration (incidence of inflamed tumors) compared with CGB7-low tumors (p=1.60x10-6) **(Figure S2-3C)**. Similarly, *CGB7*-high tumors exhibit a significantly decreased fraction of immune infiltrated tumors compared with *CGB7*-low tumors (p=0.00450) **(Figure S2-3D)**. Both of these findings are independent of *CGB3, CGB5,* and *CGB*8 expression. Conversely, selecting *CGB7*-negative samples and stratifying by summed *CGB3, CGB5*, and *CGB8* expression, we find no association between *CGB3*, *CGB5*, and *CGB8* expression and CD8+ T cell infiltration (p=0.730) or incidence of immune-infiltrated tumors (p=1) independent of *CGB7* expression **(Figure S2-3E, S2-3F)**. It is important to note, however, that our statistical power for these analyses was not equal for type I and type II CGB analyses due to *CGB7* being the most commonly expressed CGB gene **(Figure 2-1E)**.

Overall, these findings reinforce our hypothesis that *CGB7* is consistently associated with an immunosuppressive tumor microenvironment and hallmarks of immune escape. We conclude that *CGB7* is significantly associated with blunted interferon gamma signaling and is specifically and significantly associated with decreased CD8+T cell infiltration in the urothelial carcinoma cohorts investigated.

2.6 CGB expression is associated with decreased response to ICI therapy

As interferon gamma release and CD8+ T cell infiltration are associated with response to ICI therapy, we next wondered whether *CGB7* expression had implications for overall survival and response to anti-PD-L1 checkpoint inhibition. To investigate this the effect of *CGB7* on survival, we selected *CGB7*-positive (TPM >1) and *CGB7*-negative (TPM < 0.25) tumors and performed Kaplan Meier survival analysis. We found that *CGB7* expression is indeed associated with significantly decreased overall survival probability ($p= 6.87x10^{-3}$) **(Figure 4A)**. Though this decrease in survival probability associated with *CGB7* expression is strongest, *CGB3* and *CGB5,* but not *CGB8*, are also associated with significantly decreased survival probability **(Figure S4A-C)**. In contrast, *CGA* expression had no effect on overall survival **(Figure 4B)**.

We wondered whether these associations between CGB gene expression and survival persist when controlling for common potential covariates tumor mutational burden (TMB) and sex. TMB is a known predictor of response to immune checkpoint inhibition (98-101). Sex is associated with differential survival outcomes in some checkpoint immunotherapy cohorts (102-103) and in this specific dataset (**Figure S4I**). Even when survival probabilities are adjusted for the contributions of TMB and sex using Cox proportional hazards modeling, the adjusted survival probability of patients with *CGB7*-positive cancers remains significantly decreased while *CGA* has no effect on adjusted overall survival probability ($p= 0.009$, $p= 0.70$) **(Figure 2-**

4C, 2-4D). Similarly, the adjusted survival probabilities of patients with *CGB3*-positive and *CGB5*-positive tumors remains significantly decreased **(Figure S2-4D – S2-F)**. We conclude that *CGB3, CGB5,* and *CGB7* expression are associated with a significant reduction in survival probability in metastatic urothelial carcinoma patients receiving immune checkpoint blockade, with *CGB7* expression exhibiting the most robust association.

We next wondered whether *CGB7* expression impacts response to checkpoint immunotherapy. Each patient in the IMvigor 210 clinical trial was evaluated for response to anti-PD-L1 therapy by the Response Evaluation Criteria in Solid Tumors (RECIST) and scored as exhibiting progressive disease (PD), stable disease (SD), partial response (PR), or complete response (CR) (42). Again binning patients by *CGB7* expression corresponding to negative-low, moderate, or high expression levels, we compared the proportion of each clinical response classification in *CGB7*-high vs *CGB7*-low tumors to determine patterns of response associated with *CGB7* expression. *CGB7*-high tumors exhibited a significantly higher incidence of PD ($p=0.0021$), but no significant difference in incidence of CR ($p = 0.25$), PR ($p = 0.051$), or SD ($p = 0.25$) **(Figure 2-4E)**. Conversely, comparing incidence of PD between *CGA*-high vs *CGA*-low tumors demonstrated no significant differences ($p=0.71$). Similarly, we observed no significant differences in incidence of CR ($p = 0.074$), PR ($p =0.53$), or SD ($p = 0.12$) between *CGA*-high vs *CGA*-low tumors **(Figure 2-4F)**, highlighting a potential beta-subunit-specific effect on overall survival.

Repeating these analyses to parse *CGB7*-specific effects independent of *CGB3*, *CGB5*, and *CGB8* expression as described above, we determined that high *CGB7* expression is still associated with significantly increased incidence of progressive disease compared with low *CGB7* expression independently of *CGB3, CGB5,* and *CGB8* expression ($p=0.0016$) **(Figure S2-**

4G). Interestingly, when *CGB7*-high samples are filtered out to facilitate bulk *CGB3, CGB5,* and *CGB8* analyses independent of *CGB7* expression, we observe that *CGB3, CGB5,* and *CGB8* are also significantly associated with increased incidence of progressive disease (p=0.0027) independently of *CGB7*, indicating that general CGB expression is associated with progressive disease and thus resistance to ICIs **(Figure S2-4H).**

Taken together, we conclude that *CGB7* expression is strongly associated with an immunosuppressive tumor microenvironment and decreased overall survival probability, suggesting a role of *CGB7* in immune escape of tumors. We additionally conclude that *CGB3* and *CGB5* are associated with decreased survival probability. Ultimately, expression of genes encoding both type I and type II CGB genes are associated with resistance to ICIs in advanced urothelial carcinoma

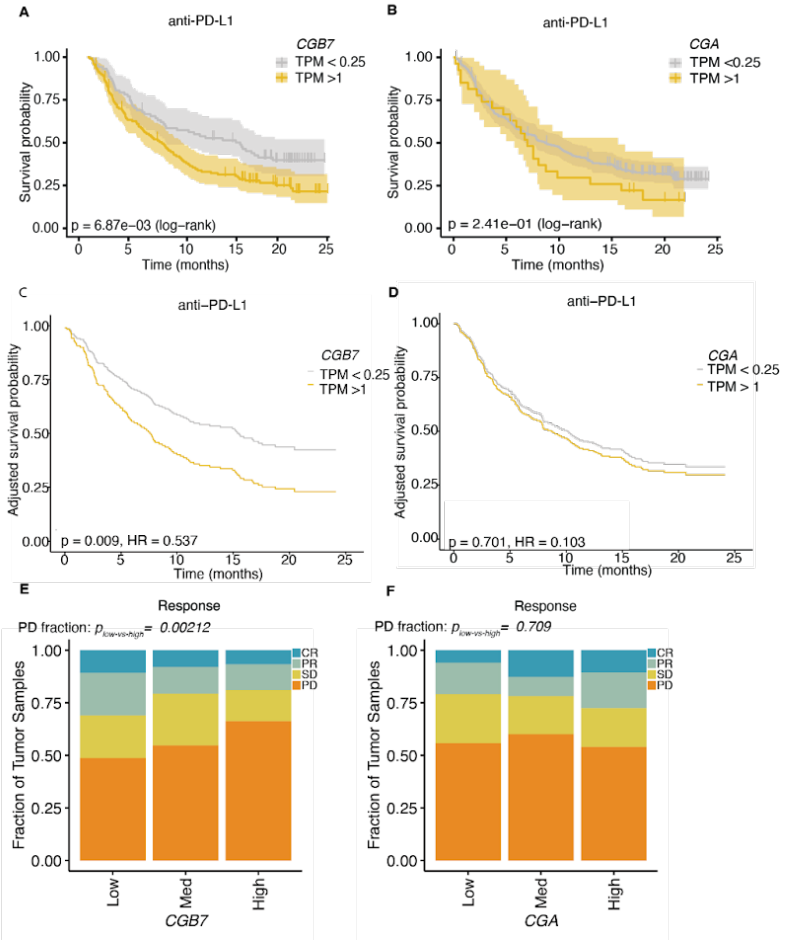

Figure 2-4. CGB expression is associated with decreased response to ICI therapy. Response Evaluation Criteria in Solid Tumors (RECIST) scoring: CR = complete response, PR = partial response, SD = stable disease, PD = progressive disease. Med = medium. (A) Kaplan Meier overall survival curves comparing patients with CGB7+ (gold) and CGB7- (gray) advanced urothelial tumors undergoing treatment with Atezolizumab (anti-PD-L1). Data re-analyzed from Mariathasan et al., 2018. P-value determined by log rank test. The estimated survival functions (solid), censored events (crosses), and 95% confidence intervals (shaded regions) are shown. (B) As in (A), but patients stratified by CGA expression. (C) Kaplan Meier overall survival curves as shown in (A) adjusted for confounding effects of sex and tumor mutational burden covariates by Cox Proportional Hazards modeling. Hazard ratio (HR) and p-value obtained from fitting a Cox Proportional Hazards model. (D) Kaplan Meier overall survival curves as shown in (B) adjusted as described in (C). (E) Response determined by RECIST criteria (data re-analyzed from Balar et al., 2017). P-values determined by proportions test with continuity correction. Chi-squared = 9.44, p-value = 0.0021. (F) As in (A), but stratified by CGA expression. Chi-squared = 0.14, p-value = 0.71.

2.7 CGB expression predicts response to ICI therapy

We next sought to analyze the effect of *CGB7* expression on survival probability by further evaluating our Cox Proportional Hazards model. We first considered the effects of clinical variables collected in the IMVigor 210 trial, including *CGB7* expression, on overall

survival using univariate Cox Proportional Hazards modeling, where variables are assessed separately, and in the multivariate setting, where confounding effects of all variables are controlled for **(Figure S5A)**. In both approaches, tumor mutational burden (TMB), Eastern Cooperative Oncology Group (ECOG) status, and *CGB7* expression, which we treat as a continuous variable, were statistically significant prognostic variables associated with overall survival. Consistent with this notion, our analyses show that TMB is associated with a decreased risk of death (HR = 0.32, $p = 1.10 \times 10^{-6}$) after controlling for all other covariates. Similarly, ECOG status negatively impacts patient survival during ICI therapy as demonstrated in the original Phase II trial of the IMvigor210 study (98), which is reflected in our own analyses (ECOG 1: HR 2.62, $p = 6.07 \times 10^{-8}$; ECOG 2: HR 3.32, $p = 2.30 \times 10^{-3}$). Accordingly, increased *CGB7* expression is correlated with increased risk of death (HR = 1.48, p = 0.026) after controlling for possible confounding (**Figure S5B**).

We next aimed to quantify the predictive value of *CGB7* as a prognostic marker over time using inferences from a Random Survival Forest (RSF) model, a machine learning ensemble consisting of multiple survival trees (104). RSF modeling enables us to predict the time-to-death in our patient cohort, and has been used widely in the literature to predict the prognosis of patients in various disease and interventional contexts (105-111). To grow the RSF, we randomly selected 70% of the patients in the cohort, utilized 1000 base learners, and included the following covariates as input: ECOG status, TMB, *CGB7* expression, platinum chemotherapy history, stage, tobacco use, sex, tumor cell PD-L1 level, and intravesical BCG administration. The resultant model had an Out-of-Bag (OOB) error of 38.9%. The OOB error is calculated from predictions for unsampled patients from each bootstrapping iteration, and represents an unbiased estimate of the test error. We also directly measured model performance using the remaining

30% of patients excluded from model training, this test error measuring 35.6% (**Figure S5B**). The RSF survival curve estimates closely mirror those generated by Kaplan Meier survival analysis, lending confidence to our model (**Figure 5A**).

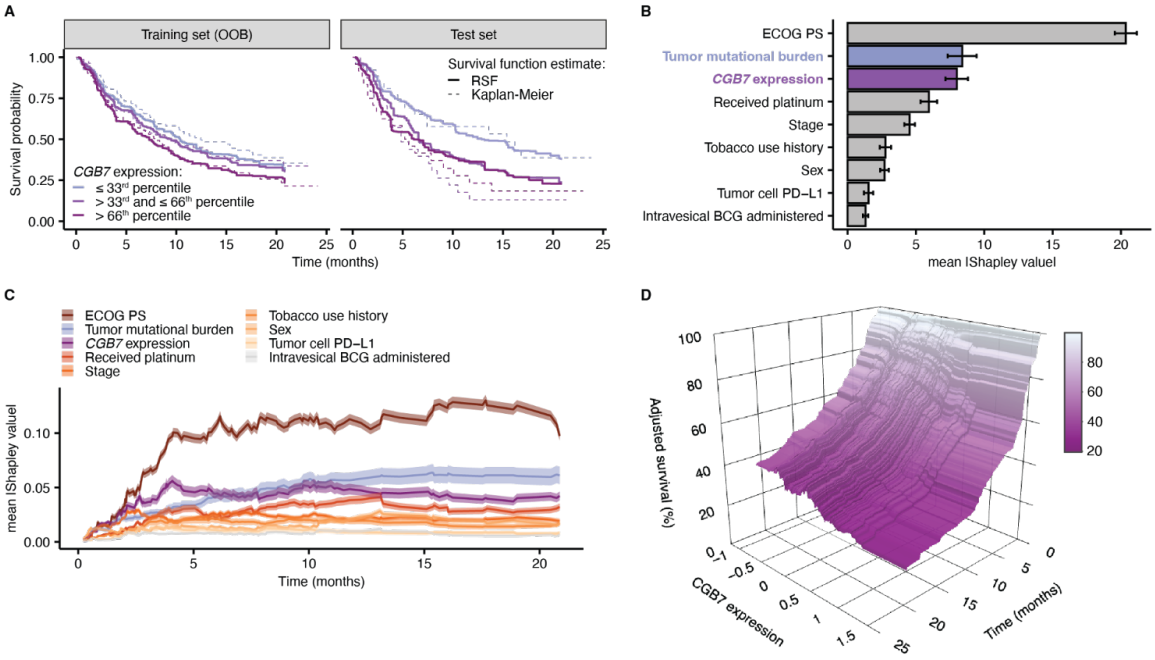

Figure 2-5. CGB7 expression is a prognostic variable associated with decreased survival (**A**) Survival estimates from the Random Survival Forest (RSF) model (median prediction, solid lines) and the Kaplan–Meier estimate (dashed lines) from the training (OOB) and test sets. Patients are stratified into terciles based on CGB7 expression. (**B**) RSF feature importance quantified via the mean absolute Shapley values. Error bars denote the 95% confidence intervals. (**C**) Time-dependent Shapley values, corresponding to survival estimates at specific timepoints. The 95% confidence interval of the mean (transparent ribbon) is shown. (**D**) Adjusted survival probability measured via partial dependence, as a function of time and CGB7 expression.

The survival probability predictions produced by the RSF model suggest that increasing *CGB7* expression is correlated with a decrease in median survival time, and conform with the aforementioned findings from the Cox Proportional Hazards regression (**Fig 5A, Fig S5C**). To quantify the contributions of *CGB7* expression to the predictions of time-to-death generated by the RSF model, we calculated the Shapley values corresponding to each variable utilized in our model (112-115). Shapley values associated with the RSF prediction for mortality, the number of expected deaths over the observation window, were calculated which showed the expected

protective effect of high TMB and the increased risk of death conferred by increased *CGB7* expression **(Figure S5D-E)**. Ranking Shapley values by the mean magnitude calculated over the entire cohort allows quantification of a feature's importance to the model prediction relative to the other model covariates. In these analyses, *CGB7* expression scored highly behind ECOG performance status and equivalently to TMB (**Figure 5B**). We extended these analyses to a time-dependent implementation. First, we verified the time frame upon which inferences from the RSF model are valid, through time-dependent Receiver Operating Characteristic (ROC) analyses. We calculated the cumulative/dynamic area under the ROC curve ($AUC^{C/D}$) which quantifies the model's accuracy at differentiating patient deaths occurring before a particular time point, versus those who survive beyond this time. Our analyses suggest a time horizon up to ~ 15 months (**Figure S5F**). Second, we calculated Shapley values associated with time point-specific survival probability, which suggest that *CGB7* expression has a dynamic relative contribution over time but preserved high importance throughout the observation window. Interestingly, *CGB7* expression is linked to greater prediction contributions compared to TMB at earlier times, up to ~ 6 months (**Figure 5C**). To obtain the adjusted or marginal effects of *CGB7* expression on overall survival, we implemented time-dependent partial dependence analyses which show a clear negative correlation between *CGB7* expression and survival probability **(Figure 5D)**. Ultimately, we observe a robust association between *CGB7* expression and predicted survival probability, in which *CGB7* expression is associated with reduced time to death in advanced urothelial cancer in the context of immune checkpoint inhibition.

Table 2. Cox Proportional Hazards Regression for Overall Survival

Characteristic	Univariate				Multivariate[a,b]			
	HR	95% CI	p-value	q-value[c]	HR	95%CI	p-value	q-value[c]
Tumor mutational burden[d]	0.43	0.28 - 0.66	1.10 x 10-4	7.72 x 10-4	0.32	0.19 - 0.50	1.10 x 10-6	7.73 x 10-6
CGB7 expression[e]	1.44	1.09 - 1.89	9.05 x 10-3	0.04	1.48	1.05 - 2.11	0.026	0.093
ECOG Performance Status[f]:								
0 (reference)	-	-	-	-	-	-	-	-
1	2.1	1.58 - 2.79	2.95 x 10-7	4.14 x 10-6	2.62	1.85 - 3.71	6.07 x 10-8	8.50 x 10-7
2	1.97	1.04 - 3.73	0.036	0.13	3.32	1.53 - 7.17	2.30 x 10-3	0.011
Received platinum:								
No (reference)	-	-	-	-	-	-	-	-
Yes	1.41	1.01 - 1.98	0.047	0.13	1.54	1.03 - 2.30	0.037	0.1
Tumor cell PD-L1[g]:								
< 1% (reference)	-	-	-	-	-	-	-	-
≥ 1% but < 50%	1.12	0.66 - 1.90	0.66	0.99	1.14	0.64 - 2.02	0.65	0.83
≥ 50%	1	0.70 - 1.44	0.99	0.99	0.77	0.49 - 1.23	0.27	0.54
Intravesical BCG administered:								
No (reference)	-	-	-	-	-	-	-	-
Yes	0.98	0.73 - 1.32	0.89	0.99	0.92	0.63 - 1.33	0.65	0.83
Tobacco use history:								
Never (reference)	-	-	-	-	-	-	-	-
Previous	0.9	0.68 - 1.19	0.45	0.78	1.01	0.72 - 1.42	0.95	0.95
Current	1.02	0.65 - 1.61	0.92	0.99	1.09	0.63 - 1.90	0.75	0.87
Stage:								
I (reference)	-	-	-	-	-	-	-	-
II	0.96	0.69 - 1.35	0.83	0.99	1.25	0.80 - 1.95	0.33	0.57
III	1.23	0.86 - 1.75	0.25	0.51	1.4	0.90 - 2.19	0.14	0.32
IV	0.98	0.68 - 1.42	0.92	0.99	0.89	0.54 - 1.46	0.65	0.83
Sex:								
Male (reference)	-	-	-	-	-	-	-	-
Female	1.23	0.91 - 1.66	0.18	0.42	1.05	0.72 - 1.53	0.81	0.87

[a]Log-rank test: p-value = 1.05 x 10-7

[b]Akaike Information Criterion =1736.51; Bayesian Information Criterion = 1780.66; Harrell's Concordance Index = 0.67

[c]Benjamini-Hochberg FDR correction

[d]$\log_{10}$(number of missense mutations)

[e]$\log_{10}$[CGB7 expression (TPM)]

[f]Eastern Oncology Cooperative Group Performance Status

[g]Fraction of tumor cells with positive PD-L1 staining

2.8 Discussion

We identify CGB genes as biomarkers of immune evasion in cancer and as prognostic factors for response to immune checkpoint inhibition. We find that all CGB genes are extensively expressed across cancer types, with *CGB7* being most frequently expressed. We confirm that CGB genes are expressed and the resultant proteins secreted from urothelial carcinoma cells *in vitro*. In a cohort of advanced urothelial carcinoma patients, *CGB7* expression is associated with reduced CD8+ T cell infiltration. *CGB7* and bulk expression of *CGB3*, *CGB5,* and *CGB8* are associated with reduced response to anti-PD-L1 checkpoint immunotherapy by RECIST criteria. We subsequently identify that tumors expressing *CGB7, CGB3,* or *CGB5* are significantly associated with decreased survival probability via Kaplan-Meier survival analyses, and this association is upheld with correction for TMB and sex via Cox Proportional Hazards modeling. As *CGB7* expression is most frequently observed in urothelial carcinoma and is associated with markers of immune evasion, we focused on investigating the predictive value of *CGB7* and ultimately demonstrate the prognostic value of *CGB7* as a marker of poor prognosis in urothelial carcinoma in the context of immune checkpoint inhibition using Random Survival Forest modeling. In fact, *CGB7* is the second most important variable in survival predictions, behind TMB, early in cancer progression. Taken together, our data suggest that *CGB7* may facilitate the conversion of the tumor microenvironment to an immunosuppressive state.

One limitation of this study is the lack of functional characterization of CGB proteins in cancer, as functional immunology efforts are made challenging by the primate-specific nature of

CGB genes and lack of murine orthologs. These functional studies, however, will be necessary to establish the immunosuppressive mechanism of action of CGB7. Our findings here demonstrate that, with careful experimental design and immune competent models, the study of CGB7 as an immunomodulator is ripe for further functional exploration. The primate-specificity of CGB gene expression further reinforces the value of analyzing high quality patient data, and the value of extending our analyses of *CGB7* to additional patient datasets.

A second limitation is the limited power of our current analyses dissecting isolated phenotypic associations with *CGB7* expression and with bulk summed *CGB3, CGB5,* and *CGB8* expression due to study size. In the analyses that we present here, it is interesting that, while *CGB7* is the only CGB gene associated with markers of immune evasion, multiple CGB genes are associated with ICI resistance and decreased survival. This might reflect a unique mechanism of action of *CGB7*, or perhaps suggest that the potential immunosuppressive functions of CGB genes are only one part of the mechanism underlying their association with poor prognosis. For example, hCG facilitates many pro-decidualization and pro-tumorigenic processes such as invasion, angiogenesis, in addition to immunosuppression. Our preliminary analyses suggest that these associations with *CGB7* are independent of *CGB3, CGB5* and *CGB8. CGB7* and bulk *CGB3, CGB5, and CGB8* are each independently associated with ICI resistance. Additional analyses to tease apart the isolated contributions of each gene will be required, and larger cohorts and study sizes will facilitate this. We hypothesize that, based on our findings in this study, while *CGB7* may uniquely be a marker of immune suppression and has great value as a marker or poor prognosis based on our analyses, that expression of any CGB gene has value as a marker of ICI resistance and worsened survival probability.

As primary and acquired resistance to checkpoint inhibitor immunotherapies remains a significant barrier to long-term remission for the majority of patients, further validation of *CGB7* as a biomarker and characterization of the mechanism by which *CGB7* suppresses the anti-cancer effects of ICIs may help us predict patient response, inform treatment, and perhaps even identify CGB7 as a potential therapeutic target. As CGB proteins are predominantly cancer-specific and readily detectable analytes in urine and plasma as the basis of modern pregnancy tests, this highlights the feasibility of CGB as a cancer biomarker. Further work will be required to validate CGB7 as a pan-cancer biomarker by confirming associations between *CGB7* expression and immunosuppressive signatures in other cancer types, and ultimately by validating this association between *CGB7* expression and ICI response in patient samples.

Ultimately, targeting CGB genes could present a promising approach for combination therapy with immunotherapies such as immune checkpoint inhibitors. As CGB proteins are secreted, there is substantial potential for development of an inhibitory anti-pan-CGB or anti-CGB7 antibody. There is precedent for potential therapeutic value of antibody neutralization of CGB proteins in the form of anti-cancer vaccines (127), and an anti-CGB therapeutic antibody could potentially provide therapeutic value on its own, or to provide specificity to a coupled anti-cancer therapeutic.

2.9 Supplementary Figures

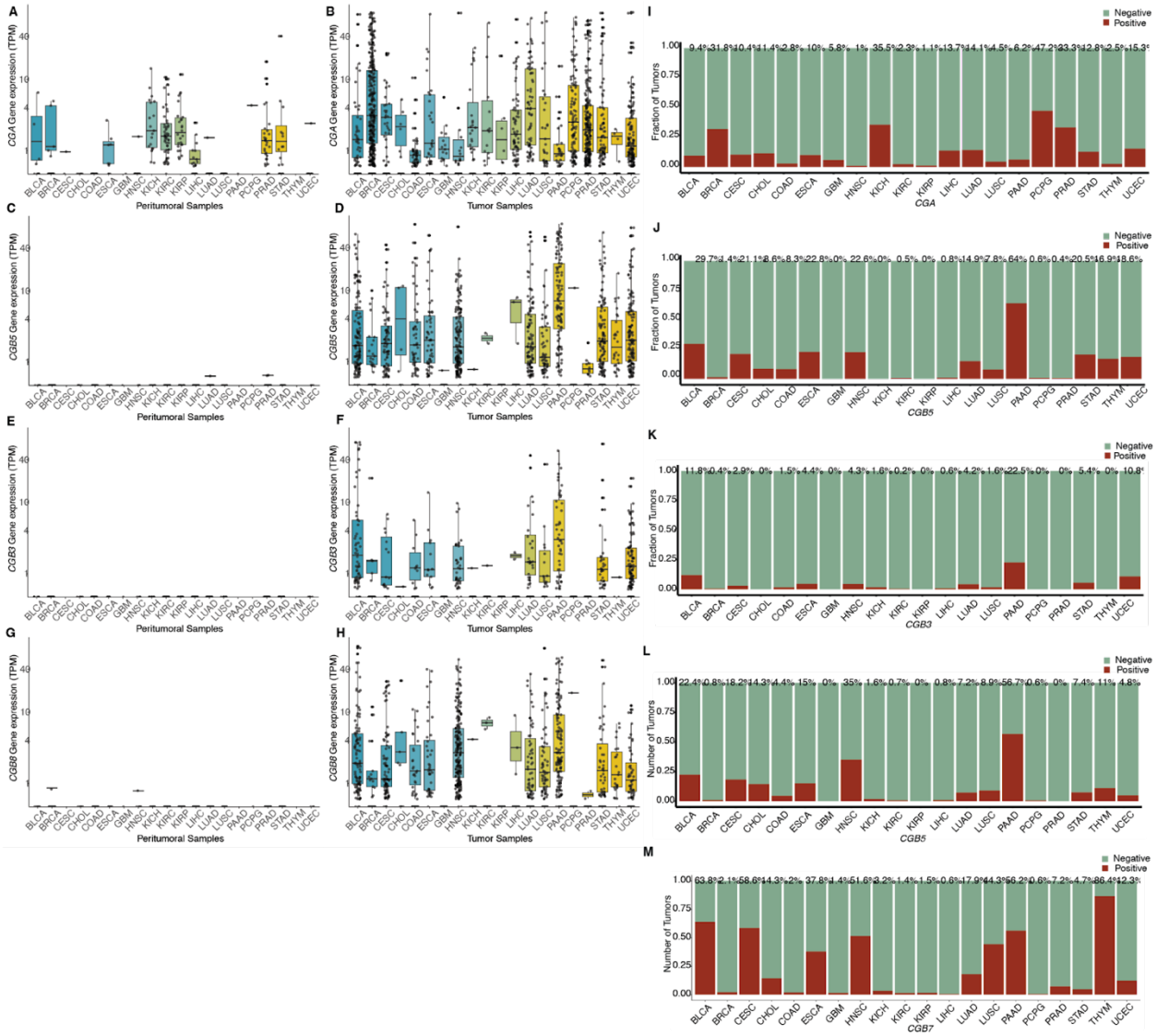

Supplemental Figure S2- 1. CGB is expressed in multiple cancer types. TPM = transcripts per million. CGA mRNA expression in healthy peritumoral tissue samples (**A**) and matched tumor tissue samples (**B**) across 20 cancer types from the TCGA. Cancer type reflects the site of the primary tumor. CGB3 mRNA expression in healthy peritumoral tissue samples (**C**) and matched tumor tissue samples (**D**) across 20 cancer types from the TCGA. Cancer type reflects the site of the primary tumor. CGB5 mRNA expression in healthy peritumoral tissue samples (**E**) and matched tumor tissue samples (**F**) across 20 cancer types from the TCGA. Cancer type reflects the site of the primary tumor. CGB8 mRNA expression in healthy peritumoral tissue samples (**G**) and matched tumor tissue samples (**H**) across 20 cancer types from the TCGA. Cancer type reflects the site of the primary tumor. (**I, J, K, L, M**) Fraction of tumors across 20 cancer types expressing CGA, CGB3, CGB5, CGB8, or CGB7, gene expression with TPM >1, respectively. Percent positive is annotated above each cancer type.

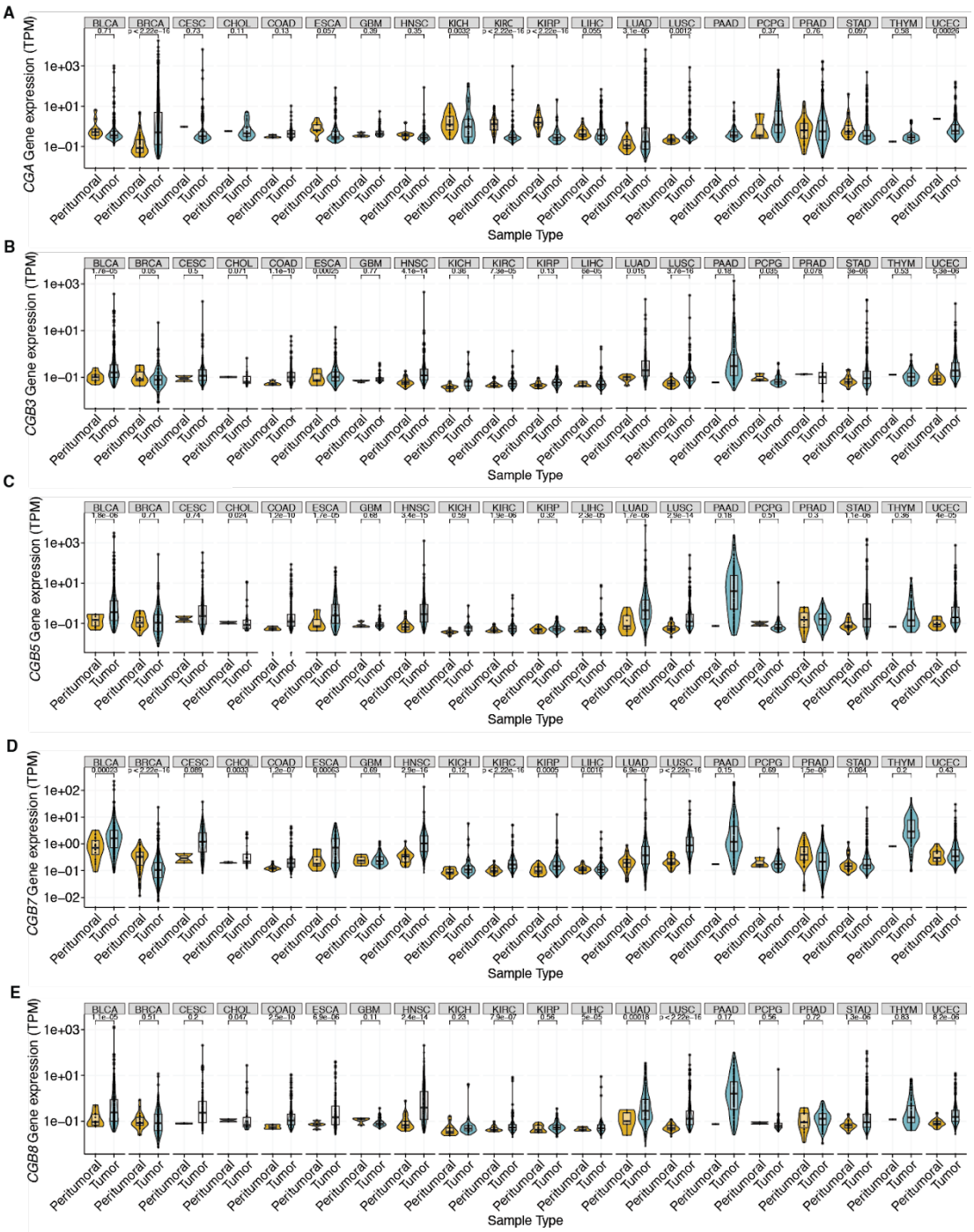

Supplemental Figure S2- 2 Supplemental Figure S2 -2. CGB expression is upregulated across cancer types. Violin plots of CGA (A), CGB3 (B), CGB5 (C), CGB7 (D), or CGB8 (E) expression in tumors and matched healthy peritumoral tissue samples across cancer type datasets from The Cancer Genome Atlas. Expression is in transcripts per million (TPM). P-values determined by wilcox signed rank test.

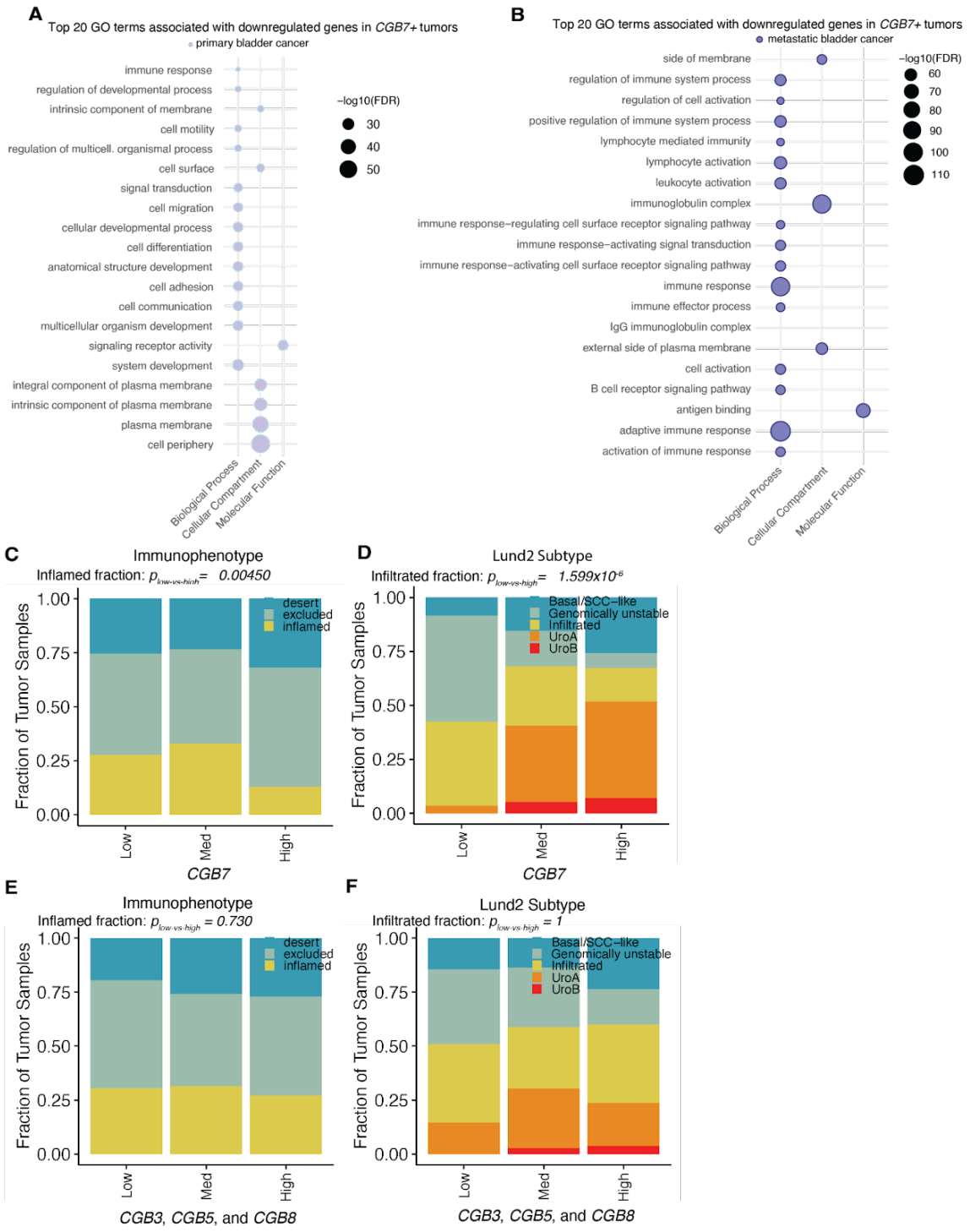

Supplemental Figure S2-3. CGB expression is associated with altered immune infiltrate. Med = medium. (**A**) The top 20 Gene Ontology terms associated with *CGB7* expression in primary urothelial cancers in the TCGA BLCA dataset. (**B**) The top 20 Gene Ontology terms associated with *CGB7* expression in metastatic urothelial cancers in the IMVigor 210 clinical trial dataset (data re-analyzed from Mariathasan et al., 2018). (**C**) Immunophenotype data: immune desert, immune excluded, or inflamed. Tumors with expression of *CGB3*, *CGB5*, or *CGB8* > 1 TPM were removed, and remaining samples stratified by *CGB7* expression. P-values determined by proportions test with continuity correction. Chi-squared = 8.072, p-value = 0.0045. (**D**) Tumor subtype data:

basal/SCC-like, genomically unstable, immune infiltrated, urothelial type A, or urothelial type B. Tumors with expression of *CGB3*, *CGB5*, or *CGB8* > 1 TPM were removed, and remaining samples stratified by *CGB7* expression. P-values determined by proportions test with continuity correction. Chi-squared = 23.025, p-value = 1.60×10^{-6}. (**E**) Immunophenotype data: immune desert, immune excluded, or inflamed. Tumors with expression of *CGB3*, *CGB5*, or *CGB8* > 1 TPM were removed, and remaining samples stratified by *CGB7* expression. P-values determined by proportions test with continuity correction. Chi-squared = 0.119p-value = 0.730. (**F**) Tumor subtype data: basal/SCC-like, genomically unstable, immune infiltrated, urothelial type A, or urothelial type B. Tumors with expression of *CGB7* > 1 TPM were removed, and remaining samples stratified by summed *CGB3*, *CGB5*, and *CGB8* expression. P-values determined by proportions test with continuity correction. Chi-squared = 0, p-value = 1.

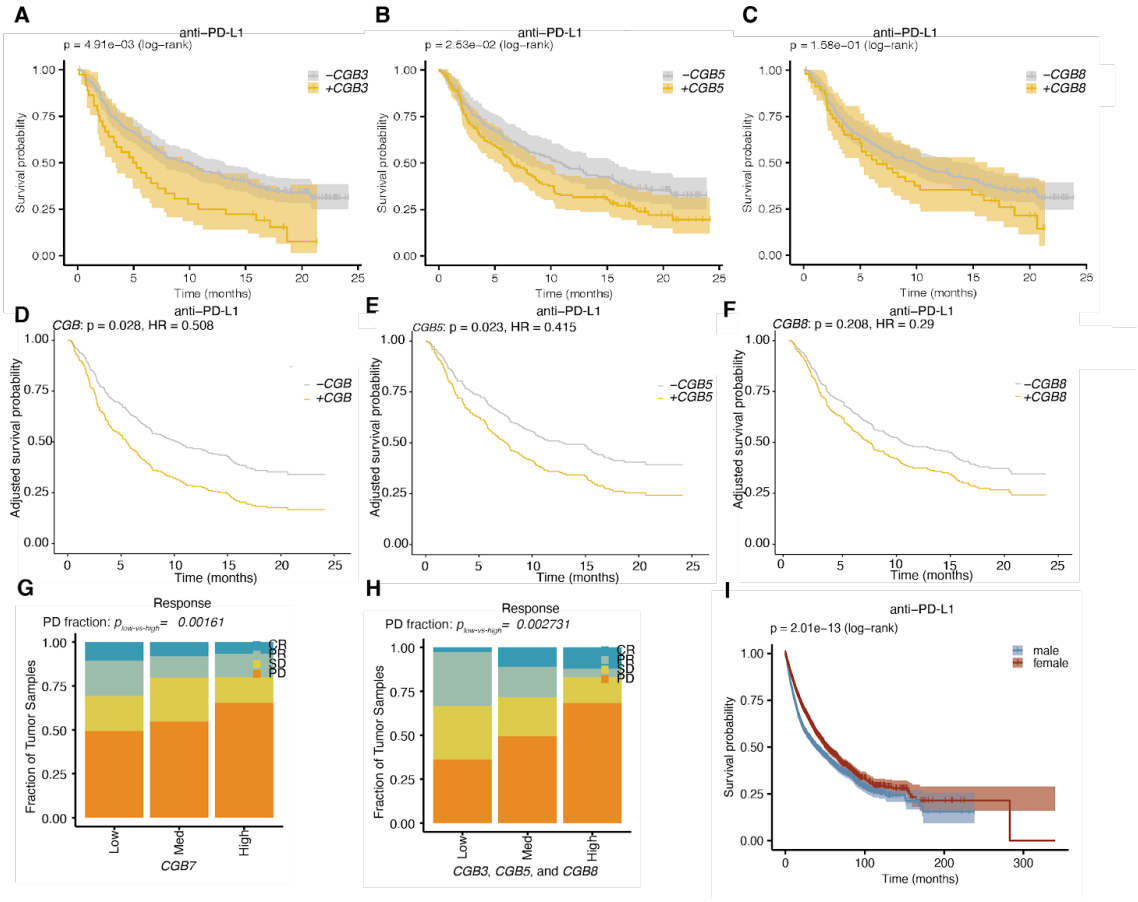

Supplemental Figure S2-4. CGB expression is associated with decreased response to ICI therapy. Response Evaluation Criteria in Solid Tumors (RECIST) scoring: CR = complete response, PR = partial response, SD = stable disease, PD = progressive disease. Med = medium. (**A**) Kaplan Meier overall survival curves comparing patients with *CGB3*+ (gold) and *CGB3*- (gray) advanced urothelial cancer tumors (data re-analyzed from Mariathasan et al., 2018). All patients received Atezolizumab (anti-PD-L1). P-value determined by log rank test. (**B**) As in (**A**), but comparing patients with *CGB5* positive (gold) and negative (gray) tumors. (**C**) As in (**A**), but comparing patients with *CGB8* positive (gold) and negative (gray) tumors. (**D**) Kaplan Meier overall survival curves as shown in (**A**) adjusted for confounding effects of sex and tumor mutational burden covariates by cox proportional hazards modeling. Hazard ratio (HR) and p-value obtained from fitting a cox proportional hazards model. (**E**) Kaplan Meier overall survival curves as shown in (**B**) adjusted as described in (**D**). (**F**) Kaplan Meier overall survival curves as shown in (**C**) adjusted as described in (**D**). (**G**) Response determined by RECIST (Mariathasan 2018). Tumors with expression of *CGB3*, *CGB5*, or *CGB8* > 1 TPM were removed, and remaining samples stratified by *CGB7* expression. P-values determined by proportions test with continuity correction. Chi-squared = 9.954, df = 1, p-value = 0.00161. (**H**) Response determined by RECIST (Mariathasan et al., 2018). Tumors with expression of *CGB7* > 1

TPM were removed, and remaining samples stratified by summed *CGB3*, *CGB5*, and *CGB8* expression. P-values determined by proportions test with continuity correction. Chi-squared = 8.979, df = 1, p-value = 0.00273.
(**I**) Kaplan Meier overall survival curves comparing male (blue) and female (red) patients with advanced urothelial carcinoma tumors. All patients received Atezolizumab (anti-PD-L1). P-value determined by log rank test.

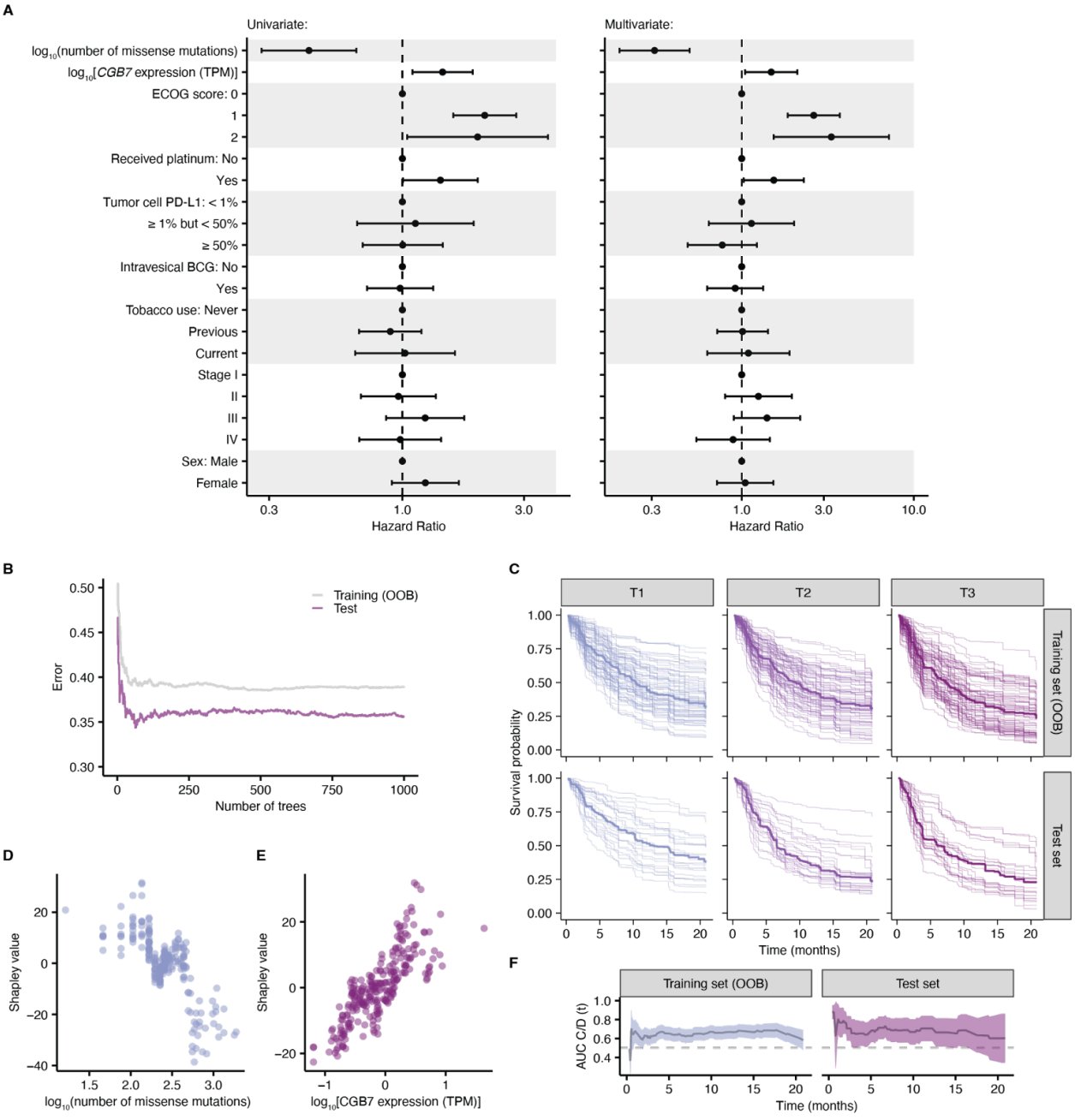

Figure S2-5. Statistical and machine learning models exhibit the negative effects of *CGB7* expression on overall survival. (**A**) Hazard ratios estimated by Cox Proportional Hazards Regression in the univariate (left) and multivariate (right) contexts. Error bars denote the 95% confidence interval of the hazard ratio. (**B**) The training out-of-bag error (OOB error, solid gray line) and the test error (solid purple line) as a function of the number of trees in the Random Survival Forest (RSF) model. Error is defined as 1 − Harrell's concordance index. (**C**) RSF predicted overall survival for individual patients (thin lines) stratified into terciles, by *CGB7* expression. OOB survival predictions are shown for the patients in the training set. The median survival function across the cohort is shown

(thick line). (**D**) Shapley dependence plot correlating tumor mutational burden (TMB, number of missense mutations) and RSF mortality. Each patient is represented by a single point. (**E**) As in (**D**), but showing *CGB7* expression. (**F**) Time-dependent receiver operating characteristic (ROC) analyses. The cumulative/dynamic area under the ROC curve ($AUC^{C/D}$) (solid line) and associated 95% confidence interval (transparent ribbon) are calculated for the training and test sets. The training set $AUC^{C/D}$ was calculated using the RSF OOB mortality predictions.

2.10 Materials and Methods

Cell lines

All cell lines utilized are human urothelial cancer cell lines cultured at 37°C and 5% CO2. SCaBER, T24, TCCSUP, J82, UM-UC-3, cell lines were purchased from ATCC (ATCC, Manassas, VA). RT-112 and KU-19-19 cell lines were purchased from DSMZ (DSMZ, Braunschweig, Germany). UM-UC-1 cell line was purchased from Sigma-Aldrich (St. Louis, MO). SCaBER, RT-112, UM-UC-1, UM-UC-3, TCCSUP and J82 cells were cultured in Eagle's Minimum Essential Medium (ATCC) supplemented with 10% FBS (Gibco, Waltham, MA) and 1% Pen Strep (Gibco). T24 cells were cultured in McCoy's 5A medium supplemented with 10% FBS and 1% Pen Strep. KU-19-19 cells were cultured in RPMI 1640 (Gibco) medium supplemented with 10% FBS and 1% Pen Strep.

CGB knockdown experiments

siRNA pools targeted all CGB genes (Horizon Discovery, Cambridge, Cambridgeshire, UK) or were a non-targeting control pool (Horizon Discovery). siRNAs transfected into cells of approximately 70% confluence with Lipofectamine™ RNAiMAX Transfection Reagent (Thermo Fisher Scientific, Waltham, MA) per the manufacturer's instructions.

ELISA

Conditioned medium: conditioned medium was collected from each indicated cell line after 72 hours of subculture in the medium described above. Bulk beta-hCG protein levels were measured and quantified using a Human CG beta (HCG beta) DuoSet ELISA kit (R&D Systems, Minneapolis, MN) DuoSet ELISA Ancillary Reagent Kit 2 (R&D Systems) according to the manufacturer's instructions. Media was diluted 1:10 from all cell lines with the exception of KU-19-19, which was diluted 1:100 prior to assay input due to high CGB protein levels. Cells were counted at collection to approximate concentration of CGB per 10,000 cells. Experiments were run in biological and technical triplicate. Raw O.D. values of standards were fit to a 4PL curve using MyAssays software.

qRT-PCR

Total RNA was extracted using a Qiagen RNeasy plus mini kit according to the manufacturer's instructions (Qiagen, Hilden, Germany). RNA was reverse transcribed to cDNA using a Verso cDNA synthesis kit (Thermo Scientific). *CGB7* transcripts detected with Applied Biosystems TaqMan Fast Advanced Master Mix (Fisher Scientific), *CGB7*-specific Taqman Probe (Thermo Scientific), *CGB3*/*CGB5*/*CGB8*-specific Taqman Probe (Thermo Scientific), and GAPDH Taqman Probe (Thermo Scientific). Experiments were run in biological and technical triplicate. Experiments were run on a ABI QuantStudio 5 Real-Time PCR System (Thermo Fisher Scientific). Data was analyzed using the ΔΔCt method.

RNA sequencing analysis, genome annotations and differential gene expression

RNA-sequencing data was analyzed as previously described (106). RNA-seq reads were mapped to an annotated transcriptome created using Ensembl 71 (116), UCSC knownGene (117), and

MISO v2.0 (118) annotations for the hg19/GRCh37 assembly using RSEM version 1.2.4 (119) modified to call Bowtie v1.0.0 with option '-v 2' (121). Unaligned reads were then mapped to the hg19/GRCh37 genome assembly using TopHat version 20.8b (121). Gene expression values in TPM (transcripts per million) were normalized via the trimmed mean of M values (TMM) method (122). For TCGA studies, we analyzed all available samples across 20 distinct cancer types that included at least one matched non-tumor tissue sample. Differential gene expression to compare positive and negative samples for expression of CGB genes in both the TCGA datasets and the dataset from the IMvigor210 clinical trial cohort (94, 42) was calculated via Mann-Whitney U Test and using several thresholds: the absolute value of log-fold-change threshold of 1.5 or greater, a maximum p-value of 0.05, a minimum bayes factor of 100, and maximum FDR of 0.01. We defined positive expression of CGB genes as TPM >1 and negative expression as TPM < 0.25 unless otherwise noted.

Clinical variable analyses

Clinical variables were reported for patients enrolled in the IMVigor210 clinical trial (94, 42). Patient response to Atezolizumab was scored according to the Response Evaluation Criteria for Solid Tumors (RECIST) (42). Tumor subtype was determined according to Lund 2 taxonomy for bladder cancer classification (94). Immunophenotype was determined based on the level and pattern of CD8+ T cell infiltration by CD8a IHC staining (94). For each analysis, patients were first stratified by expression of each CGB gene, or by summed expression of multiple CGBs where indicated. NAs were filtered out for each response, immunophenotype, and subtype analysis individually after CGB gene stratification. We determined the proportions of each RECIST score, immunophenotype, and subtype in CGB-high (>75%) and CGB-low/negative

(<25%) tumors, and quantified the difference in proportions via 1-sample proportions test with continuity correction.

Survival analyses

Survival analyses were performed with the Kaplan–Meier estimator and statistical tests were performed with a logrank test (R package survival) (123). Samples were stratified by expression of individual genes, where positive expression was defined as exhibiting TPM >1, and negative expression was defined as exhibiting TPM <0.25. Adjusted survival probabilities were calculated by fitting a Cox Proportional Hazards model to adjust for the covariates sex and tumor mutational burden.

Random Survival Forest and Feature Importance computation

The Random Survival Forest Model, Shapley value estimation, and partial dependence analyses was implemented as previously described (106). In brief, we randomly assigned patients into training (70%) and test (30%) datasets. We determined optimal hyperparameters via a grid search. That is, we evaluated 10,608 RSF models representing various values and combinations of the RSF hyperparameters: number of trees, minimum terminal node size, number of randomly selected splitting variables, handling of missing data, splitting rule, and bootstrapping method. The model which minimized both the OOB training and the test errors (defined as 1 − concordance index) was selected: ntree = 1000, nodesize = 6, mtry = 3, na.action = "na.impute", splitrule = "logrank", and samptype = "swr". We set the hyperparameter nsplit = 0 to evaluate all possible split points. The predictions associated with the test cohort were handled using na.action = "na.omit" which excluded patients with missing data. Shapley values were

calculated using the fastshap package (124). We used 1000 Monte Carlo repetitions and set the parameter adjust = TRUE to correct the estimated Shapley values such that local accuracy was satisfied. Shapley values associated with mortality and per time point overall survival predictions from the RSF model were used to quantify overall feature importance and time-dependent importance, respectively. The marginal effect of CGB7 expression on survival probability was assessed using partial dependence, implemented using the partial() function from the randomForestSRC package. Visualizations were created in the R programming environment using the dplyr (125), ggplot2 (126), pammtools (127), and plotly (128) packages.

Measuring survival model predictive accuracy

We evaluated the RSF model's accuracy over time using time-dependent ROC curve analyses. For each timepoint, we calculated the cumulative/dynamic area under the ROC curve ($AUC^{C/D}$) and 95% confidence interval using the timeROC package, which additionally corrects for bias due to right-censoring (129). The training (OOB) or the test predictions for mortality were used as input.

Chapter 3 Major vault protein is a critical regulator of tumor-immune interactions

Please note that this chapter reflects work in progress. I greatly appreciate the collaboration of Tracy Yang and Dominik Otto in the lab of Manu Setty for their work processing the single cell RNA-seq data that was generated by me, and applying their novel methodology to quantify abundance in single cell data to our dataset (Kompot). They contributed several of the plots shown in Figure 3-3, supplemental Figure S3-3, and Supplemental Figure S3-4. We collaborated to devise a plan for analysis and annotated cell types with consultation from Dr. Susan De Wolf and Dr. Erik Kimble. Andrea Belleville worked with the preclinical modeling facility to develop the MVP-/- mouse model utilized in this chapter. We worked collaboratively to conduct some of the work described in this chapter, including several allograft cohorts and optimization of efficient CRISPR/Cas9 genome editing of *Mvp* in B16-OVA cells.

3.1 Abstract

The major vault protein (MVP) is the main component of the vault complex, an organelle found ubiquitously in cells and involved in immune regulation in the numerous contexts, including host-pathogen interactions and metabolic disease. While numerous studies have demonstrated roles of MVP in immune modulation, MVP has not yet been studied as a regulator of anti-tumor immunity. We identify that *Mvp* expression is associated with adaptive immune response across multiple cohorts of advanced melanoma patients. We demonstrate that *Mvp* expression in both the host and in the tumor each separately promote survival, and notably tumor-intrinsic expression of *Mvp* exerts this survival effect in an immune-dependent manner, by utilizing a series of *in vivo* allograft experiments. Single cell RNA-sequencing reveals that MVP

knockout (KO) tumors exhibit higher abundance of exhausted CD8+ T cells compared with control tumors. Finally, we demonstrate that *Mvp* expression is associated with increased overall survival probability and decreased incidence of progressive disease in cohorts of patients treated with immune checkpoint inhibitors, suggesting that therapeutically augmenting *Mvp* expression may be a strategy to enhance response to checkpoint immunotherapy.

3.2 Introduction

Since its discovery in 1986, the vault complex organelle has been shrouded in mystery. The striking hollow barrel-like structure of the vault is composed primarily of the major vault protein (MVP), which accounts for > 70% of the complex, along with two additional associated proteins, Telomerase-associated protein 1 (TEP1) and vault ADP-ribose polymerase (VPARP), and varying numbers of short untranslated vtRNAs; three in humans (131-133). MVP, however, is sufficient for vault assembly, with minor changes noted in vault structure (134,136). Though the vault has been linked to and implicated in many biological processes, the core function of the vault, however, remains a mystery.

Consistent with varied and diverse functions, vaults are found and *Mvp* is expressed ubiquitously across almost all cell types. *Mvp* can be upregulated in epithelium, in professional antigen presenting cells such as differentiated macrophages and dendritic cells, and in some cancer cells including lung, colon, thyroid, and melanoma, supporting a functional role of MVP in barrier epithelium, antigen presenting immune cells, and cancer (137-143) .

MVP was first discovered as the lung resistance-related protein (LRP), and was initially studied as a multidrug and chemoresistance protein (144,146). In addition to being implicated in multidrug resistance in cancer, MVP has demonstrated critical function in numerous cellular

processes across a range of biological contexts. MVP has been shown to function as a potential scaffold for signaling pathway transduction (136), facilitate the formation and function of lipid raft microdomains in the plasma membrane (146-147), facilitate nucleocytoplasmic transport (148-149), in exocytosis (150), in cell survival (151), in dendritic cell maturation (138,139), in macrophage polarity (152,153), inflammatory signaling in disease and normal biology (136, 154, 159), and in host-protective anti-pathogen immune responses (138, 146,148,154). MVP is recognized as an interferon gamma stimulated gene in cancer that may additionally regulate interferon response and induction by regulating STAT1- and STAT3- directed transcription (158, 154, 137). As Vaults are highly evolutionarily conserved, this suggests a critical function of vaults in host response to infection, disease, and general stress (157). Thus, the described roles of MVP are broad, and the involvement of MVP in inflammatory signaling is particularly extensive.

Development of the first MVP-/- mouse enabled further study of several of these functions and elucidated a role of MVP on host-pathogen interactions. Intriguingly, no function of MVP in drug resistance or as a regulator of dendritic cell maturation was identified under the conditions tested (155,156) In fact, MVP-/- mice appear to display no distinct phenotype unless challenged by disease or infection, as in the case of host-pathogen interactions. Here, MVP aids in maximizing P. aeruginosa internalization and clearance via translocation to and stabilization of lipid rafts (146). In influenza A infection, MVP is also host protective, and is shown to enhance expression of inflammatory cytokines by facilitating AP-1 nuclear translocation in multiple cell types, including host macrophages and lung epithelium (148). In both of these infectious contexts, P. aeruginosa and Influenza A, MVP-/- mice clear significantly less

pathogens than WT counterparts, and ultimately succumb faster to infection than WT mice (146, 148). These data solidify a clear involvement of MVP in anti-pathogen immune responses.

From these data, we wondered whether MVP may be involved in host-protective anti-tumor immunity by regulating inflammatory signaling either in host cells, such as dendritic cells and macrophages, or in tumor cells. There is some evidence that MVP could protect against immunoediting, and thus immune escape, by attenuating apoptotic signaling (147). Consistent with a potential role of MVP in inflammation are suggestions of a positive association between MVP expression and immune cell infiltration gene expression signatures in cancer (141,160). Should MVP augment anti-tumor immune responses, MVP may additionally have farther-reaching implications for response to checkpoint immunotherapy.

Here we examine a previously unexplored role of MVP in anti-cancer immunity. We identify that elevated *Mvp* expression is associated with upregulated adaptive immune response across four cohorts of patients with cutaneous melanoma. This elevated *Mvp* expression is associated with increased CYT score, a measure of cytolytic activity, in all four cohorts. We generate a novel MVP-/- murine model and validate that, as in infectious contexts, host *Mvp* expression increases survival probability in a syngeneic melanoma allograft model. We additionally identify that *Mvp* expression in the tumor similarly increases survival probability in an immune-dependent manner. *Mvp* expressing tumors exhibit decreased abundance of exhausted CD8+ T cells. Finally, we determine that *Mvp* expression is associated with increased survival probability and decreased incidence of progressive disease in multiple cohorts of patients treated with immune checkpoint inhibitors. Taken together, our findings suggest that augmenting *Mvp* expression may ultimately improve immunotherapy response in cancer.

3.3 *MVP* expression is associated with inflammation and cytotoxic T cell activity in patient cohorts

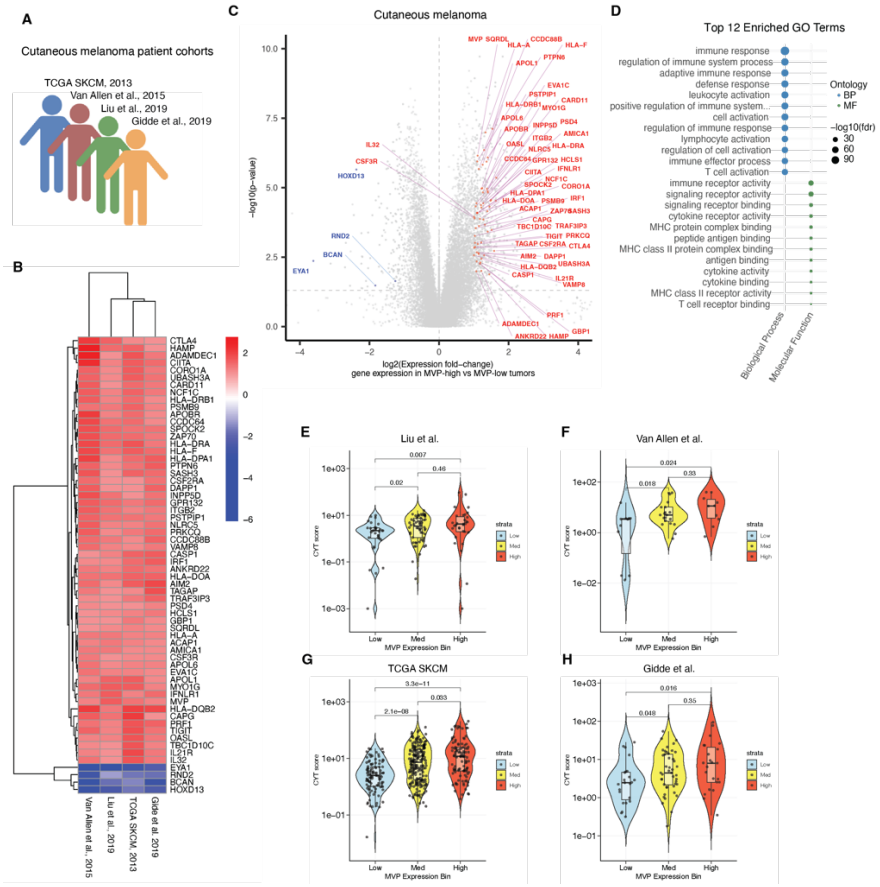

Figure 3-1. *MVP* expression is associated with increased inflammatory response in patient cohorts *MVP* -high tumors: *MVP* expression > 66th percentile, *MVP* -med tumors: >33rd percentile and <66th percentile, *MVP* -low tumors: *MVP* expression < 33th percentile. (A) Selection of 4 melanoma patient cohort datasets for analysis. (B) Heatmap of log fold change of differentially expressed genes that overlap across all four cohorts. (C) Gene expression comparison in *MVP* -high vs *MVP* -low tumors. Labeled genes correspond to overlapping differentially expressed genes across all four cohorts. Differentially expressed genes: log fold change > 1 and p-value <0.05. Upregulated genes in red, downregulated in blue. (D) The top 12 biological process and molecular function gene ontology terms enriched in genes upregulated in *MVP MVP* -high tumors in a representative dataset: Liu et al., 2019. (E-H) CYT score for tumors with low, medium, or high *MVP* expression.

As MVP is an established regulator of immune response in inflammatory diseases and in host response to viral and bacterial infections, we sought to determine whether *Mvp* expression is associated with immune activity in tumors. We selected four cutaneous melanoma patient

cohorts, all of which had RNA-sequencing data available from pretreatment biopsies: Van Allen et al., Liu et al., Gide et al., and the TCGA SKCM datasets (163-165) **(Figure 3-1A)**.

We compared gene expression profiles in *MVP* -high (>66th percentile) vs *MVP*-low tumors (<33rd percentile) in each dataset, enabling us to survey unbiased gene expression changes associated with *MVP* expression. Upregulated genes that overlap between all four datasets is extensive and includes numerous HLA proteins, other genes involved in antigen processing by HLA class II proteins such as *CD74* and *CTSS*, and checkpoints that are upregulated with T cell activation such as *TIGIT* and *CTLA-4* **(Figure 3-1B, 3-1C)**. Here we utilized a threshold of log fold change > 1. In each dataset, Gene Ontology analysis of differentially expressed genes revealed remarkably similar expression profiles based on the top 12 enriched molecular functions and biological processes **(Figure 3-1D, S3-1A - S3-1C)**. Genes upregulated (log fold change > 1.5 and $p < 0.05$) in *MVP*-high tumors compared with *MVP* -low tumors in each dataset are involved in antigen display, immune receptor activity, leukocyte or T cell activation, suggesting an association between *MVP* expression and adaptive immunity **(Figure S3-1D – S3-1F)**. This led us to hypothesize that *MVP* expression may be associated with CD8+ T cell activity. Indeed, *MVP* -high tumors exhibit a significantly higher CYT score, a metric to quantify cytotoxic activity of CD8+ cytotoxic T cells, in all four cohorts **(Figure 3-1E - 3-1H)**. We conclude that *MVP* is associated with inflammation, and specifically adaptive immune response, and CD8+ T cell activity in multiple patient cohorts.

3.4 Tumoral MVP expression and host MVP expression individually increase survival probability *in vivo*

MVP is an established interferon-stimulated gene (ISG) (158). This leads to the question of whether *MVP* expression is merely a consequence of anti-tumor immune activation, such as

retained sensitivity to interferon gamma signaling, or whether MVP is an active driver of anti-tumor immunity. Furthermore, an additional question remained: if indeed MVP is a driver of anti-tumor immunity, does expression in the tumor, or in the host drive this phenotype? *MVP* is expressed across cell types, and has been previously studied in the context of dendritic cell maturation and macrophage polarization. Our prior re-analyses of bulk RNA-seq data do not provide information at a cell-type or compartment resolution. To investigate these questions, we designed two parallel *in vivo* survival studies using an immune competent syngeneic B16-F10 and C57BL/6 murine tumor allograft model.

To investigate the effect of host *Mvp* expression on survival, we developed a novel MVP-/- mouse model. For our syngeneic studies, we elected to engineer an updated model by targeting *Mvp* with CRISPR/Cas9 gene editing technology in a C57BL/6 background. We targeted exon 4 of *Mvp* with paired guides that were injected along with purified Cas9 into one-cell C57BL/6 embryos. Generation of indels at this locus was identified for each F0 mouse by PCR with primers flanking a region of exon 4 **(Figure S3-2A)**. Heterozygous MVP+/- F1 mice were obtained by backcrossing to C57BL/6 mice, and MVP-/-, MVP-/+, and MVP+/+ mice were obtained from heterozygous intercrosses. MVP protein in liver lysate appeared completely depleted in MVP-/- mice, partially depleted in MVP-/+ as expected, and intact in MVP+/+ mice by western blot **(Figure S3-2B)**. MVP-/- mice were ultimately backcrossed four generations.

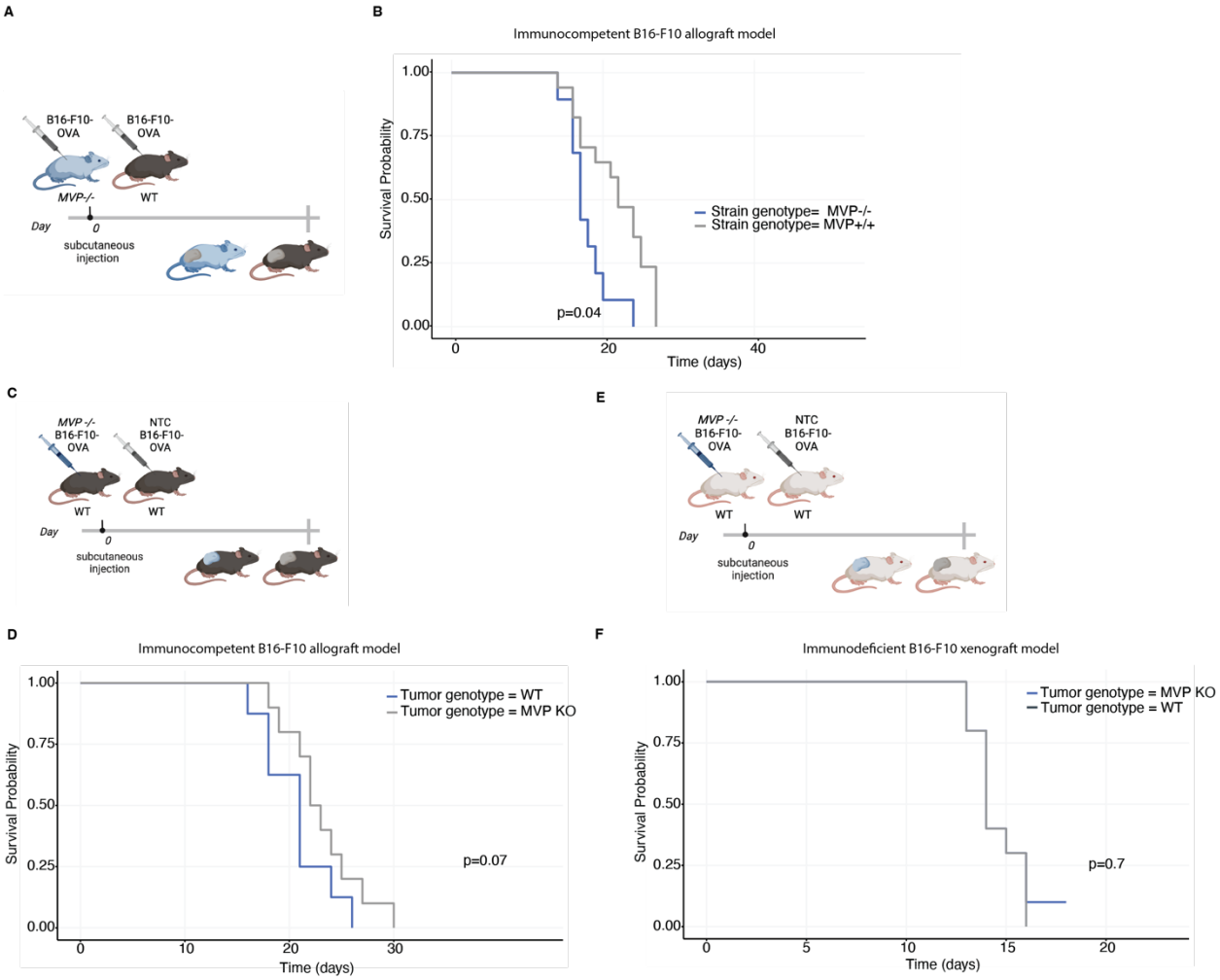

Figure 3-2: Host MVP and tumoral MVP individually increase survival probability in vivo (A) Design of host MVP knockout allograft experiment. (B) Kaplan-Meier survival curves for each strain. Significance determined by log-rank test. (C) Design of tumor MVP knockout allograft experiment. (D) Kaplan-Meier survival curves for each tumor genotype. Significance determined by log-rank test. (E) Design of tumor MVP knockout xenograft experiment. (F) Kaplan-Meier survival curves for each tumor genotype. Significance determined by log-rank test.

We had previously engineered polyclonal MVP knockout and control (NTC) cells with CRISPR/Cas9 and MVP-targeting or non-targeting control guide RNAs. Because B16-F10 cells have rapid doubling time and are extremely aggressive, it is challenging to detect and quantify increases in growth and aggressiveness. To increase the immunogenicity of these cells, we overexpressed transgenic chicken ovalbumin in each cell line. Depletion of MVP protein in the MVP KO line and expression of OVA in both cell lines were validated by western blot **(Figure S3-2C)**. We engrafted the NTC cell line into the flanks of age- and sex-matched MVP-/- and WT

C57BL/6 mice and sacrificed animals once tumor burden met standard endpoint criteria as defined by IACUC **(Figure 3-2A)**. MVP-/- mice had a significantly decreased survival probability compared with WT C57BL/6 mice (log rank test, p=0.04) **(Figure 3-2B)**. While we detected no significant difference in tumor volumes prior to initiation of the survival study, there is an observable impact of host MVP on tumor growth **(Figure S3-2D,E)**. Though this finding is in a single model, this result suggests for the first time that host MVP expression impacts survival probability in cancer.

As MVP is also expressed, and sometimes upregulated, in some tumor cells (137), we next wondered whether tumoral MVP expression may similarly impact survival. To test this, we performed a similar survival study, this time knocking out MVP expression in the tumor. We engrafted the MVP KO and NTC cell lines expressing transgenic Ova into the flanks of age and sex-matched C57BL/6 mice and performed a survival study as described **(Figure 3-2C)**. Mice bearing MVP KO tumors exhibited decreased survival probability (log rank test, p=0.07) **(Figure 3-2D)**. Though this survival phenotype does not reach significance, this is an exciting finding due to the challenging nature of identifying a growth-enhancing phenotype in the B16-F10 tumor model.

While this result was intriguing, we next sought to confirm that the pro-survival phenotype observed in mice bearing *Mvp* -expressing tumors was immune-dependent. Here we performed the same survival study with the same two MVP knockout and MVP expressing cell lines in a xenograft model with the immunodeficient strain of NSG mice **(Figure 3-2E)**. We observed no significant difference in survival probability, suggesting that this effect on survival is immune-dependent (p=0.7) **(Figure 3-2F)**. Again, though we detected no significant difference in volumes of MVP KO vs WT (NTC) tumors prior to initiation of the survival study,

there is an observable difference in the growth of MVP KO tumors in an immunocompetent model than in our immunodeficient model **(Figure S3-2F, Figure S3-2I)**. These results suggest that tumoral MVP expression influences survival in an immune-dependent manner.

We conclude that in our studies in murine melanoma, knocking out MVP in both the tumor and in the host results in decreased survival probability, suggesting multiple potential anti-tumor MVP-driven mechanisms across distinct cell types. Repeating these studies in additional models and perhaps with increased cohort sizes would be critical to generalize and solidify these findings. As our discovery that tumoral *Mvp* expression leads to greater survival probability was a more surprising finding, we next sought to explore the function of tumoral MVP at a molecular and cellular level with our syngeneic B16-F10 murine allograft model.

3.5 MVP KO tumors display increased abundance of exhausted CD8+ T cells *in vivo*

Here we utilized single cell RNA-sequencing (scRNA-seq) to profile cellular changes associated with tumoral *Mvp* expression. To investigate this, we performed a limited-size fixed-endpoint study with our syngeneic tumor MVP KO model to enable direct comparisons between tumors of both genotypes at the same stage. We collected tumor tissue from n=10 tumors and processed samples for scRNA-seq library generation using the 10X Genomics Flex protocol. We prepared tumor tissue samples and generated libraries with 5 MVP KO tumor samples and 5 NTC tumor samples.

We obtained a minimum of 4,200 cells with a mitochondrial fraction < 0.8, molecule count between the 3rd and 98th percentiles, and with expression of > 50 genes **(Figure S3-3A)**. Nineteen clusters were identified by Leiden clustering with standard parameters that organized into four compartments encompassing tumor, lymphoid, myeloid, and fibroblast **(Figure 3-3A)**.

We annotated clusters based on gene expression profiles consistent with previous scRNA-seq studies. Cells from each sample can be found in each cluster (**Figure S3-3B**). Samples from mice of both genotypes clustered together, highlighting our ability to isolate similar cell populations in tumors of both genotypes **(Figure 3-3B)**.

To determine which compartments changed most with *Mvp* expression, we quantified the abundance of each cell type per genotype with a methodology based on Mellon, a continuous density function to compare densities across genotypes in single cell data (161). This method provides statistical measures of differential abundance at single-cell resolution (citation to come). We visualized this abundance distribution across clusters on the full dataset UMAP and identified significantly altered abundance between genotypes in the lymphoid compartment, as well as in the myeloid compartment and fibroblast compartment **(Figure 3-3C)**. As we hypothesized that *Mvp* may impact CD8+ T cell infiltration or cytolytic activity based on our prior analysis of patient cohorts, we sought to focus on the lymphoid compartment.

We re-clustered the lymphoid compartment to increase the resolution of lymphoid cell types identified, and again, cells from both genotypes could be found in each region of the UMAP **(Figure 3-3D)** though here it was noticeable that some samples clustered more similarly across the UMAP than did others **(Figure S3-3C).** We annotated these clusters based on consistency of gene expression profile with established cell type annotations. Higher-resolution clustering revealed NK cells, NK T cells, conventional CD4+ T cells, T regulatory cells, naïve or central memory T cells, intermediate CD8+ T cells, and two clusters of effector CD8+ T cells **(Figure 3-3E)**. We identified two clusters of effector CD8+ T cells expressing multiple inhibitory receptors, which is a hallmark of T cell exhaustion **(Figure 3-3F, Figure S3-4A).** The first cluster of cytotoxic CD8+ T cells expresses moderate levels of cytotoxic and exhaustion

markers: *Gzmb*^{mid}, *Prf1*^{mid}, *Pdcd1*^{mid}, *Lag-3*^{mid}, *Havcr2*^{mid}, *Ifng*^{mid}. Thes second cluster of effector CD8+ T cells exhibited high levels of cytotoxic markers, interferon gamma, and exhaustion markers, including the addition of *Tox*: *Gzmb*^{hi}, *Prf1*^{hi}, *Pdcd1*^{hi}, Lag-3^{hi}, *Havcr2*^{hi}, *Tox*, *Ifng*^{hi}. Despite expressing high levels of multiple exhaustion markers, these cells also express higher levels of *Mki67*, suggesting that these cells are proliferating despite appearing fated for the exhaustion pathway.

We performed differential abundance analysis within the lymphoid compartment and observed enrichment of two subtypes of exhausted cytotoxic CD8+ T cells in MVP KO tumors: Gzmb^{mid}, *Prf1*^{mid}, *Pdcd1*^{mid}, *Lag3*^{mid}, *Havcr2*^{mid}, *Ifng*^{lo} cells and *Gzmb*^{hi}, Prf1^{hi}, *Pdcd1*^{hi}, *Lag3*^{hi}, *Havcr2*^{hi}, Tox, *Ifng*^{mid} **(Figure 3-3G).** T cell exhaustion encompasses a spectrum of functional and dysfunctional states. Indeed, subsets of exhausted cells with high exhaustion markers that paradoxically retain high expression of granzymes and interferon gamma are observed in myeloma and in a previous report of the syngeneic B16-F10 tumor model (166-168). In myeloma, these cells retain some tumor-killing ability despite being their exhausted phenotype (166,167). In B16-F10 melanoma, these cells are similarly characterized as a terminally exhausted population with superior cytotoxicity, but ultimately reduced long-term survival, suggesting that these cells in our dataset may have limited functional capacity that would need to be confirmed functionally (168).

We next validated that this increased abundance of highly cytotoxic terminally exhausted cells was not due to increased CD8+ T cell infiltration into MVP KO tumors. To investigate whether this difference in abundance of exhausted CD8+ T cells reflected an overall difference in CD8+ T cell infiltration, or increased incidence of exhaustion, we analyzed overall CD8+ T cell infiltration by fluorescent IHC in the same tumors we assayed by single cell RNA-seq, as

well as in three additional tumors harvested from the same cohort (n=13). We identified that while there was no significant difference in CD8+ infiltration between MVP KO and WT tumors, there was a trend toward increased infiltration in NTC tumors, all together suggesting that the increased abundance of exhausted cells in MVP KO tumors was not a reflection of increased overall CD8+ infiltration **(Figure 3-3H).** We conclude that MVP KO tumors exhibit increased abundance of cytotoxic CD8+ T cells that appear to be fated for the exhaustion pathway.

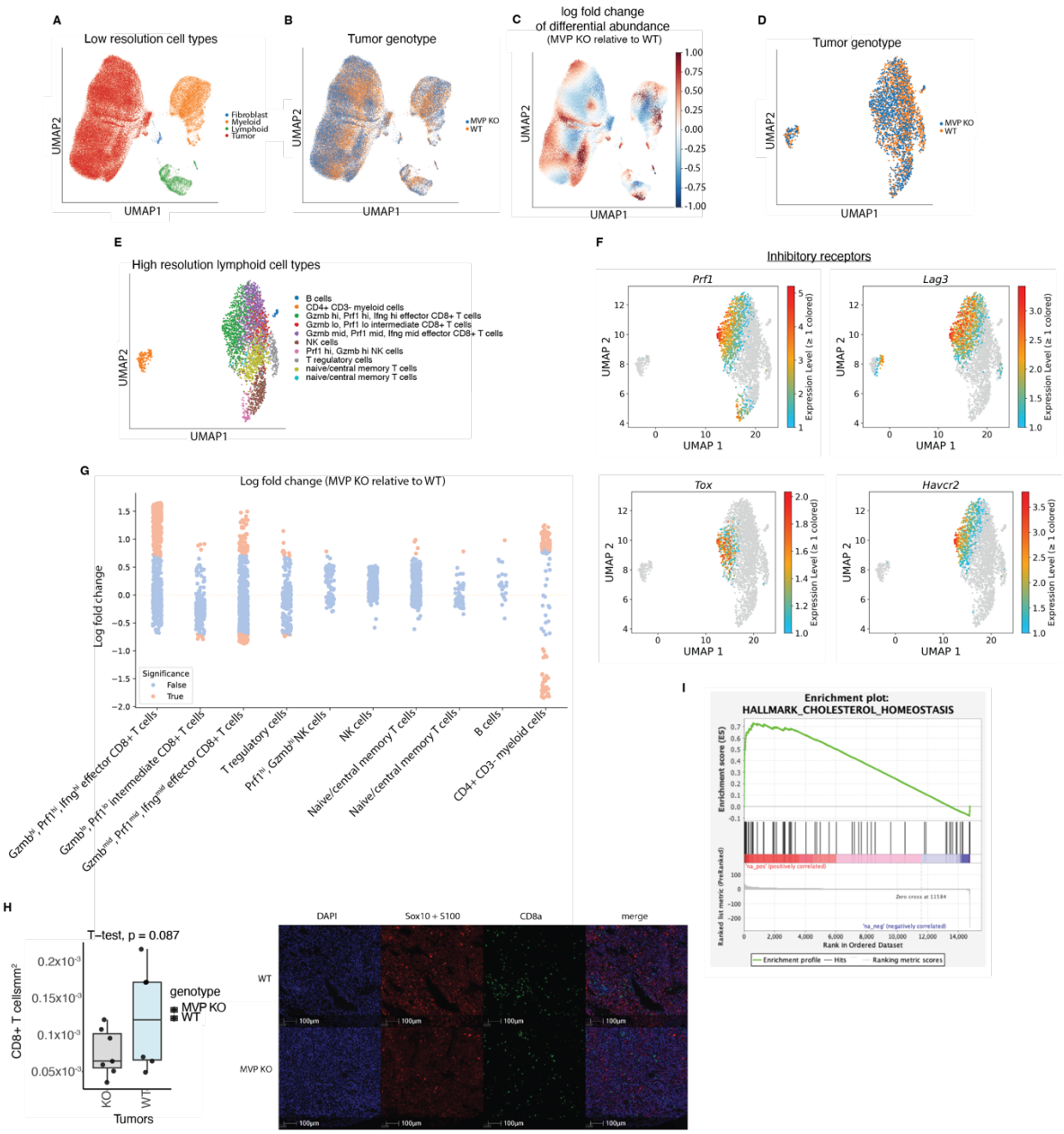

Figure 3-3: MVP KO tumors display increased abundance of exhausted CD8+ T cells *in vivo*. (A) UMAP visualization colored by low resolution leiden clustering of all ten scRNA-seq samples. (B) UMAP visualization colored by genotype of each scRNA-seq sample. (C) UMAP visualization of leiden clusters as described above. Color reflects differential abundance between tumor genotypes. Red = increased abundance in MVP KO tumors, blue = increased abundance in WT (non-targeting control; NTC) tumors. (D) UMAP visualization of re-clustered lymphoid cell types colored by genotype of each scRNA-seq sample. (E) UMAP visualization of re-clustered lymphoid cell types colored by higher resolution lymphoid cell type. (F) Feature plots showing expression patterns of inhibitory receptors in lymphoid cells. (G) Differential abundance per higher-resolution lymphoid cluster in MVP KO vs WT (NTC) tumors. Positive log fold change indicates increased abundance in MVP KO tumors, while negative log fold change indicates increased abundance in MVP WT tumors. Cells with absolute value of log fold change > 0.75 reach significance. (H) Quantification and representative images of CD8a+ immune cell infiltration per tumor area, determined by CD8a IHC staining. n=6-7 samples per genotype (MVP KO, WT) (I) Gene set enrichment analysis of differentially expressed genes reveals enrichment of genes involved in cholesterol

homeostasis. Normalized Enrichment Score (NES) 1.29, FDR q-value 0.035. Data subset by cell cycle phase; representative plot shown.

How tumoral *Mvp* expression influences tumor-immune interactions remains a question. To explore the effect of intratumoral *Mvp* expression on gene expression in the tumor, we isolated the entire tumor cell compartment of each sample, which accounts for the majority of cells in the dataset. Number of molecules per cell was identified to be a source of variation in the gene expression data and variation in molecule counts was adjusted for **(Figure 3-3A)**. We also observed that cell cycle phase was a substantial source of variability **(Figure S3-4B)**.

We first computed differential gene expression in the tumor compartment, comparing expression in MVP KO tumors to expression in WT tumors as reference and observed modest gene expression changes in MVP KO tumors as determined by Mahalanobis distance and weighted log fold change **(Figure S3-4C)**. Mahalanobis distance is a quantification of distance between expression of each gene and average gene expression across samples, ultimately incorporating correlation between expression of genes in the dataset. The observation of modest gene expression changes between genotypes, which was expected due to the intrinsic heterogeneity of MVP expression in these tumors.

Re-clustering the tumor cell compartment revealed that the cell cycle was a major source of variation in the gene expression data, so we computed differential gene expression per phase of the cell cycle **(Figure S3-4D - S3-4F).** Given the subtlety of shifts in gene expression between tumor genotypes, we defined significantly upregulated genes (Mahalanobis distance > 50, weighted log fold change > 1) and significantly downregulated genes (Mahalanobis distance > 50 and a weighted log fold change < 1). Notably more genes are upregulated in MVP KO tumors than are downregulated.

We performed Gene Set Enrichment Analysis (GSEA) and were surprised to find that genes upregulated in MVP KO tumors were significantly enriched for genes involved in cholesterol homeostasis (FDR q-value 0.035) **(Figure 3-3I).** Differentially expressed genes between WT and MVP KO tumors that are involved in cholesterol homeostasis are similar in each phase of the cell cycle **(Figure S4-3D-F)**. MVP has been linked to lipid and cholesterol metabolism previously in the context of an atherosclerosis model. Here Ben et al. identified that MVP-/- mice bear higher plasma levels of fatty acids, triglycerides, and total cholesterol than WT mice on a high fat diet (139). Ben et al. ultimately demonstrates that MVP macrophage expression is protective against atherosclerosis. With a precedent for MVP regulation of cholesterol in a disease context in a distinct MVP-/- murine model, MVP regulation of cholesterol in melanoma could be an interesting model of MVP-driven tumorigenesis and modulation of the tumor microenvironment.

3.6 MVP expression is associated with response to immune checkpoint inhibition in clinical human cancer

Given our observation that MVP KO tumors are associated with increased CD8+ T cell exhaustion, we hypothesized that MVP expression may have implications for response to checkpoint immunotherapy. Returning to the large-scale melanoma patient cohorts we analyzed previously, we selected the three patient cohorts treated with immune checkpoint inhibitors: anti-PD-1 (166), anti-PD-1 or combination anti-PD-1/anti-CTLA-4 (167), and anti-CTLA-4 (168). Higher MVP expression, as hypothesized, is significantly associated with increased survival probably in two of these three cohorts **(Figure 3-4A, 3-4B)**. In the third cohort, some patients were treated with anti-PD-1 monotherapy, and others were treated with anti-PD-1 and anti-

CTLA-4 combination therapy. As patients treated with combination therapy exhibited much higher response rates overall, and for consistency with our prior analyses, we selected patients treated with monotherapy for analysis.

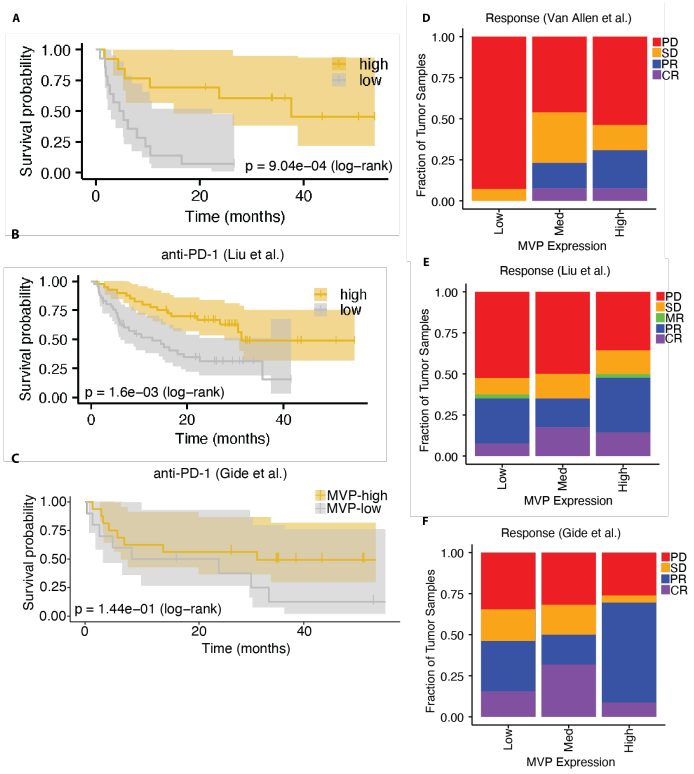

Figure 3-4: *MVP* expression is associated with response to immune checkpoint inhibition *MVP* -high tumors: *MVP* expression > 66th percentile; *MVP* -low tumors: *MVP* expression < 33rd percentile. RECIST: CR = complete response, PR = partial response, MR = mixed response, SD = stable disease, PD = progressive disease. (A-C) Kaplan Meier survival curves comparing *MVP* -high and *MVP* -low tumors across Van Allen et al. 2015, Liu et al., 2019, and Gide et al., 2019 patient cohorts, respectively. (D-F) Response determined by RECIST criteria (data re-analyzed from Van Allen et al. 2015, Liu et al., 2019, and Gide et al., 2019, respectively).

Here we observed a trend toward increased survival probability in patients with *MVP* -high tumors **(Figure 3-4C).** This may be influenced by the smaller sample size present in this cohort. We stratified each cohort into terciles by *MVP* expression, computed Kaplan Meier survival curves comparing *MVP* -low tumors (< 33 percentile) and MVP-high tumors (>66 percentile), and determined significance by log-rank test (Van Allen et al., p= 9.04E-04; Liu et al., p=1.6E-3; Gide et al., p=1.4E-1). Even when survival probabilities are adjusted for the

contributions of common covariates such as TMB and sex using Cox proportional hazards modeling, the adjusted survival probabilities are highly similar **(Figure S5-4A – S5-4C)**.

Patients in the three melanoma cohorts treated with immune checkpoint inhibitors (Liu et al., Van Allen et al., and Gide et al.) were evaluated for response with the Response Evaluation Criteria in Solid Tumors (RECIST) in solid tumors. To test the effect of *MVP* expression on response to immune checkpoint blockade therapeutics, we again compared *MVP* -high and *MVP* -low tumors, this time comparing the proportion of tumors scored as complete response (CR), partial response (PR), mixed response (MR), stable disease (SD), or progressive disease (PD). In the cohort described in Liu et al., we observe decreased incidence of progressive disease ($p=0.040$) in patients with *MVP*-high tumors (**Figure 3-4D)**. We observe no significant difference in incidence of PD between *MVP* -high and *MVP* -low tumors, however there is significantly increased incidence of stable disease in *MVP* -low tumors ($p=0.0012$) and increased incidence of PR ($p=0.003$) in *MVP* -high tumors in the cohort described by Gide et al. **(Figure 3-4E)**. In the cohort described by Van Allen et al., patients with *MVP* -high tumors exhibit decreased incidence of progressive disease ($p=0.0078$) **(Figure 3-4F).**

Taken together, we conclude that high *MVP* expression is associated with increased survival probability and improved response to checkpoint immunotherapy in multiple melanoma patient cohorts. We further describe associations between high *MVP* expression in the tumor, dendritic cells, and macrophages and ICB response in an additional cancer type; renal cell carcinoma.

3.7 Discussion

For the diversity and breadth of cellular and molecular functions linked to *MVP* expression, a function of MVP in anti-tumor immunity has not yet been elucidated. Here we

make progress toward characterizing a novel role of MVP in anti-tumor immunity. We identify that *MVP* expression is associated with adaptive immune response across multiple melanoma patient cohorts. We find that immune-related gene expression changes associated with *MVP* are consistent across all four cohorts of patients surveyed. As this analysis is associative, and does not differentiate *MVP* expression from the tumor vs from the host, we designed a series of *in vivo* tumor allograft and xenograft experiments with an immunocompetent host MVP knockout model, an immunocompetent tumor MVP knockout model, and an immunodeficient tumor MVP knockout model. For the first time, we suggest that MVP in both the host and in the tumor each separately impact survival, and this tumoral-expression driven effect on survival is immune-dependent. We identify that MVP KO tumors exhibit higher abundance of exhausted CD8+ T cells compared with control tumors by scRNA-seq profiling. MVP KO tumors upregulate genes involved in multiple signaling pathways as well as cholesterol homeostasis. Finally, we demonstrate that high *Mvp* expression is associated with significantly increased survival probability in multiple melanoma patient cohorts, as well as decreased incidence of progressive disease.

Though functional studies would be essential to demonstrate this, we hypothesize that this protection against exhaustion may underlie the positive effects of MVP expression on overall survival and response to immune checkpoint blockade, as CD8+ T cell exhaustion is an established barrier to immune control of tumors and checkpoint immunotherapy response.

Our studies, however, do not explain how tumoral *Mvp* expression influences tumor-immune interactions. *Mvp* may influence immune cells in the tumor microenvironment by regulating genes involved in cholesterol homeostasis. Accumulation of cholesterol within the plasma membrane of cells enhances the formation of lipid rafts, which are plasma membrane

domains rich in cholesterol that are critical for transduction of many different signaling pathways. Of note, MVP is important for lipid raft formation in response to P. aeruginosa infection (149). It is possible that the effects of lipid raft stabilization are amplified in an immune checkpoint inhibitor treatment context. Upregulated LDLR expression in tumor cells, which we observe in MVP KO tumors, can lead not only to the accumulation of cholesterol in tumor cells, but also the accumulation of cholesterol in the tumor microenvironment and thus contribute to CD8+ T cell dysfunction (171, 172).

There are several limitations to this study. First is the use of a single cohort per *in vivo* experiment. Second is our use of a single tumor model to test our hypotheses *in vivo*. Extending these experiments to an additional tumor model would inform whether these results are generalizable across cancer types. Third, while our study lays the foundation for future investigation of MVP as a regulator of anti-tumor immunity, further mechanistic validation is required to confirm the effects on infiltrating cytotoxic CD8+ T cell function as well as validate the effect of *Mvp* expression on the tumor.

As a positive regulator of anti-tumor immunity and potential protector from CD8+ T cell exhaustion, MVP expression may have potential as a previously unrecognized therapeutic target to augment response to checkpoint immunotherapies. Augmenting MVP expression in tumors in combination with checkpoint immunotherapy may protect against terminal and irreversible CD8+ T cell exhaustion to enable sustained checkpoint immunotherapy response.

3.8 Supplemental Figures

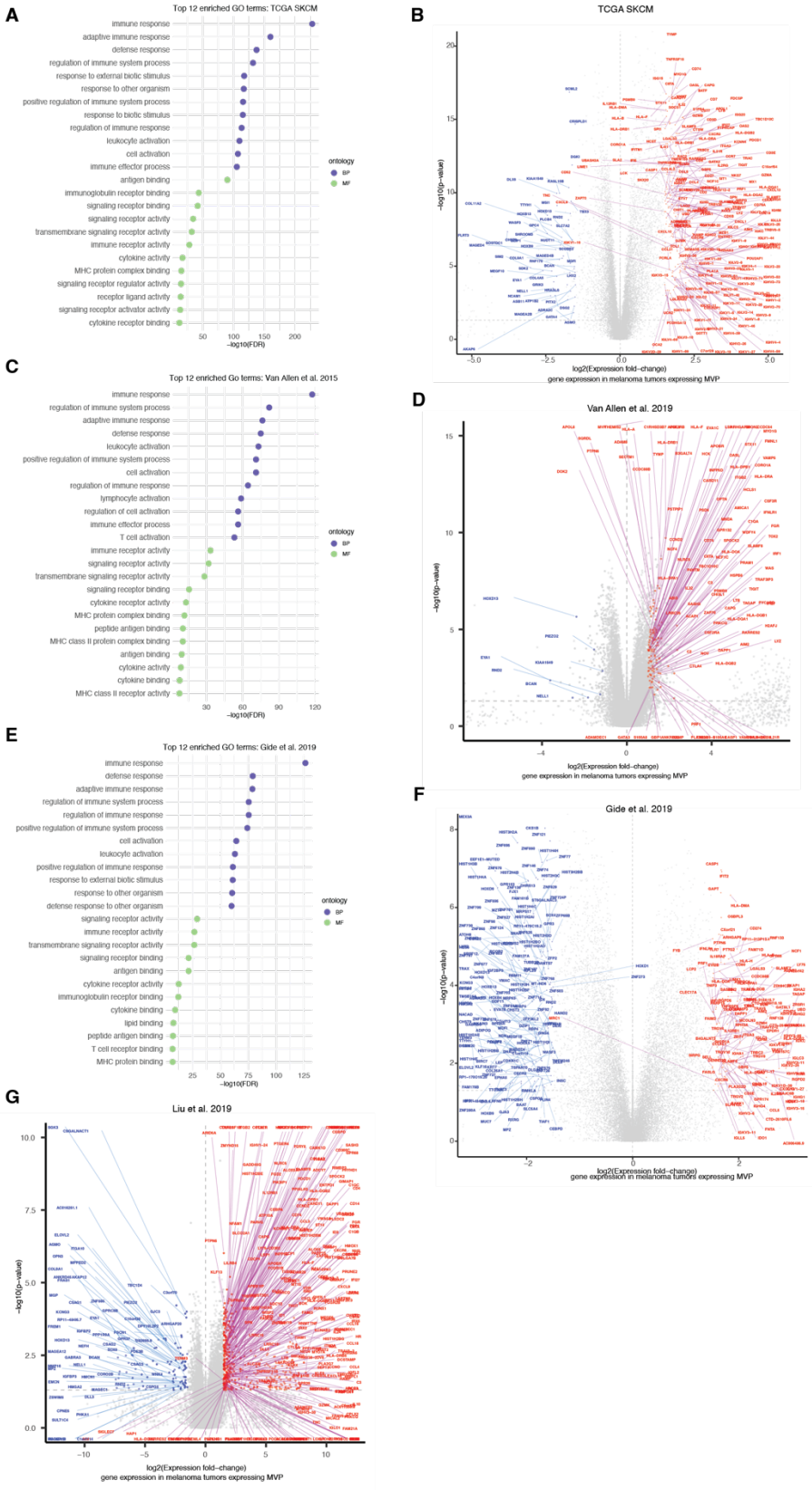

Supplemental figure S3-1: *MVP* expression is associated with increased inflammatory response in patient cohorts *MVP* -high tumors: *MVP* expression > 66th percentile, *MVP* -med tumors: >33rd percentile and <66th percentile, *MVP* -low tumors: *MVP* expression < 33th percentile. (A) The top 12 biological process and molecular function gene ontology terms enriched in genes upregulated in MVP-high tumors in the TCGA SKCM dataset (C) As in A, but in the Van Allen et al., 2015 dataset (E) As in A, but in the Gide et al., 2019 dataset (B,D,F,G) Gene expression comparison in *MVP* -high vs *MVP* -low tumors. Labeled genes correspond to overlapping differentially expressed genes across all four cohorts. Differentially expressed genes: log fold change > 1.5 and p-value <0.05. Upregulated genes in red, downregulated in blue. Volcano plots of differentially expressed genes in each dataset: TCGA SKCM; Van Allen et al., 2015; Gide et al., 2019; Liu et al., 2019

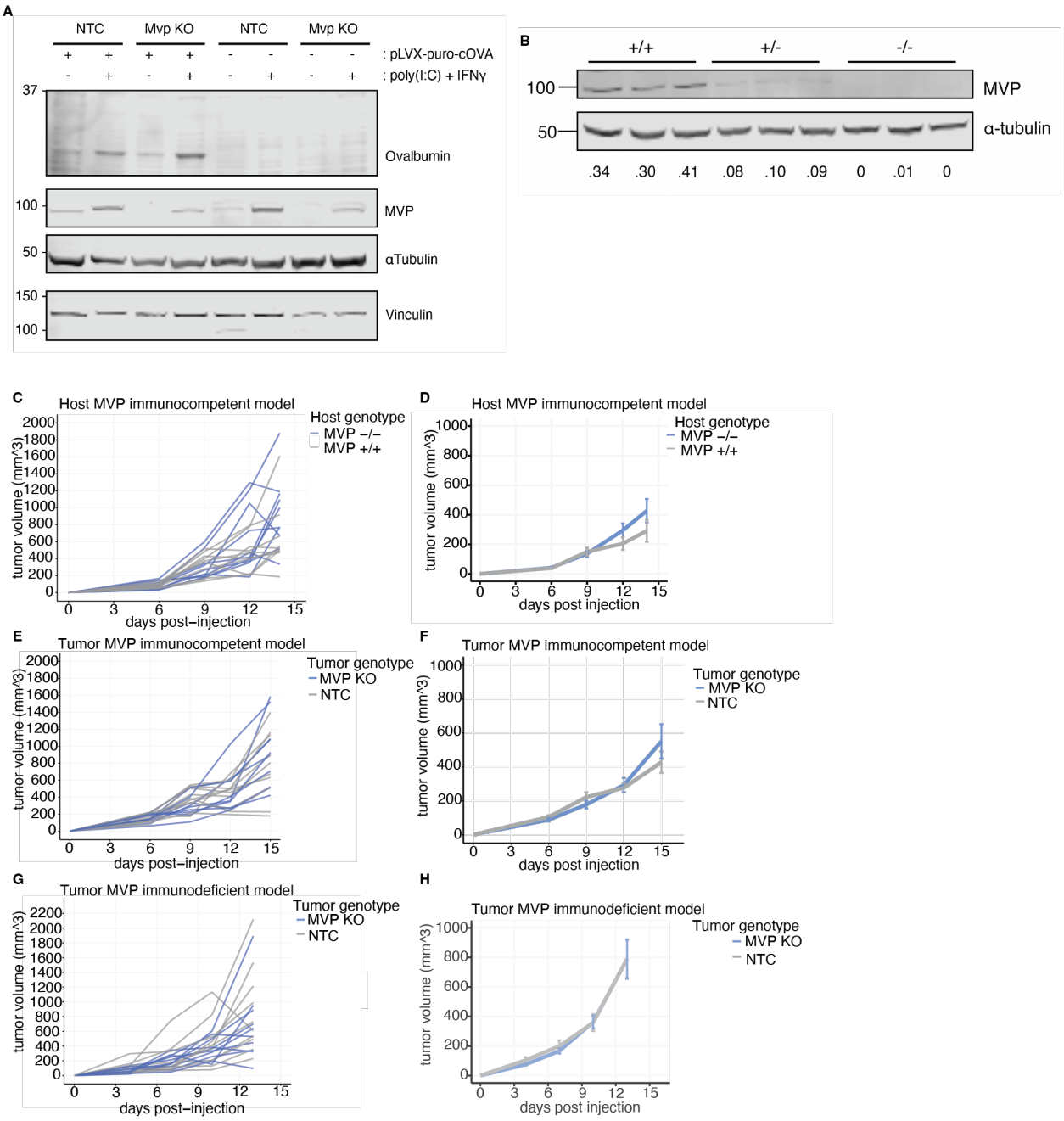

Supplemental figure S3-2: Tumoral MVP expression and host MVP expression uniquely increase survival probability *in vivo*. (A) Depletion of MVP protein is observed in liver lysate from an MVP-/- founder mouse. MVP signal is reduced in a MVP+/- littermate. (B) Validation of depletion of MVP protein in MVP KO B16-F10 cells and OVA expression in MVP KO and NTC B16-OVA cells. (C) Total tumor burden per animal; host MVP KO allograft model. n=10 mice per condition. (D) Mean volume of tumors per genotype; host MVP KO allograft model. n=20 tumors per condition. (E) Total tumor burden per animal; tumor MVP KO allograft model. n=10 mice per condition. (F) Mean volume of tumors per genotype; tumor MVP KO allograft model. n=20 tumors per condition. (G) Total tumor burden per animal; tumor MVP KO xenograft model. n=9-10 mice per condition. (H) Mean volume of tumors per genotype; tumor MVP KO xenograft model. n=19-20 tumors per condition.

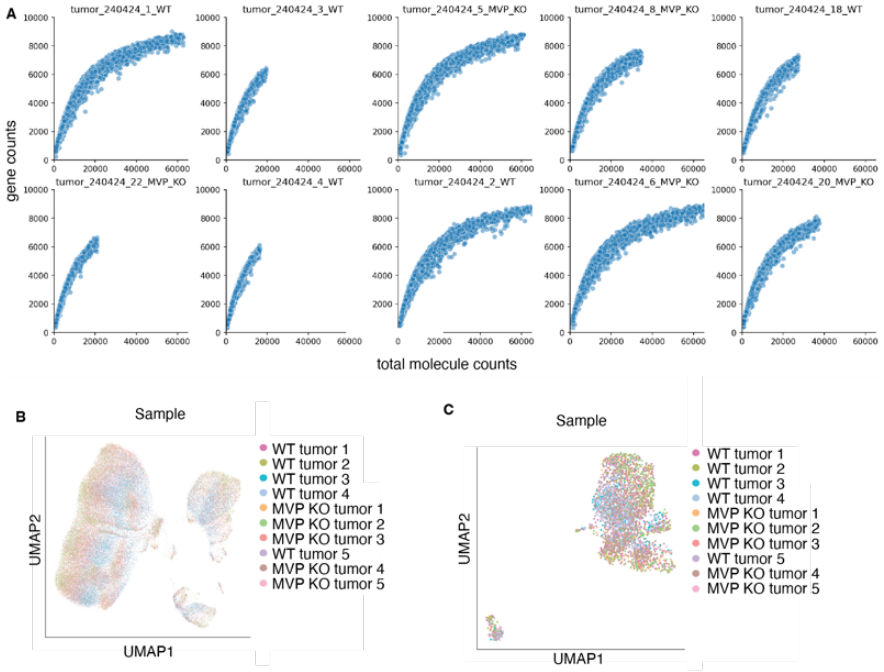

Supplemental Figure S3-3: Sample-level validation of single cell RNA-sequencing data. (A) Molecule counts vs gene counts per sample (B) UMAP visualization of all cells colored by each sample. (C) UMAP visualization of lymphoid cells colored by each sample.

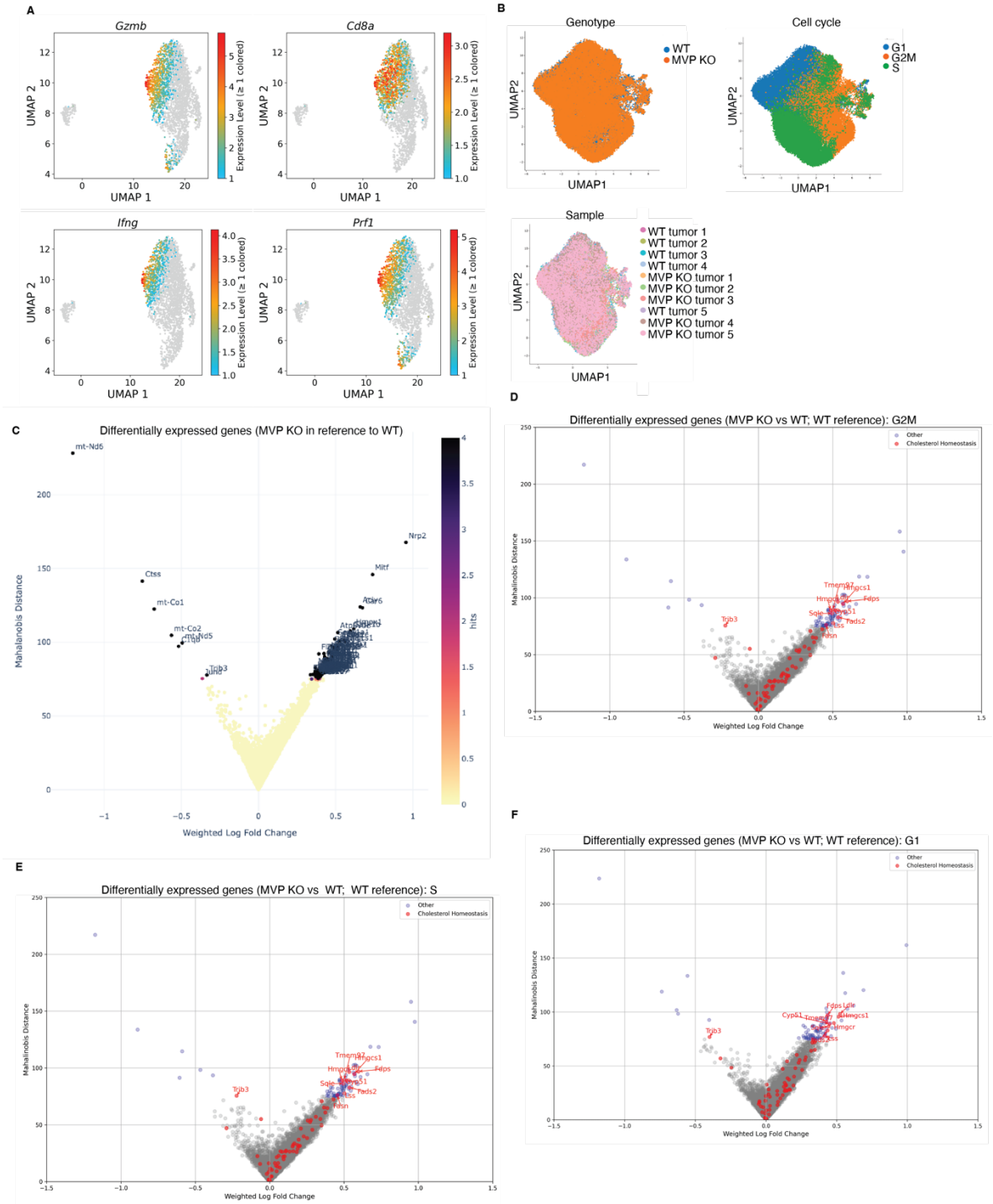

Supplemental Figure S3-4: MVP KO tumors display increased abundance of exhausted CD8+ T cells *in vivo*. (A) Expression of markers of effector CD8 T cells visualized on UMAP of lymphoid cells. (B) UMAP visualization of tumor cells colored by genotype, cell cycle phase, or sample. (C) Differentially expressed genes between WT and MVP KO tumors determined by Mahalanobis distance and log fold change > 0.75. The top 50 differentially expressed genes are labeled. Reference: WT. (D-F) Differentially expressed genes between WT and MVP KO tumors determined by Mahalanobis distance corresponding to cells in G2M, S, and G1 phases of the cell cycle respectively. Points colored in red are involved in cholesterol homeostasis. Labeled points in red are significantly differentially expressed. Points in blue are other significantly differentially expressed genes.

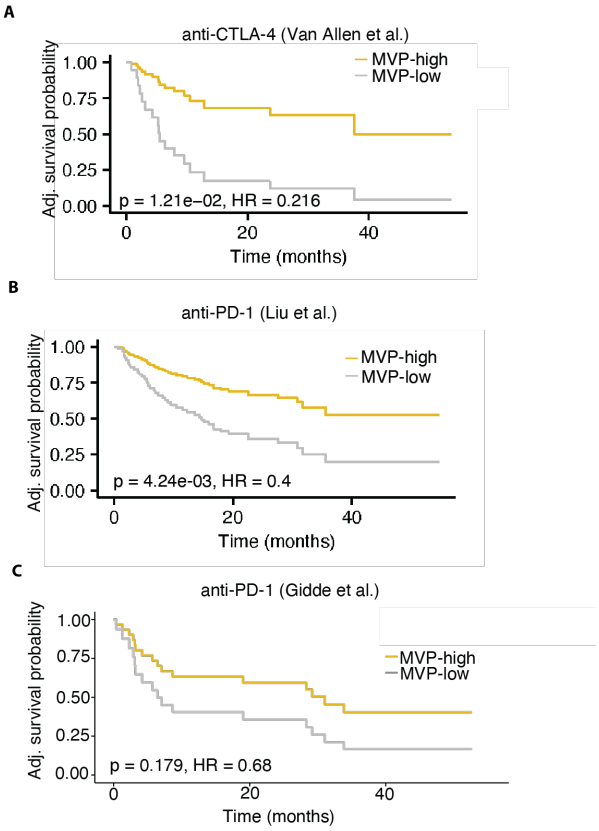

Supplemental Figure S3-5: *MVP* expression is associated with response to immune checkpoint inhibition. *MVP*-high tumors: *MVP* expression > 66th percentile; *MVP* -low tumors: *MVP* expression < 33rd percentile. Kaplan Meier survival curves comparing *MVP* -high and *MVP* -low tumors adjusted for confounding effects of sex and tumor mutational burden covariates by Cox Proportional Hazards modeling. Hazard ratio (HR) and p-value obtained from fitting a Cox Proportional Hazards model. (A) Data re-analyzed from Van Allen et al. 2015. (B) Data re-analyzed from Liu et al., 2019. (C) Data re-analyzed from Gide et al., 2019.

3.9 Materials and Methods

Cell lines

B16-F10 mouse melanoma cell line derivatives were cultured at 37°C and 5% CO2. B16-F10 parental cell line was purchased from ATCC (ATCC, Manassas, VA) and cultured in Debeco's Minimum Essential Medium (Gibco, Waltham, MA) supplemented with 10% FBS (Gibco) and 1% Pen Strep (Gibco). MVP KO cells were generated using an alt-R genome editing kit (IDT, Coralville, Iowa) with two predesigned csRNAs from IDT: Mm.Cas9.MVP.1.AA MVP and Mm.Cas9.MVP.1.AC MVP. RNP complexes were electroporated into B16-F10 cells. Knockout

of MVP was validated with the alt-R Genome Editing Detection Kit and by western blot. MVP KO and NTC B16-OVA were generated by lentiviral transduction of pLVX-puro-cOVA (Plasmid #135073, Addgene, Watertown, Massachusetts)

Generation of MVP-/- mouse model

We designed paired guide RNAs to target the 3' splice site of exon 4: guides = MVP_KO3 and MVP_KO4 = CCAAGTATCAGGTTTGAGCT and GGGCAGAACCACCTGCAGCG. The resulting deletion allele contains an indel in intron 3 and indel in exon 4. As a result of this frameshift mutation, a premature termination codon is introduced in exon 4. These guide RNAs and Cas9 were delivered into one-cell C57BL/6J embryos by pronuclear microinjection. DNA was isolated from tail clips and used to genotype F0 mice. Mice were genotyped with forward and reverse primers, where wildtype tissue yields in a 478 bp product. Primer sequences: MVP Geno 5F- GAGGAGGAGACAGCTGATGC, MVP Geno 5R- AGTTCTTCAGACCTGGTGGC. F0 mice with presence of a non-WT band on PCR were crossed with WT C57BL/6 mice to assess the transmission of the mutant allele. Recovered mutant alleles in the MVP exon 4 locus were propagated by backcrossing F0 mice and intercrossing heterozygous F1 mice to generate MVP-/-, MVP+/-, and MVP+/+ progeny. MVP-/- mice were backcrossed four generations.

Tumor allograft and xenograft experiments

For the host MVP KO experiment, all mice used were in the C57BL/6 background, with age- and sex-matched WT controls purchased from Jackson Labs as we required more mice than we could produce as littermates. All mice used in the immunocompetent tumor MVP KO experiments were age- and sex-matched WT C57BL/6 mice purchased from Jackson Labs. All mice used in

the immunodeficient tumor MVP KO experiments were age- and sex-matched NOD scid gamma (NSG) mice purchased from Jackson Labs. For all experiments, we infected 500,000 cells subcutaneously into each flank and monitored tumors for growth daily. Once palpable or visible, we began measuring tumors to track changes in volume. Survival studies utilized endpoint criteria defined by Fred Hutchinson Cancer Center IACUC. Tumor size criteria: tumors to not exceed 1.5cm in either direction nor combined total tumor burden of 2000mm^3.

Single cell RNA-sequencing data processing and expression analysis

Data underwent initial processing in CellRanger (173) by the Fred Hutch Genomics Shared Resource core facility, where samples were demultiplexed. Quality control and downstream analyses were performed in python by Tracy Yang and Dominik Otto. Individual samples underwent quality control, where cells with mitochondrial reads exceeding 20% were removed. Thresholds for RNA content were >3rd and <98th percentiles of molecule counts and expression of greater than 50 genes. Data were then combined and normalized per cell and log transformed. Using CellRanger, the top 2500 highly variable genes were selected and informed cell-cell variability. PCA analysis was used to reduce dimensionality in the data, and the data were ultimately visualized by UMAP, with Leiden clustering used with standard parameters to determine groups of similar and different cells. Cell type annotations were determined by expression of defined cell type phenotypic markers.

Differential abundance analysis

Method to be described in new manuscript in process by the Setty Lab: Otto D, Yang R, Arriaga-Gomez E, Thieme E, Lee SC, Setty M. kompot statistical framework for single-cell resolution

differential abundance and differential expression testing. In preparation (2025) . This methodology builds upon methodology published previously (164).

Immunohistochemistry

Tissues from tumors were processed, embedded and stained through the Fred Hutch Experimental Histopathology core. Mouse CD8A and SOX10/S100 (cocktail to stain for mouse melanoma cells). Staining was performed with a BOND RX autostainer (Leica Biosystems) and images were then acquired with an Aperio ImageScope at 40x magnification (Leica Biosystems). Image analysis was completed using HALO Image Analysis software.

Survival analyses

Survival analyses were performed with the Kaplan–Meier estimator and statistical tests were performed with a log rank test (R package survival) (123). Samples were stratified by expression of *Mvp*, where high and low expressing samples were defined by tercile > 66th percentile or < 33rd percentile respectively, and compared. Adjusted survival probabilities were calculated by fitting a Cox Proportional Hazards model to adjust for the covariates sex and tumor mutational burden.

Chapter 4 Perspectives and future directions

Here we explore the contributions of two candidate modulators of tumor-immune interactions. In the case of *CGB7*, we characterize a biomarker of reduced anti-tumor immunity and in the case of MVP, we describe a positive regulator of anti-tumor immunity.

4.1 Validation of CGB as a biomarker of immune evasion and resistance to ICI in cancer

Our investigation describes the potential value of the expression of CGB genes as cancer biomarkers, and ultimately suggests that *CGB7* expression in particular may be a biomarker of tumor immune escape, and may have prognostic value to predict poor response to immune checkpoint inhibitor therapies. Further validation of CGB is required to facilitate use of CGB expression as a clinical-grade biomarker.

Potential modalities for CGB biomarker detection might be qRT-PCR based biomarker assay to detect transcripts of CGB genes, or an Enzyme Linked Immunosorbent Assay (ELISA) to detect secreted protein. We, and others as described in chapter 2, have validated that detection of CGB is possible at a gene expression level, where we can parse expression of individual CGB genes, as well as at the protein level, where CGB proteins are secreted, and perhaps more challenging to detect as individual type-I vs type-II CGB proteins due to the three amino acid difference between type-I and type-II proteins.

Interestingly, as described in our data, it appears that detection of bulk, or any, CGB transcripts may have value as biomarkers of poor response or resistance to immune checkpoint inhibition. This affords the possibility of utilizing an ELISA assay that detects bulk CGB secreted protein from patient sera or plasma. A bulk CGB ELISA assay is already FDA approved and widely clinically utilized for use in pregnancy testing, making this assay an attractive candidate assay to apply widely for cancer detection and prognosis.

As *CGB7* appears to be the only CGB gene associated with a suppressed tumor immune microenvironment, it is possible that CGB7 uniquely impacts tumor-immune interactions through mechanisms not conferred by type-I CGBs. It is possible that there could be utility in development of a CGB7-specific biomarker assay to be used in parallel with a bulk/any CGB

detection assay if indeed it is validated that *CGB7* expression uniquely impacts prognosis in certain disease or therapeutic contexts. ELISA with a highly CGB7-specific antibody, or qRT-PCR for *CGB7* transcripts could have potential as biomarker assays. Another interesting potential biomarker assay to explore to detect CGB protein is immunohistochemistry (IHC) detection of CGB.

Final critical consideration for validation of CGB as a cancer biomarker are a need to 1) measure CGB expression or secretion in a prospective study to determine whether CGB accurately predicts response to checkpoint immunotherapy and 2) the need to extend these predictive analyses to additional patient cohorts, larger patient cohorts, and ultimately to additional cancer types, as CGB is expressed in many cancers.

4.2 Perspectives for determining CGB7 mechanism of immune evasion in cancer

Our work elucidated an exciting association between expression of CGB genes and prediction of response to immune checkpoint inhibition in advanced bladder cancer. It also revealed an association between *CGB7* and markers of immune evasion. Thus, characterizing the molecular mechanism of CGB7 and other CGB proteins in cancer would be a critical next step.

A major limitation of studying primate-specific CGBs is the challenge of immunocompetent murine modeling. In any context, CGB proteins would be foreign proteins in mice not exposed to hCG during development, likely masking any potential immunosuppressive effect of CGB. A potential way around this would be through generation of CGB centrally tolerized mouse model inspired by Grzelak et al. (180).

Pilot experiments not described in chapter 2 were performed to explore potential molecular and cellular mechanisms of CGB proteins in tumor-immune interactions. A role of

CGB proteins as regulators of T regulatory cell recruitment was explored by co-culturing CD4+ T cells isolated from PBMCs with conditioned media from CGB-expressing cancer cell lines or supplemented with recombinant CGB protein. The effect of CGB on immune cell phenotype and function was investigated with a pilot assay where donor-derived whole blood was treated with recombinant CGB protein or conditioned media from CGB+ tumor cell lines as well as stimulatory positive controls and negative vehicle control. As CGB proteins are hypothesized to be immunosuppressive, future investigation may be more informative performed under immune-stimulating conditions, such as with IFNg or TNFa stimulation. Tumor-intrinsic effects of CGB expression were also investigated, such as an effect on proliferation, or expression of genes in inflammatory signaling, were largely negative, again suggesting the value of investigating the mechanisms of action of CGB7 and other CGB proteins in an immune-activating context.

4.3 Functional characterization of MVP-associated effector CD8+ T cells

Our work in chapter three identified a previously uncharacterized function of MVP in tumor-immune interactions. We have shown that MVP KO tumors are associated with increased abundance of effector CD8+ T cells that, while expressing high levels of *Gzmb*, *Prf1*, and *Ifng*, appear fated for the exhaustion pathway with high expression of multiple immune checkpoints or markers of exhaustion: *Pdcd1*, Tim-3 (*Havcr2*), *Lag-3*, *Tox*. Previously, cells of a similar phenotype have been characterized in myeloma by Minnie et al. (167) and a highly similar B16-OVA melanoma by Miller et al. (168). Minnie et al. suggest that these cells retain effector function and may be able to be functionally rescued by immunotherapy (167). Miller et al. describes these cells as retaining some effector function, but ultimately these effectors are short lived and do not contribute to durable anti-tumor effects. Miller et al. goes on to demonstrate that anti-PD-1 therapy does not act on these cells (168). Ultimately, there are multiple reports of

highly cytotoxic CD8+ T cells with features of exhaustion that appear phenotypically similar to a population of cells significantly more present in MVP KO tumors than in control (NTC) tumors. As there are variable findings surrounding the function of these highly cytotoxic cells with features of exhaustion, and their sensitivity to checkpoint immunotherapy, it is clear that functional follow up studies would be essential to functionally characterize this population of cells in our model.

A next step that could be taken toward functionally characterizing these cells in our model would be a co-culture assay with CD8+ T cells isolated from OT-1 mice and MVP KO or NTC B16-OVA cells. Here, tumor killing could be measured, as could surface marker expression on CD8+ T cells after co-culture, by flow cytometry. After co-culture, levels of cytokines in the supernatant could be measured by ELISA. These data would provide a snapshot of the effector function of CD8+ T cells cultured with MVP KO or NTC control tumor cells coupled with profiling of CD8+ phenotypes present in the co-culture, and could guide future functional studies.

To determine whether the positive survival effect of tumor MVP expression is dependent on CD8+ T cells, the same survival cohort we performed in our study could be performed in the presence of a CD8+ T cell antibody. If CD8+ T cells are necessary for the MVP-driven pro-survival phenotype, it would be expected that the survival curves would be highly similar for mice bearing MVP KO and NTC tumors in this context.

Additional experimentation to better understand functional implications of MVP-associated CD8+ T cell exhaustion in the context of immune checkpoint inhibitors would be valuable. Here, tumor allograft studies could be performed by engrafting MVP KO or NTC B16-OVA cells into C57BL/6 mice and treating them with PD-1 or CTLA-4 monotherapy. A survival

study would inform the effect of *MVP* expression on response to immune checkpoint inhibition. A parallel fixed-endpoint study would enable collection of tumors for subsequent analysis (scRNA-seq, flow cytometry, etc.).

4.4 Concluding perspectives

This work characterizes two novel therapeutic targets and/or biomarkers of resistance or response to immune checkpoint inhibitors and contributes to our overall understanding of the multifaceted landscape of factors that influence immunotherapy response and tumor-immune interactions. Many patients upwards of 50% do not ultimately achieve a durable response to ICI therapy, and in this context, we propose that targeting of MVP or CGB7 (or CGB proteins broadly) may be valuable in combination with ICI to enhance response rates for subsets of patients.

CGB proteins have been studied as oncofetal antigens and subsequently cancer biomarkers for decades. This work further expands our understanding of CGB proteins in cancer by establishing previously unrecognized associations between *CGB7* and markers of immune evasion, decreased survival probability in the context of immune checkpoint inhibition, and lack of response to immune checkpoint inhibition in urothelial carcinoma. We go on to extend this association by demonstrating that *CGB7* expression can predict this decreased survival probability with a similar predictive value as established and widely used biomarker tumor mutational burden (TMB). This reinforces that CGB proteins are valuable biomarkers not just of cancer in general, but can actually be utilized to predict checkpoint immunotherapy outcomes.

As *CGB7*, and other CGB genes, are expressed widely across cancers, they may be widely valuable as clinical biomarkers in this setting. With additional validation of associations

between CGB protein levels in blood or urine and survival in checkpoint immunotherapy treatment, it may be possible to rapidly repurpose pre-existing clinical CGB tests for cancer, as clinical tests already exist to detect CGB proteins in pregnancy and testicular cancer. As CGB proteins are secreted, they are excellent candidates for inhibitory targeting with CGB-specific therapeutic antibodies. This is one strategy for developing an anti-CGB therapeutic to be used in combination with checkpoint immunotherapy.

This work additionally expands our understanding of the vault complex, which has been shrouded in mystery for decades. Though the vault, and expression of the main component of the vault MVP, have since been linked to diverse biological processes and molecular functions, fundamentally we lack complete understanding of the functions of the vault complex. Here we contribute to this understanding by describing a previously unappreciated role of MVP in tumor-immune interactions, with both host and tumor-derived *Mvp* enhancing survival probability in melanoma. We further identify associations between *MVP* and increased survival probability in the context of immune checkpoint inhibition, which may be explained by our finding that MVP KO tumors exhibit increased abundance of effector CD8+ T cells that express high levels of multiple markers of exhaustion and therefore may exist along the spectrum of dysfunction.

As MVP is expressed widely across healthy cells, augmenting *MVP* expression or MVP protein levels in cancer cells may offer protection against exhaustion of effector CD8+ T cells. Indeed, therapeutic vault nanoparticle shells have been developed to delivery targeted therapeutics to cancers, and here we suggest that delivery of the vault shell—composed largely of MVP-- alone may afford some therapeutic benefit in both within the context of melanoma cancers treated with checkpoint immunotherapy and perhaps even in those untreated with checkpoint immunotherapy.

Taken together, this work advances our understanding of factors that influence tumor-immune interactions and survival in checkpoint immunotherapy treated cancers in multiple types.

References

1. Hanahan D, Weinberg RA. Hallmarks of cancer: the next generation. Cell. 2011 Mar 4;144(5):646-74. doi: 10.1016/j.cell.2011.02.013. PMID: 21376230.
2. Hanahan D. Hallmarks of Cancer: New Dimensions. Cancer Discov. 2022 Jan;12(1):31-46. doi: 10.1158/2159-8290.CD-21-1059. PMID: 35022204.
3. Kastan, M., Bartek, J. Cell-cycle checkpoints and cancer. Nature 432, 316–323 (2004).
4. Norbury CJ, Zhivotovsky B. DNA damage-induced apoptosis. Oncogene. 2004 Apr 12;23(16):2797-808. doi: 10.1038/sj.onc.1207532. PMID: 15077143.
5. Jackson, S., Bartek, J. The DNA-damage response in human biology and disease. Nature 461, 1071–1078 (2009). https://doi.org/10.1038/nature08467
6. Lykke-Andersen, S., Jensen, T. Nonsense-mediated mRNA decay: an intricate machinery that shapes transcriptomes. Nat Rev Mol Cell Biol 16, 665–677 (2015).
7. Hetz, C., Zhang, K. & Kaufman, R.J. Mechanisms, regulation and functions of the unfolded protein response. Nat Rev Mol Cell Biol 21, 421–438 (2020).
8. Zitvogel, L., Tesniere, A. & Kroemer, G. Cancer despite immunosurveillance: immunoselection and immunosubversion. Nat Rev Immunol 6, 715–727 (2006).
9. Swann JB, Smyth MJ. Immune surveillance of tumors. J Clin Invest. 2007 May;117(5):1137-46. doi: 10.1172/JCI31405. PMID: 17476343; PMCID: PMC1857231.
10. Mortaz E, Tabarsi P, Mansouri D, Khosravi A, Garssen J, Velayati A, Adcock IM. Cancers Related to Immunodeficiencies: Update and Perspectives. Front Immunol. 2016 Sep 20;7:365. doi: 10.3389/fimmu.2016.00365. PMID: 27703456; PMCID: PMC5028721.
11. Shankaran V, Ikeda H, Bruce AT, White JM, Swanson PE, Old LJ, Schreiber RD. IFNgamma and lymphocytes prevent primary tumour development and shape tumour immunogenicity. Nature. 2001 Apr 26;410(6832):1107-11. doi: 10.1038/35074122. PMID: 11323675.
12. Dhatchinamoorthy K, Colbert JD, Rock KL. Cancer Immune Evasion Through Loss of MHC Class I Antigen Presentation. Front Immunol. 2021 Mar 9;12:636568. doi: 10.3389/fimmu.2021.636568. PMID: 33767702; PMCID: PMC7986854.
13. Zaretsky JM, Garcia-Diaz A, Shin DS, Escuin-Ordinas H, Hugo W, Hu-Lieskovan S, Torrejon DY, Abril-Rodriguez G, Sandoval S, Barthly L, Saco J, Homet Moreno B, Mezzadra R, Chmielowski B, Ruchalski K, Shintaku IP, Sanchez PJ, Puig-Saus C, Cherry G, Seja E, Kong X, Pang J, Berent-Maoz B, Comin-Anduix B, Graeber TG, Tumeh PC, Schumacher TN, Lo RS, Ribas A. Mutations Associated with Acquired Resistance to PD-1 Blockade in Melanoma. N Engl J Med. 2016 Sep 1;375(9):819-29. doi: 10.1056/NEJMoa1604958. Epub 2016 Jul 13. PMID: 27433843; PMCID: PMC5007206.
14. He, X., Xu, C. Immune checkpoint signaling and cancer immunotherapy. Cell Res 30, 660–669 (2020). https://doi.org/10.1038/s41422-020-0343-4
15. Lehmann C, Zeis M, Schmitz N, Uharek L. Impaired Binding of Perforin on the Surface of Tumor Cells is a Cause of Target Cell Resistance Against Cytotoxic Effector Cells (2000).

16. Otten HG, van Ginkel WGJ, Hagenbeek A, Petersen EJ. Prevalence and Clinical Significance of Resistance to Perforin- and FAS-Mediated Cell Death in Leukemia. Leukemia (2004) 18:1401–5. doi: 10.1038/sj.leu.2403414
17. Kaiserman, D., Bird, P. Control of granzymes by serpins. Cell Death Differ 17, 586–595 (2010). https://doi.org/10.1038/cdd.2009.169
18. Alturki NA. Review of the Immune Checkpoint Inhibitors in the Context of Cancer Treatment. J Clin Med. 2023 Jun 27;12(13):4301. doi: 10.3390/jcm12134301. PMID: 37445336; PMCID: PMC10342855.
19. Vaddepally RK, Kharel P, Pandey R, Garje R, Chandra AB. Review of Indications of FDA-Approved Immune Checkpoint Inhibitors per NCCN Guidelines with the Level of Evidence. Cancers (Basel). 2020 Mar 20;12(3):738. doi: 10.3390/cancers12030738. PMID: 32245016; PMCID: PMC7140028.
20. Wang Y, Tong Z, Zhang W, Zhang W, Buzdin A, Mu X, Yan Q, Zhao X, Chang HH, Duhon M, Zhou X, Zhao G, Chen H, Li X. FDA-Approved and Emerging Next Generation Predictive Biomarkers for Immune Checkpoint Inhibitors in Cancer Patients. Front Oncol. 2021 Jun 7;11:683419. doi: 10.3389/fonc.2021.683419. PMID: 34164344; PMCID: PMC8216110.
21. Sharma P, Goswami S, Raychaudhuri D, Siddiqui BA, Singh P, Nagarajan A, Liu J, Subudhi SK, Poon C, Gant KL, Herbrich SM, Anandhan S, Islam S, Amit M, Anandappa G, Allison JP. Immune checkpoint therapy-current perspectives and future directions. Cell. 2023 Apr 13;186(8):1652-1669. doi: 10.1016/j.cell.2023.03.006. PMID: 37059068.
22. Ishida Y, Agata Y, Shibahara K, Honjo T. Induced expression of PD-1, a novel member of the immunoglobulin gene superfamily, upon programmed cell death. EMBO J. 1992 Nov;11(11):3887-95. doi: 10.1002/j.1460-2075.1992.tb05481.x. PMID: 1396582; PMCID: PMC556898.
23. Leach DR, Krummel MF, Allison JP. Enhancement of antitumor immunity by CTLA-4 blockade. Science. 1996 Mar 22;271(5256):1734-6. doi: 10.1126/science.271.5256.1734. PMID: 8596936.
24. Triebel F, Jitsukawa S, Baixeras E, Roman-Roman S, Genevee C, Viegas-Pequignot E, Hercend T, LAG-3, a novel lymphocyte activation gene closely related to CD4, J Exp Med 171(5) (1990) 1393–405.
25. Yu X, Harden K, Gonzalez LC, Francesco M, Chiang E, Irving B, Tom I, Ivelja S, Refino CJ, Clark H, Eaton D, Grogan JL. The surface protein TIGIT suppresses T cell activation by promoting the generation of mature immunoregulatory dendritic cells. Nat Immunol. 2009 Jan;10(1):48-57. doi: 10.1038/ni.1674. Epub 2008 Nov 16. PMID: 19011627.
26. Monney, L. et al. TH1-specific cell surface protein Tim-3 regulates macrophage activation and severity of an autoimmune disease. Nature 415, 536–541 (2002).
27. Seidel JA, Otsuka A, Kabashima K. Anti-PD-1 and Anti-CTLA-4 Therapies in Cancer: Mechanisms of Action, Efficacy, and Limitations. Front Oncol. 2018 Mar 28;8:86. doi: 10.3389/fonc.2018.00086. PMID: 29644214; PMCID: PMC5883082.
28. Larkin J, Chiarion-Sileni V, Gonzalez R, Grob JJ, Rutkowski P, Lao CD, Cowey CL, Schadendorf D, Wagstaff J, Dummer R, Ferrucci PF, Smylie M, Hogg D, Hill A, Márquez-Rodas I, Haanen J, Guidoboni M, Maio M, Schöffski P, Carlino MS, Lebbé C, McArthur G, Ascierto PA, Daniels GA, Long GV, Bastholt L, Rizzo JI,

Balogh A, Moshyk A, Hodi FS, Wolchok JD. Five-Year Survival with Combined Nivolumab and Ipilimumab in Advanced Melanoma. N Engl J Med. 2019 Oct 17;381(16):1535-1546. doi: 10.1056/NEJMoa1910836. Epub 2019 Sep 28. PMID: 31562797.

29. Rossi E, Schinzari G, Maiorano BA, Indellicati G, Di Stefani A, Pagliara MM, Fragomeni SM, De Luca EV, Sammarco MG, Garganese G, Galli J, Blasi MA, Paludetti G, Scambia G, Peris K, Tortora G. Efficacy of immune checkpoint inhibitors in different types of melanoma. Hum Vaccin Immunother. 2021 Jan 2;17(1):4-13. doi: 10.1080/21645515.2020.1771986. Epub 2020 Jul 14. PMID: 32663057; PMCID: PMC7872095.
30. Keilholz U, Mehnert JM, Bauer S, Bourgeois H, Patel MR, Gravenor D, Nemunaitis JJ, Taylor MH, Wyrwicz L, Lee KW, Kasturi V, Chin K, von Heydebreck A, Gulley JL. Avelumab in patients with previously treated metastatic melanoma: phase 1b results from the JAVELIN Solid Tumor trial. J Immunother Cancer. 2019 Jan 16;7(1):12. doi: 10.1186/s40425-018-0459-y. PMID: 30651126; PMCID: PMC6335739.
31. McDermott D, Haanen J, Chen TT, Lorigan P, O'Day S; MDX010-20 investigators. Efficacy and safety of ipilimumab in metastatic melanoma patients surviving more than 2 years following treatment in a phase III trial (MDX010-20). Ann Oncol. 2013 Oct;24(10):2694-2698. doi: 10.1093/annonc/mdt291. Epub 2013 Aug 13. PMID: 23942774.
32. Maio M, Grob JJ, Aamdal S, Bondarenko I, Robert C, Thomas L, Garbe C, Chiarion-Sileni V, Testori A, Chen TT, Tschaika M, Wolchok JD. Five-year survival rates for treatment-naive patients with advanced melanoma who received ipilimumab plus dacarbazine in a phase III trial. J Clin Oncol. 2015 Apr 1;33(10):1191-6. doi: 10.1200/JCO.2014.56.6018. Epub 2015 Feb 23. PMID: 25713437; PMCID: PMC5795709.
33. Cha JH, Chan LC, Li CW, Hsu JL, Hung MC. Mechanisms Controlling PD-L1 Expression in Cancer. Mol Cell. 2019 Nov 7;76(3):359-370. doi: 10.1016/j.molcel.2019.09.030. Epub 2019 Oct 24. PMID: 31668929; PMCID: PMC6981282.
34. Ascierto PA, Long GV, Robert C, Brady B, Dutriaux C, Di Giacomo AM, Mortier L, Hassel JC, Rutkowski P, McNeil C, et al. Survival outcomes in patients with previously untreated braf wild-type advanced melanoma treated with nivolumab therapy: three-year follow-up of a randomized phase 3 trial. JAMA Oncol. 2019;5(2):187–194. doi: 10.1001/jamaoncol.2018.4514.
35. Robert C, Long GV, Brady B, Dutriaux C, Maio M, Mortier L, Hassel JC, Rutkowski P, McNeil C, Kalinka-Warzocha E, Savage KJ, Hernberg MM, Lebbé C, Charles J, Mihalcioiu C, Chiarion-Sileni V, Mauch C, Cognetti F, Arance A, Schmidt H, Schadendorf D, Gogas H, Lundgren-Eriksson L, Horak C, Sharkey B, Waxman IM, Atkinson V, Ascierto PA. Nivolumab in previously untreated melanoma without BRAF mutation. N Engl J Med. 2015 Jan 22;372(4):320-30. doi: 10.1056/NEJMoa1412082. Epub 2014 Nov 16. PMID: 25399552.
36. Robert C, Schachter J, Long GV, Arance A, Grob JJ, Mortier L, Daud A, Carlino MS, McNeil C, Lotem M, et al. Pembrolizumab versus ipilimumab in advanced melanoma. N Engl J Med. 2015;372(26):2521–2532. doi: 10.1056/NEJMoa1503093.

37. Schachter J, Ribas A, Long GV, Arance A, Grob JJ, Mortier L, Daud A, Carlino MS, McNeil C, Lotem M, et al. Pembrolizumab versus ipilimumab for advanced melanoma: final overall survival results of a multicentre, randomised, open-label phase 3 study (KEYNOTE-006). Lancet. 2017;390(10105):1853–1862. doi: 10.1016/S0140-6736(17)31601-X.
38. Wolchok JD, Chiarion-Sileni V, Rutkowski P, Cowey CL, Schadendorf D, Wagstaff J, Queirolo P, Dummer R, Butler MO, Hill AG, Postow MA, Gaudy-Marqueste C, Medina T, Lao CD, Walker J, Márquez-Rodas I, Haanen JBAG, Guidoboni M, Maio M, Schöffski P, Carlino MS, Sandhu S, Lebbé C, Ascierto PA, Long GV, Ritchings C, Nassar A, Askelson M, Benito MP, Wang W, Hodi FS, Larkin J; CheckMate 067 Investigators. Final, 10-Year Outcomes with Nivolumab plus Ipilimumab in Advanced Melanoma. N Engl J Med. 2025 Jan 2;392(1):11-22. doi: 10.1056/NEJMoa2407417. Epub 2024 Sep 15. PMID: 39282897.
39. Motzer RJ, Escudier B, George S, Hammers HJ, Srinivas S, Tykodi SS, Sosman JA, Plimack ER, Procopio G, McDermott DF, Castellano D, Choueiri TK, Donskov F, Gurney H, Oudard S, Richardet M, Peltola K, Alva AS, Carducci M, Wagstaff J, Chevreau C, Fukasawa S, Tomita Y, Gauler TC, Kollmannsberger CK, Schutz FA, Larkin J, Cella D, McHenry MB, Saggi SS, Tannir NM. Nivolumab versus everolimus in patients with advanced renal cell carcinoma: Updated results with long-term follow-up of the randomized, open-label, phase 3 CheckMate 025 trial. Cancer. 2020 Sep 15;126(18):4156-4167. doi: 10.1002/cncr.33033. Epub 2020 Jul 16. PMID: 32673417; PMCID: PMC8415096.
40. Motzer RJ, Tannir NM, McDermott DF, Arén Frontera O, Melichar B, Choueiri TK, Plimack ER, Barthélémy P, Porta C, George S, Powles T, Donskov F, Neiman V, Kollmannsberger CK, Salman P, Gurney H, Hawkins R, Ravaud A, Grimm MO, Bracarda S, Barrios CH, Tomita Y, Castellano D, Rini BI, Chen AC, Mekan S, McHenry MB, Wind-Rotolo M, Doan J, Sharma P, Hammers HJ, Escudier B; CheckMate 214 Investigators. Nivolumab plus Ipilimumab versus Sunitinib in Advanced Renal-Cell Carcinoma. N Engl J Med. 2018 Apr 5;378(14):1277-1290. doi: 10.1056/NEJMoa1712126. Epub 2018 Mar 21. PMID: 29562145; PMCID: PMC5972549.
41. Albiges L, Tannir NM, Burotto M, McDermott D, Plimack ER, Barthélémy P, Porta C, Powles T, Donskov F, George S, Kollmannsberger CK, Gurney H, Grimm MO, Tomita Y, Castellano D, Rini BI, Choueiri TK, Saggi SS, McHenry MB, Motzer RJ. Nivolumab plus ipilimumab versus sunitinib for first-line treatment of advanced renal cell carcinoma: extended 4-year follow-up of the phase III CheckMate 214 trial. ESMO Open. 2020 Nov;5(6):e001079. doi: 10.1136/esmoopen-2020-001079. PMID: 33246931; PMCID: PMC7703447.
42. Balar AV, Galsky MD, Rosenberg JE, Powles T, Petrylak DP, Bellmunt J, Loriot Y, Necchi A, Hoffman-Censits J, Perez-Gracia JL, Dawson NA, van der Heijden MS, Dreicer R, Srinivas S, Retz MM, Joseph RW, Drakaki A, Vaishampayan UN, Sridhar SS, Quinn DI, Durán I, Shaffer DR, Eigl BJ, Grivas PD, Yu EY, Li S, Kadel EE 3rd, Boyd Z, Bourgon R, Hegde PS, Mariathasan S, Thåström A, Abidoye OO, Fine GD, Bajorin DF; IMvigor210 Study Group. Atezolizumab as first-line treatment in cisplatin-ineligible patients with locally advanced and metastatic urothelial carcinoma: a single-arm, multicentre, phase 2 trial. Lancet. 2017 Jan

7;389(10064):67-76. doi: 10.1016/S0140-6736(16)32455-2. Epub 2016 Dec 8. Erratum in: Lancet. 2017 Aug 26;390(10097):848. doi: 10.1016/S0140-6736(17)32213-4. PMID: 27939400; PMCID: PMC5568632.
43. Powles T, Durán I, van der Heijden MS, Loriot Y, Vogelzang NJ, De Giorgi U, Oudard S, Retz MM, Castellano D, Bamias A, Fléchon A, Gravis G, Hussain S, Takano T, Leng N, Kadel EE 3rd, Banchereau R, Hegde PS, Mariathasan S, Cui N, Shen X, Derleth CL, Green MC, Ravaud A. Atezolizumab versus chemotherapy in patients with platinum-treated locally advanced or metastatic urothelial carcinoma (IMvigor211): a multicentre, open-label, phase 3 randomised controlled trial. Lancet. 2018 Feb 24;391(10122):748-757. doi: 10.1016/S0140-6736(17)33297-X. Epub 2017 Dec 18. Erratum in: Lancet. 2018 Oct 20;392(10156):1402. doi: 10.1016/S0140-6736(18)32516-9. PMID: 29268948.
44. Powles T, Park SH, Voog E, Caserta C, Valderrama BP, Gurney H, Kalofonos H, Radulović S, Demey W, Ullén A, Loriot Y, Sridhar SS, Tsuchiya N, Kopyltsov E, Sternberg CN, Bellmunt J, Aragon-Ching JB, Petrylak DP, Laliberte R, Wang J, Huang B, Davis C, Fowst C, Costa N, Blake-Haskins JA, di Pietro A, Grivas P. Avelumab Maintenance Therapy for Advanced or Metastatic Urothelial Carcinoma. N Engl J Med. 2020 Sep 24;383(13):1218-1230. doi: 10.1056/NEJMoa2002788. Epub 2020 Sep 18. PMID: 32945632.
45. Pilard, C., Ancion, M., Delvenne, P. et al. Cancer immunotherapy: it's time to better predict patients' response. Br J Cancer 125, 927–938 (2021). https://doi.org/10.1038/s41416-021-01413-x
46. Sharma P, Hu-Lieskovan S, Wargo JA, Ribas A. Primary, Adaptive, and Acquired Resistance to Cancer Immunotherapy. Cell. 2017 Feb 9;168(4):707-723. doi: 10.1016/j.cell.2017.01.017. PMID: 28187290; PMCID: PMC5391692.
47. Grasso CS, Tsoi J, Onyshchenko M, Abril-Rodriguez G, Ross-Macdonald P, Wind-Rotolo M, Champhekar A, Medina E, Torrejon DY, Shin DS, Tran P, Kim YJ, Puig-Saus C, Campbell K, Vega-Crespo A, Quist M, Martignier C, Luke JJ, Wolchok JD, Johnson DB, Chmielowski B, Hodi FS, Bhatia S, Sharfman W, Urba WJ, Slingluff CL Jr, Diab A, Haanen JBAG, Algarra SM, Pardoll DM, Anagnostou V, Topalian SL, Velculescu VE, Speiser DE, Kalbasi A, Ribas A. Conserved Interferon-γ Signaling Drives Clinical Response to Immune Checkpoint Blockade Therapy in Melanoma. Cancer Cell. 2021 Jan 11;39(1):122. doi: 10.1016/j.ccell.2020.11.015. Epub 2020 Dec 10. Erratum for: Cancer Cell. 2020 Oct 12;38(4):500-515.e3. doi: 10.1016/j.ccell.2020.08.005. PMID: 33306984; PMCID: PMC7885306.
48. Doroshow, D.B., Bhalla, S., Beasley, M.B. et al. PD-L1 as a biomarker of response to immune-checkpoint inhibitors. Nat Rev Clin Oncol 18, 345–362 (2021).
49. Gunjur A, Shao Y, Rozday T, Klein O, Mu A, Haak BW, Markman B, Kee D, Carlino MS, Underhill C, Frentzas S, Michael M, Gao B, Palmer J, Cebon J, Behren A, Adams DJ, Lawley TD. A gut microbial signature for combination immune checkpoint blockade across cancer types. Nat Med. 2024 Mar;30(3):797-809. doi: 10.1038/s41591-024-02823-z. Epub 2024 Mar 1. PMID: 38429524; PMCID: PMC10957475.
50. Tagliamonte M, Petrizzo A, Tornesello ML, Buonaguro FM, Buonaguro L. Antigen-specific vaccines for cancer treatment. Hum Vaccin Immunother. 2014;10(11):3332-46. doi: 10.4161/21645515.2014.973317. PMID: 25483639; PMCID: PMC4514024.

51. Simpson AJ, Caballero OL, Jungbluth A, Chen YT, Old LJ. Cancer/testis antigens, gametogenesis and cancer. Nat Rev Cancer. 2005 Aug;5(8):615-25. doi: 10.1038/nrc1669. PMID: 16034368.
52. Garrett PE, Kurtz SR. Clinical utility of oncofetal proteins and hormones as tumor markers. Med Clin North Am. 1986 Nov;70(6):1295-306. doi: 10.1016/s0025-7125(16)30899-9. PMID: 2431237.
53. Wepsic HT. Overview of oncofetal antigens in cancer. Ann Clin Lab Sci. 1983 Jul-Aug;13(4):261-6. PMID: 6194734.
54. Sisinni L, Landriscina M. The Role of Human Chorionic Gonadotropin as Tumor Marker: Biochemical and Clinical Aspects. Adv Exp Med Biol. 2015;867:159-76. doi: 10.1007/978-94-017-7215-0_11. PMID: 26530366.
55. Go VL. Carcinoembryonic antigen: clinical application. Cancer. 1976 Jan;37(1 suppl):562-6. doi: 10.1002/1097-0142(197601)37:1+<562::aid-cncr2820370721>3.0.co;2-0. PMID: 1247982.
56. Zhou L, Liu J, Luo F. Serum tumor markers for detection of hepatocellular carcinoma. World J Gastroenterol. 2006 Feb 28;12(8):1175-81. doi: 10.3748/wjg.v12.i8.1175. PMID: 16534867; PMCID: PMC4124425.
57. Lin, M.J., Svensson-Arvelund, J., Lubitz, G.S. et al. Cancer vaccines: the next immunotherapy frontier. Nat Cancer 3, 911–926 (2022).
58. D'Angelo SP, Araujo DM, Abdul Razak AR, Agulnik M, Attia S, Blay JY, Carrasco Garcia I, Charlson JA, Choy E, Demetri GD, Druta M, Forcade E, Ganjoo KN, Glod J, Keedy VL, Le Cesne A, Liebner DA, Moreno V, Pollack SM, Schuetze SM, Schwartz GK, Strauss SJ, Tap WD, Thistlethwaite F, Valverde Morales CM, Wagner MJ, Wilky BA, McAlpine C, Hudson L, Navenot JM, Wang T, Bai J, Rafail S, Wang R, Sun A, Fernandes L, Van Winkle E, Elefant E, Lunt C, Norry E, Williams D, Biswas S, Van Tine BA. Afamitresgene autoleucel for advanced synovial sarcoma and myxoid round cell liposarcoma (SPEARHEAD-1): an international, open-label, phase 2 trial. Lancet. 2024 Apr 13;403(10435):1460-1471. doi: 10.1016/S0140-6736(24)00319-2. Epub 2024 Mar 27. PMID: 38554725; PMCID: PMC11419333.
59. Lázaro-Gorines, R., Ruiz-de-la-Herrán, J., Navarro, R. et al. A novel Carcinoembryonic Antigen (CEA)-Targeted Trimeric Immunotoxin shows significantly enhanced Antitumor Activity in Human Colorectal Cancer Xenografts. Sci Rep 9, 11680 (2019). https://doi.org/10.1038/s41598-019-48285-z
60. Terentiev AA, Moldogazieva NT. Alpha-fetoprotein: a renaissance. Tumour Biol. 2013 Aug;34(4):2075-91. doi: 10.1007/s13277-013-0904-y. Epub 2013 Jun 14. PMID: 23765762.
61. Sandberg ML, Wang X, Martin AD, Nampe DP, Gabrelow GB, Li CZ, McElvain ME, Lee WH, Shafaattalab S, Martire S, Fisher FA, Ando Y, Liu E, Ju D, Wong LM, Xu H, Kamb A. A carcinoembryonic antigen-specific cell therapy selectively targets tumor cells with HLA loss of heterozygosity in vitro and in vivo. Sci Transl Med. 2022 Mar 2;14(634):eabm0306. doi: 10.1126/scitranslmed.abm0306. Epub 2022 Mar 2. PMID: 35235342.
62. Munson PV, Adamik J, Butterfield LH. Immunomodulatory impact of α-fetoprotein. Trends Immunol. 2022 Jun;43(6):438-448. doi: 10.1016/j.it.2022.04.001. Epub 2022 May 9. PMID: 35550875.

63. Lapthorn AJ, Harris DC, Littlejohn A, Lustbader JW, Canfield RE, Machin KJ, Morgan FJ, Isaacs NW. Crystal structure of human chorionic gonadotropin. Nature. 1994 Jun 9;369(6480):455-61. doi: 10.1038/369455a0. PMID: 8202136.
64. Douglas, J. et al. Serum total hCGβ level is an independent prognostic factor in transitional cell carcinoma of the urothelial tract. Brit J Cancer 110, 1759–1766 (2014).
65. Iles RK. Ectopic hCGbeta expression by epithelial cancer: malignant behaviour, metastasis and inhibition of tumor cell apoptosis. Mol Cell Endocrinol. 2007 Jan 2;260-262:264-70. doi: 10.1016/j.mce.2006.02.019. Epub 2006 Oct 27. PMID: 17069968.
66. Chew GL, Campbell AE, De Neef E, Sutliff NA, Shadle SC, Tapscott SJ, Bradley RK. DUX4 Suppresses MHC Class I to Promote Cancer Immune Evasion and Resistance to Checkpoint Blockade. Dev Cell. 2019 Sep 9;50(5):658-671.e7. doi: 10.1016/j.devcel.2019.06.011. Epub 2019 Jul 18. PMID: 31327741; PMCID: PMC6736738.
67. Chang C, Chen YL, Wang YW, Chen HW, Hsu CW, Lin KC, Ou YC, Liu T, Chen WL, Chu CA, Ho CL, Lee CT, Chow NH. Aberrant trophoblastic differentiation in human cancer: An emerging novel therapeutic target (Review). Oncol Rep. 2024 Mar;51(3):43. doi: 10.3892/or.2024.8701. Epub 2024 Jan 19. PMID: 38240107; PMCID: PMC10823338.
68. Cheng HL, Chou LP, Tsai HW, Lee CT, Wang YW, Chung-Liang H, Ou JH, Tsai YS, Chow NH. Urothelial carcinoma with trophoblastic differentiation: Reappraisal of the clinical implication and immunohistochemically features. Urol Oncol. 2021 Oct;39(10):732.e17-732.e23. doi: 10.1016/j.urolonc.2021.03.006. Epub 2021 Mar 26. PMID: 33773916.
69. Fluhr H, Bischof-Islami D, Krenzer S, Licht P, Bischof P, Zygmunt M. Human chorionic gonadotropin stimulates matrix metalloproteinases-2 and -9 in cytotrophoblastic cells and decreases tissue inhibitor of metalloproteinases-1, -2, and -3 in decidualized endometrial stromal cells. Fertil Steril. 2008 Oct;90(4 Suppl):1390-5. doi: 10.1016/j.fertnstert.2007.08.023. Epub 2008 Mar 4. PMID: 18291374.
70. J. Guibourdenche, K. Handschuh, V. Tsatsaris, P. Gerbaud, M. C. Leguy, F. Muller, D. Evain Brion, T. Fournier, Hyperglycosylated hCG Is a Marker of Early Human Trophoblast Invasion, The Journal of Clinical Endocrinology & Metabolism, Volume 95, Issue 10, 1 October 2010, Pages E240–E244, https://doi.org/10.1210/jc.2010-0138
71. Zygmunt M, Herr F, Keller-Schoenwetter S, Kunzi-Rapp K, Münstedt K, Rao CV, Lang U, Preissner KT. Characterization of human chorionic gonadotropin as a novel angiogenic factor. J Clin Endocrinol Metab. 2002 Nov;87(11):5290-6. doi: 10.1210/jc.2002-020642. PMID: 12414904.
72. Berndt S, Perrier d'Hauterive S, Blacher S, Péqueux C, Lorquet S, Munaut C, Applanat M, Hervé MA, Lamandé N, Corvol P, van den Brûle F, Frankenne F, Poutanen M, Huhtaniemi I, Geenen V, Noël A, Foidart JM. Angiogenic activity of human chorionic gonadotropin through LH receptor activation on endothelial and epithelial cells of the endometrium. FASEB J. 2006 Dec;20(14):2630-2. doi: 10.1096/fj.06-5885fje. Epub 2006 Oct 25. PMID: 17065221.

73. Berndt S, Blacher S, Perrier d'Hauterive S, Thiry M, Tsampalas M, Cruz A, Péqueux C, Lorquet S, Munaut C, Noël A, Foidart JM. Chorionic gonadotropin stimulation of angiogenesis and pericyte recruitment. J Clin Endocrinol Metab. 2009 Nov;94(11):4567-74. doi: 10.1210/jc.2009-0443. Epub 2009 Oct 16. PMID: 19837939.
74. Schumacher A, Brachwitz N, Sohr S, Engeland K, Langwisch S, Dolaptchieva M, Alexander T, Taran A, Malfertheiner SF, Costa SD, Zimmermann G, Nitschke C, Volk HD, Alexander H, Gunzer M, Zenclussen AC. Human chorionic gonadotropin attracts regulatory T cells into the fetal-maternal interface during early human pregnancy. J Immunol. 2009 May 1;182(9):5488-97. doi: 10.4049/jimmunol.0803177. PMID: 19380797.
75. Schumacher A, Heinze K, Witte J, Poloski E, Linzke N, Woidacki K, Zenclussen AC. Human chorionic gonadotropin as a central regulator of pregnancy immune tolerance. J Immunol. 2013 Mar 15;190(6):2650-8. doi: 10.4049/jimmunol.1202698. Epub 2013 Feb 8. PMID: 23396945.
76. Dauven D, Ehrentraut S, Langwisch S, Zenclussen AC, Schumacher A. Immune Modulatory Effects of Human Chorionic Gonadotropin on Dendritic Cells Supporting Fetal Survival in Murine Pregnancy. Front Endocrinol (Lausanne). 2016 Nov 15;7:146. doi: 10.3389/fendo.2016.00146. PMID: 27895621; PMCID: PMC5108759.
77. Poloski E, Oettel A, Ehrentraut S, Luley L, Costa SD, Zenclussen AC, Schumacher A. JEG-3 Trophoblast Cells Producing Human Chorionic Gonadotropin Promote Conversion of Human CD4+FOXP3- T Cells into CD4+FOXP3+ Regulatory T Cells and Foster T Cell Suppressive Activity. Biol Reprod. 2016 May 1;94(5):106. doi: 10.1095/biolreprod.115.135541. Epub 2016 Mar 9. PMID: 26962115.
78. Schumacher A. Human Chorionic Gonadotropin as a Pivotal Endocrine Immune Regulator Initiating and Preserving Fetal Tolerance. Int J Mol Sci. 2017 Oct 17;18(10):2166. doi: 10.3390/ijms18102166. PMID: 29039764; PMCID: PMC5666847.
79. Bellet D, Lazar V, Bieche I, Paradis V, Giovangrandi Y, Paterlini P, Lidereau R, Bedossa P, Bidart J-M, Vidaud M. Malignant transformation of nontrophoblastic cells is associated with the expression of chorionic gonadotropin beta genes normally transcribed in trophoblastic cells. Cancer Res 1997; 57:516–523.
80. Sohr S, Engeland K. The tumor suppressor p53 induces expression of the pregnancy-supporting human chorionic gonadotropin (hCG) CGB7 gene. Cell Cycle. 2011 Nov 1;10(21):3758-67. doi: 10.4161/cc.10.21.17946. Epub 2011 Nov 1. PMID: 22032922; PMCID: PMC3266010.
81. Zimmermann G, Ackermann W, Alexander H. Expression and production of human chorionic gonadotropin (hCG) in the normal secretory endometrium: evidence of CGB7 and/or CGB6 beta hCG subunit gene expression. Biol Reprod. 2012 Mar 30;86(3):87. doi: 10.1095/biolreprod.111.092429. PMID: 21832169.
82. Subramanian A, Tamayo P, Mootha VK, Mukherjee S, Ebert BL, Gillette MA, Paulovich A, Pomeroy SL, Golub TR, Lander ES, Mesirov JP. Gene set enrichment analysis: a knowledge-based approach for interpreting genome-wide expression profiles. Proc Natl Acad Sci U S A. 2005 Oct 25;102(43):15545-50. doi:

10.1073/pnas.0506580102. Epub 2005 Sep 30. PMID: 16199517; PMCID: PMC1239896.
83. Cook AM, Huddart RA, Jay G, Norman A, Dearnaley DP, Horwich A. The utility of tumour markers in assessing the response to chemotherapy in advanced bladder cancer. Br J Cancer. 2000 Jun;82(12):1952-7. doi: 10.1054/bjoc.2000.1147. PMID: 10864203; PMCID: PMC2363245.
84. Hotakainen K, Haglund C, Paju A, Nordling S, Alfthan H, Rintala E, Stenman UH. Chorionic gonadotropin beta-subunit and core fragment in bladder cancer: mRNA and protein expression in urine, serum and tissue. Eur Urol. 2002 Jun;41(6):677-85. doi: 10.1016/s0302-2838(02)00125-2. PMID: 12074787.
85. Hotakainen K, Lintula S, Jarvinen R, Paju A, Stenman J, Rintala E, Stenman UH. Overexpression of human chorionic gonadotropin beta genes 3, 5 and 8 in tumor tissue and urinary cells of bladder cancer patients. Tumour Biol. 2007;28(1):52-6. doi: 10.1159/000097703. Epub 2006 Dec 1. PMID: 17139196.
86. Moutzouris G, Yannopoulos D, Barbatis C, Zaharof A, Theodorou C. Is beta-human chorionic gonadotrophin production by transitional cell carcinoma of the bladder a marker of aggressive disease and resistance to radiotherapy? Br J Urol. 1993 Dec;72(6):907-9. doi: 10.1111/j.1464-410x.1993.tb16294.x. PMID: 7508330.
87. Dirnhofer S, Koessler P, Ensinger C, Feichtinger H, Madersbacher S, Berger P. Production of trophoblastic hormones by transitional cell carcinoma of the bladder: association to tumor stage and grade. Hum Pathol. 1998 Apr;29(4):377-82. doi: 10.1016/s0046-8177(98)90119-8. PMID: 9563788.
88. Przybycin CG, McKenney JK, Nguyen JK, Shah RB, Umar SA, Harik L, Shih IM, Cox RM. Urothelial Carcinomas With Trophoblastic Differentiation, Including Choriocarcinoma: Clinicopathologic Series of 16 Cases. Am J Surg Pathol. 2020 Oct;44(10):1322-1330. doi: 10.1097/PAS.0000000000001532. PMID: 32931680.
89. Iles RK, Oliver RT, Kitau M, Walker C, Chard T. In vitro secretion of human chorionic gonadotrophin by bladder tumour cells. Br J Cancer. 1987 Jun;55(6):623-6. doi: 10.1038/bjc.1987.126. PMID: 2441730; PMCID: PMC2002027.
90. Fukutani K, Libby JM, Panko WB, Scardino PT. Human chorionic gonadotropin detected in urinary concentrates from patients with malignant tumors of the testis, prostate, bladder, ureter and kidney. J Urol. 1983 Jan;129(1):74-7. doi: 10.1016/s0022-5347(17)51926-6. PMID: 6827688.
91. Dexeus F, Logothetis C, Hossan E, Samuels ML. Carcinoembryonic antigen and beta-human chorionic gonadotropin as serum markers for advanced urothelial malignancies. J Urol. 1986 Aug;136(2):403-7. doi: 10.1016/s0022-5347(17)44882-8. PMID: 2426474.
92. Iles RK, Jenkins BJ, Oliver RT, Blandy JP, Chard T. Beta human chorionic gonadotrophin in serum and urine. A marker for metastatic urothelial cancer. Br J Urol. 1989 Sep;64(3):241-4. doi: 10.1111/j.1464-410x.1989.tb06006.x. PMID: 2478247.
93. Hotakainen K, Lintula S, Stenman J, Rintala E, Lindell O, Stenman UH. Detection of messenger RNA for the beta-subunit of chorionic gonadotropin in urinary cells from patients with transitional cell carcinoma of the bladder by reverse transcription-polymerase chain reaction. Int J Cancer. 1999 Jun 21;84(3):304-8. doi:

10.1002/(sici)1097-0215(19990621)84:3<304::aid-ijc18>3.0.co;2-b. PMID: 10371351.

94. Mariathasan S, Turley SJ, Nickles D, Castiglioni A, Yuen K, Wang Y, Kadel EE III, Koeppen H, Astarita JL, Cubas R, Jhunjhunwala S, Banchereau R, Yang Y, Guan Y, Chalouni C, Ziai J, Şenbabaoğlu Y, Santoro S, Sheinson D, Hung J, Giltnane JM, Pierce AA, Mesh K, Lianoglou S, Riegler J, Carano RAD, Eriksson P, Höglund M, Somarriba L, Halligan DL, van der Heijden MS, Loriot Y, Rosenberg JE, Fong L, Mellman I, Chen DS, Green M, Derleth C, Fine GD, Hegde PS, Bourgon R, Powles T. TGFβ attenuates tumour response to PD-L1 blockade by contributing to exclusion of T cells. Nature. 2018 Feb 22;554(7693):544-548. doi: 10.1038/nature25501. Epub 2018 Feb 14. PMID: 29443960; PMCID: PMC6028240.
95. Zaretsky JM, Garcia-Diaz A, Shin DS, Escuin-Ordinas H, Hugo W, Hu-Lieskovan S, Torrejon DY, Abril-Rodriguez G, Sandoval S, Barthly L, Saco J, Homet Moreno B, Mezzadra R, Chmielowski B, Ruchalski K, Shintaku IP, Sanchez PJ, Puig-Saus C, Cherry G, Seja E, Kong X, Pang J, Berent-Maoz B, Comin-Anduix B, Graeber TG, Tumeh PC, Schumacher TN, Lo RS, Ribas A. Mutations Associated with Acquired Resistance to PD-1 Blockade in Melanoma. N Engl J Med. 2016 Sep 1;375(9):819-29. doi: 10.1056/NEJMoa1604958. Epub 2016 Jul 13. PMID: 27433843; PMCID: PMC5007206.
96. Sjödahl G, Lauss M, Lövgren K, Chebil G, Gudjonsson S, Veerla S, Patschan O, Aine M, Fernö M, Ringnér M, Månsson W, Liedberg F, Lindgren D, Höglund M. A molecular taxonomy for urothelial carcinoma. Clin Cancer Res. 2012 Jun 15;18(12):3377-86. doi: 10.1158/1078-0432.CCR-12-0077-T. Epub 2012 May 2. PMID: 22553347.
97. Sjödahl G, Lövgren K, Lauss M, Patschan O, Gudjonsson S, Chebil G, Aine M, Eriksson P, Månsson W, Lindgren D, Fernö M, Liedberg F, Höglund M. Toward a molecular pathologic classification of urothelial carcinoma. Am J Pathol. 2013 Sep;183(3):681-91. doi: 10.1016/j.ajpath.2013.05.013. Epub 2013 Jul 1. PMID: 23827819.
98. Samstein RM, Lee CH, Shoushtari AN, Hellmann MD, Shen R, Janjigian YY, Barron DA, Zehir A, Jordan EJ, Omuro A, Kaley TJ, Kendall SM, Motzer RJ, Hakimi AA, Voss MH, Russo P, Rosenberg J, Iyer G, Bochner BH, Bajorin DF, Al-Ahmadie HA, Chaft JE, Rudin CM, Riely GJ, Baxi S, Ho AL, Wong RJ, Pfister DG, Wolchok JD, Barker CA, Gutin PH, Brennan CW, Tabar V, Mellinghoff IK, DeAngelis LM, Ariyan CE, Lee N, Tap WD, Gounder MM, D'Angelo SP, Saltz L, Stadler ZK, Scher HI, Baselga J, Razavi P, Klebanoff CA, Yaeger R, Segal NH, Ku GY, DeMatteo RP, Ladanyi M, Rizvi NA, Berger MF, Riaz N, Solit DB, Chan TA, Morris LGT. Tumor mutational load predicts survival after immunotherapy across multiple cancer types. Nat Genet. 2019 Feb;51(2):202-206. doi: 10.1038/s41588-018-0312-8. Epub 2019 Jan 14. PMID: 30643254; PMCID: PMC6365097.
99. Ricciuti B, Wang X, Alessi JV, Rizvi H, Mahadevan NR, Li YY, Polio A, Lindsay J, Umeton R, Sinha R, Vokes NI, Recondo G, Lamberti G, Lawrence M, Vaz VR, Leonardi GC, Plodkowski AJ, Gupta H, Cherniack AD, Tolstorukov MY, Sharma B, Felt KD, Gainor JF, Ravi A, Getz G, Schalper KA, Henick B, Forde P, Anagnostou V, Jänne PA, Van Allen EM, Nishino M, Sholl LM, Christiani DC, Lin X, Rodig SJ, Hellmann MD, Awad MM. Association of High Tumor Mutation Burden in Non-

Small Cell Lung Cancers With Increased Immune Infiltration and Improved Clinical Outcomes of PD-L1 Blockade Across PD-L1 Expression Levels. JAMA Oncol. 2022 Aug 1;8(8):1160-1168. doi: 10.1001/jamaoncol.2022.1981. Erratum in: JAMA Oncol. 2022 Nov 1;8(11):1702. doi: 10.1001/jamaoncol.2022.5957. PMID: 35708671; PMCID: PMC9204620.

100. Hellmann MD, Paz-Ares L, Bernabe Caro R, Zurawski B, Kim SW, Carcereny Costa E, Park K, Alexandru A, Lupinacci L, de la Mora Jimenez E, Sakai H, Albert I, Vergnenegre A, Peters S, Syrigos K, Barlesi F, Reck M, Borghaei H, Brahmer JR, O'Byrne KJ, Geese WJ, Bhagavatheeswaran P, Rabindran SK, Kasinathan RS, Nathan FE, Ramalingam SS. Nivolumab plus Ipilimumab in Advanced Non-Small-Cell Lung Cancer. N Engl J Med. 2019 Nov 21;381(21):2020-2031. doi: 10.1056/NEJMoa1910231. Epub 2019 Sep 28. PMID: 31562796.
101. Hellmann MD, Ciuleanu TE, Pluzanski A, Lee JS, Otterson GA, Audigier-Valette C, Minenza E, Linardou H, Burgers S, Salman P, Borghaei H, Ramalingam SS, Brahmer J, Reck M, O'Byrne KJ, Geese WJ, Green G, Chang H, Szustakowski J, Bhagavatheeswaran P, Healey D, Fu Y, Nathan F, Paz-Ares L. Nivolumab plus Ipilimumab in Lung Cancer with a High Tumor Mutational Burden. N Engl J Med. 2018 May 31;378(22):2093-2104. doi: 10.1056/NEJMoa1801946. Epub 2018 Apr 16. PMID: 29658845; PMCID: PMC7193684.
102. Ye Y, Jing Y, Li L, Mills GB, Diao L, Liu H, Han L. Sex-associated molecular differences for cancer immunotherapy. Nat Commun. 2020 Apr 14;11(1):1779. doi: 10.1038/s41467-020-15679-x. PMID: 32286310; PMCID: PMC7156379.
103. Jang SR, Nikita N, Banks J, Keith SW, Johnson JM, Wilson M, Lu-Yao G. Association Between Sex and Immune Checkpoint Inhibitor Outcomes for Patients With Melanoma. JAMA Netw Open. 2021 Dec 1;4(12):e2136823. doi: 10.1001/jamanetworkopen.2021.36823. PMID: 34854905; PMCID: PMC8640892.
104. Ishwaran H, Kogalur Udaya B., Blackstone Eugene H., Lauer Michael S.. "Random survival forests." The Annals of Applied Statistics, 2(3) 841-860 September 2008. https://doi.org/10.1214/08-AOAS169
105. Ishwaran H, Malley JD. Synthetic learning machines. BioData Min. 2014 Dec 18;7(1):28. doi: 10.1186/s13040-014-0028-y. PMID: 25614764; PMCID: PMC4279689.
106. Pineda JMB, Bradley RK. DUX4 is a common driver of immune evasion and immunotherapy failure in metastatic cancers. Elife. 2024 Jun 3;12:RP89017. doi: 10.7554/eLife.89017. PMID: 38829686; PMCID: PMC11147511.
107. Pickett KL, Suresh K, Campbell KR, Davis S, Juarez-Colunga E. Random survival forests for dynamic predictions of a time-to-event outcome using a longitudinal biomarker. BMC Med Res Methodol. 2021 Oct 17;21(1):216. doi: 10.1186/s12874-021-01375-x. PMID: 34657597; PMCID: PMC8520610.
108. Zhao B, Nguyen VK, Xu M, Colacino JA, Jolliet O. Random survival forest for predicting the combined effects of multiple physiological risk factors on all-cause mortality. Sci Rep. 2024 Jul 6;14(1):15566. doi: 10.1038/s41598-024-66261-0. PMID: 38971926; PMCID: PMC11227534.
109. Sarica A, Aracri F, Bianco MG, Arcuri F, Quattrone A, Quattrone A; Alzheimer's Disease Neuroimaging Initiative. Explainability of random survival forests in predicting conversion risk from mild cognitive impairment to Alzheimer's disease.

Brain Inform. 2023 Nov 18;10(1):31. doi: 10.1186/s40708-023-00211-w. PMID: 37979033; PMCID: PMC10657350.
110. Bohannan ZS, Coffman F, Mitrofanova A. Random survival forest model identifies novel biomarkers of event-free survival in high-risk pediatric acute lymphoblastic leukemia. Comput Struct Biotechnol J. 2022 Jan 6;20:583-597. doi: 10.1016/j.csbj.2022.01.003. PMID: 35116134; PMCID: PMC8777142.
111. Jung SY, Papp JC, Sobel EM, Yu H, Zhang ZF. Breast Cancer Risk and Insulin Resistance: Post Genome-Wide Gene-Environment Interaction Study Using a Random Survival Forest. Cancer Res. 2019 May 15;79(10):2784-2794. doi: 10.1158/0008-5472.CAN-18-3688. Epub 2019 Apr 1. PMID: 30936085; PMCID: PMC6522308.
112. Lundberg SM, Erion G, Chen H, DeGrave A, Prutkin JM, Nair B, Katz R, Himmelfarb J, Bansal N, Lee SI. From Local Explanations to Global Understanding with Explainable AI for Trees. Nat Mach Intell. 2020 Jan;2(1):56-67. doi: 10.1038/s42256-019-0138-9. Epub 2020 Jan 17. PMID: 32607472; PMCID: PMC7326367.
113. Maksymiuk AW, Tappia PS, Bux RA, Moyer D, Huang G, Joubert P, Miller DW, Ramjiawan B, Sitar DS. Use of amantadine in the evaluation of response to chemotherapy in lung cancer: a pilot study. Future Sci OA. 2021 Jan 27;7(4):FSO679. doi: 10.2144/fsoa-2020-0176. PMID: 33815824; PMCID: PMC8015664.
114. Shapley, L. S. (1953). A Value for n-Person Games. Contributions to the Theory of Games, 2, 307-317.https://doi.org/10.1515/9781400881970-018
115. Štrumbelj E., Kononenko I. 2014. Explaining prediction models and individual predictions with feature contributions. Knowledge and Information Systems 41:647–665. https://doi.org/10.1007/s10115-013-0679-x
116. Flicek P, Ahmed I, Amode MR, Barrell D, Beal K, Brent S, Carvalho-Silva D, Clapham P, Coates G, Fairley S, Fitzgerald S, Gil L, García-Girón C, Gordon L, Hourlier T, Hunt S, Juettemann T, Kähäri AK, Keenan S, Komorowska M, Kulesha E, Longden I, Maurel T, McLaren WM, Muffato M, Nag R, Overduin B, Pignatelli M, Pritchard B, Pritchard E, Riat HS, Ritchie GR, Ruffier M, Schuster M, Sheppard D, Sobral D, Taylor K, Thormann A, Trevanion S, White S, Wilder SP, Aken BL, Birney E, Cunningham F, Dunham I, Harrow J, Herrero J, Hubbard TJ, Johnson N, Kinsella R, Parker A, Spudich G, Yates A, Zadissa A, Searle SM. Ensembl 2013. Nucleic Acids Res. 2013 Jan;41(Database issue):D48-55. doi: 10.1093/nar/gks1236. Epub 2012 Nov 30. PMID: 23203987; PMCID: PMC3531136.
117. Meyer LR, Zweig AS, Hinrichs AS, Karolchik D, Kuhn RM, Wong M, Sloan CA, Rosenbloom KR, Roe G, Rhead B, Raney BJ, Pohl A, Malladi VS, Li CH, Lee BT, Learned K, Kirkup V, Hsu F, Heitner S, Harte RA, Haeussler M, Guruvadoo L, Goldman M, Giardine BM, Fujita PA, Dreszer TR, Diekhans M, Cline MS, Clawson H, Barber GP, Haussler D, Kent WJ. The UCSC Genome Browser database: extensions and updates 2013. Nucleic Acids Res. 2013 Jan;41(Database issue):D64-9. doi: 10.1093/nar/gks1048. Epub 2012 Nov 15. PMID: 23155063; PMCID: PMC3531082.
118. Katz Y, Wang ET, Airoldi EM, Burge CB. Analysis and design of RNA sequencing experiments for identifying isoform regulation. Nat Methods. 2010

Dec;7(12):1009-15. doi: 10.1038/nmeth.1528. Epub 2010 Nov 7. PMID: 21057496; PMCID: PMC3037023.
119. Li B, Dewey CN. RSEM: accurate transcript quantification from RNA-Seq data with or without a reference genome. BMC Bioinformatics. 2011 Aug 4;12:323. doi: 10.1186/1471-2105-12-323. PMID: 21816040; PMCID: PMC3163565.
120. Langmead B, Trapnell C, Pop M, Salzberg SL. Ultrafast and memory-efficient alignment of short DNA sequences to the human genome. Genome Biol. 2009;10(3):R25. doi: 10.1186/gb-2009-10-3-r25. Epub 2009 Mar 4. PMID: 19261174; PMCID: PMC2690996.
121. Trapnell C, Pachter L, Salzberg SL. TopHat: discovering splice junctions with RNA-Seq. Bioinformatics. 2009 May 1;25(9):1105-11. doi: 10.1093/bioinformatics/btp120. Epub 2009 Mar 16. PMID: 19289445; PMCID: PMC2672628.
122. Robinson MD, Oshlack A. A scaling normalization method for differential expression analysis of RNA-seq data. Genome Biol. 2010;11(3):R25. doi: 10.1186/gb-2010-11-3-r25. Epub 2010 Mar 2. PMID: 20196867; PMCID: PMC2864565.
123. Therneau T (2024). A Package for Survival Analysis in R. R package version 3.7-0, https://CRAN.R-project.org/package=survival.
124. Greenwell B (2024). fastshap: Fast Approximate Shapley Values. R package version 0.1.1, https://bgreenwell.github.io/fastshap/, https://github.com/bgreenwell/fastshap.
125. Wickham H, François R, Henry L, Müller K, Vaughan D (2023). dplyr: A Grammar of Data Manipulation. R package version 1.1.4, https://github.com/tidyverse/dplyr, https://dplyr.tidyverse.org.
126. Wickham H (2016). ggplot2: Elegant Graphics for Data Analysis. Springer-Verlag New York. ISBN 978-3-319-24277-4, https://ggplot2.tidyverse.org.
127. Bender A, Scheipl F (2018). "pammtools: Piece-wise exponential Additive Mixed Modeling tools." arXiv:1806.01042 [stat]. https://arxiv.org/abs/1806.01042.
128. Sievert C (2020). Interactive Web-Based Data Visualization with R, plotly, and shiny. Chapman and Hall/CRC. ISBN 9781138331457, https://plotly-r.com.
129. Blanche P, Dartigues J, Jacqmin-Gadda H (2013). "Estimating and Comparing time-dependent areas under receiver operating characteristic curves for censored event times with competing risks." Statistics in Medicine, 32(30), 5381–5397. http://onlinelibrary.wiley.com/doi/10.1002/sim.5958/full.
130. Moulton HM, Yoshihara PH, Mason DH, Iversen PL, Triozzi PL. Active specific immunotherapy with a beta-human chorionic gonadotropin peptide vaccine in patients with metastatic colorectal cancer: antibody response is associated with improved survival. Clin Cancer Res. 2002 Jul;8(7):2044-51. PMID: 12114402.
131. Tanaka H, Kato K, Yamashita E, Sumizawa T, Zhou Y, Yao M, Iwasaki K, Yoshimura M, Tsukihara T. The structure of rat liver vault at 3.5 angstrom resolution. Science. 2009 Jan 16;323(5912):384-8. doi: 10.1126/science.1164975. PMID: 19150846.
132. Kong LB, Siva AC, Kickhoefer VA, Rome LH, Stewart PL. RNA location and modeling of a WD40 repeat domain within the vault. RNA. 2000 Jun;6(6):890-900. doi: 10.1017/s1355838200000157. PMID: 10864046; PMCID: PMC1369965.

133. van Zon A, Mossink MH, Schoester M, Scheffer GL, Scheper RJ, Sonneveld P, Wiemer EA. Multiple human vault RNAs. Expression and association with the vault complex. J Biol Chem. 2001 Oct 5;276(40):37715-21. doi: 10.1074/jbc.M106055200. Epub 2001 Jul 30. PMID: 11479319.
134. Guerra P, González-Alamos M, Llauró A, Casañas A, Querol-Audí J, de Pablo PJ, Verdaguer N. Symmetry disruption commits vault particles to disassembly. Sci Adv. 2022 Feb 11;8(6):eabj7795. doi: 10.1126/sciadv.abj7795. Epub 2022 Feb 9. PMID: 35138889; PMCID: PMC8827651.
135. Stephen AG, Raval-Fernandes S, Huynh T, Torres M, Kickhoefer VA, Rome LH. Assembly of vault-like particles in insect cells expressing only the major vault protein. J Biol Chem. 2001 Jun 29;276(26):23217-20. doi: 10.1074/jbc.C100226200. Epub 2001 May 10. PMID: 11349122.
136. Ben J, Jiang B, Wang D, Liu Q, Zhang Y, Qi Y, Tong X, Chen L, Liu X, Zhang Y, Zhu X, Li X, Zhang H, Bai H, Yang Q, Ma J, Wiemer EAC, Xu Y, Chen Q. Major vault protein suppresses obesity and atherosclerosis through inhibiting IKK-NF-κB signaling mediated inflammation. Nat Commun. 2019 Apr 17;10(1):1801. doi: 10.1038/s41467-019-09588-x. PMID: 30996248; PMCID: PMC6470148.
137. Bai H, Wang C, Qi Y, Xu J, Li N, Chen L, Jiang B, Zhu X, Zhang H, Li X, Yang Q, Ma J, Xu Y, Ben J, Chen Q. Major vault protein suppresses lung cancer cell proliferation by inhibiting STAT3 signaling pathway. BMC Cancer. 2019 May 15;19(1):454. doi: 10.1186/s12885-019-5665-6. PMID: 31092229; PMCID: PMC6521381.
138. Anouk B. Schroeijers, Anneke W. Reurs, George L. Scheffer, Anita G. M. Stam, Mariska C. de Jong, Thomas Rustemeyer, Erik A. C. Wiemer, Tanja D. de Gruijl, Rik J. Scheper; Up-Regulation of Drug Resistance-Related Vaults During Dendritic Cell Development1. J Immunol 15 February 2002; 168 (4): 1572–1578. https://doi.org/10.4049/jimmunol.168.4.1572
139. Schroeijers AB, Reurs AW, Scheffer GL, Stam AG, de Jong MC, Rustemeyer T et al. Up-regulation of drug resistance-related vaults during dendritic cell development. J Immunol 2002; 168: 1572–1578.
140. Berger W, Spiegl-Kreinecker S, Buchroithner J, Elbling L, Pirker C, Fischer J et al. Overexpression of the human major vault protein in astrocytic brain tumor cells. Int J Cancer 2001; 94: 377–382.
141. Dong X, Akuetteh PDP, Song J, Ni C, Jin C, Li H, Jiang W, Si Y, Zhang X, Zhang Q, Huang G. Major Vault Protein (MVP) Associated With BRAFV600E Mutation Is an Immune Microenvironment-Related Biomarker Promoting the Progression of Papillary Thyroid Cancer via MAPK/ERK and PI3K/AKT Pathways. Front Cell Dev Biol. 2022 Mar 31;9:688370. doi: 10.3389/fcell.2021.688370. PMID: 35433709; PMCID: PMC9009514.
142. Schadendorf D, Makki A, Stahr C, van Dyck A, Wanner R, Scheffer GL et al. Membrane transport proteins associated with drug resistance expressed in human melanoma. Am J Pathol 1995; 147: 1545–1552.
143. Meijer GA, Schroeijers AB, Flens MJ, Meuwissen SG, van der Valk P, Baak JP et al. Increased expression of multidrug resistance related proteins Pgp, MRP1, and LRP/MVP occurs early in colorectal carcinogenesis. J Clin Pathol 1999; 52: 450–454.

144. Scheffer GL, Wijngaard PL, Flens MJ, Izquierdo MA, Slovak ML, Pinedo HM, Meijer CJ, Clevers HC, Scheper RJ. The drug resistance-related protein LRP is the human major vault protein. Nat Med. 1995 Jun;1(6):578-82. doi: 10.1038/nm0695-578. PMID: 7585126.
145. Kickhoefer VA, Rajavel KS, Scheffer GL, Dalton WS, Scheper RJ, Rome LH . Vaults are up-regulated in multidrug-resistant cancer cell lines. J Biol Chem 1998; 273: 8971–8974.
146. Kowalski MP, Dubouix-Bourandy A, Bajmoczi M, Golan DE, Zaidi T, Coutinho-Sledge YS, et al. Host Resistance to Lung Infection Mediated by Major Vault Protein in Epithelial Cells. Science (2007) 317(5834):130–2. doi: 10.1126/science.1142311
147. Rayo J, Gregor R, Jacob NT, Dandela R, Dubinsky L, Yashkin A, Aranovich A, Thangaraj M, Ernst O, Barash E, Malitsky S, Florea BI, Krom BP, Wiemer EAC, Kickhoefer VA, Rome LH, Mathison JC, Kaufmann GF, Overkleeft HS, Cravatt BF, Zor T, Janda KD, Ulevitch RJ, Kravchenko VV, Meijler MM. Immunoediting role for major vault protein in apoptotic signaling induced by bacterial N-acyl homoserine lactones. Proc Natl Acad Sci U S A. 2021 Mar 23;118(12):e2012529118. doi: 10.1073/pnas.2012529118. PMID: 33723037; PMCID: PMC8000436.
148. Peng N, Liu S, Xia Z, Ren S, Feng J, Jing M, Gao X, Wiemer EA, Zhu Y. Inducible Major Vault Protein Plays a Pivotal Role in Double-Stranded RNA- or Virus-Induced Proinflammatory Response. J Immunol. 2016 Mar 15;196(6):2753-66. doi: 10.4049/jimmunol.1501481. Epub 2016 Feb 3. PMID: 26843330.
149. Borer RA, Lehner CF, Eppenberger HM, Nigg EA. Major nucleolar proteins shuttle between nucleus and cytoplasm. Cell. 1989 Feb 10;56(3):379-90. doi: 10.1016/0092-8674(89)90241-9. PMID: 2914325.
150. Teng Y, Ren Y, Hu X, Mu J, Samykutty A, Zhuang X, Deng Z, Kumar A, Zhang L, Merchant ML, Yan J, Miller DM, Zhang HG. MVP-mediated exosomal sorting of miR-193a promotes colon cancer progression. Nat Commun. 2017 Feb 17;8:14448. doi: 10.1038/ncomms14448. PMID: 28211508; PMCID: PMC5321731.
151. Ryu, S., An, H., Oh, Y. et al. On the role of major vault protein in the resistance of senescent human diploid fibroblasts to apoptosis. Cell Death Differ 15, 1673–1680 (2008). https://doi.org/10.1038/cdd.2008.96
152. Yu C, Zhu Q, Ma C, Luo C, Nie L, Cai H, Wang Q, Wang F, Ren H, Yan H, Xu K, Zhou L, Zhang C, Lu G, Lu Z, Zhu Y, Liu S. Major vault protein regulates tumor-associated macrophage polarization through interaction with signal transducer and activator of transcription 6. Front Immunol. 2024 Jan 9;14:1289795. doi: 10.3389/fimmu.2023.1289795. PMID: 38264642; PMCID: PMC10803552.
153. Yang Y, Zhao N, Wang R, Zhan Z, Guo S, Song H, Wiemer EAC, Ben J, Ma J. Macrophage MVP regulates fracture repair by promoting M2 polarization via JAK2-STAT6 pathway. Int Immunopharmacol. 2023 Jul;120:110313. doi: 10.1016/j.intimp.2023.110313. Epub 2023 May 31. PMID: 37267856.
154. Liu S, Peng N, Xie J, Hao Q, Zhang M, Zhang Y, Xia Z, Xu G, Zhao F, Wang Q, Han T, Zhu Y. Human hepatitis B virus surface and e antigens inhibit major vault protein signaling in interferon induction pathways. J Hepatol. 2015 May;62(5):1015-23. doi: 10.1016/j.jhep.2014.11.035. Epub 2014 Dec 3. PMID: 25481566.

155. Mossink MH, van Zon A, Fränzel-Luiten E, Schoester M, Kickhoefer VA, Scheffer GL, Scheper RJ, Sonneveld P, Wiemer EA. Disruption of the murine major vault protein (MVP/LRP) gene does not induce hypersensitivity to cytostatics. Cancer Res. 2002 Dec 15;62(24):7298-304. PMID: 12499273.
156. Mossink MH, de Groot J, van Zon A, Fränzel-Luiten E, Schoester M, Scheffer GL, Sonneveld P, Scheper RJ, Wiemer EA. Unimpaired dendritic cell functions in MVP/LRP knockout mice. Immunology. 2003 Sep;110(1):58-65. doi: 10.1046/j.1365-2567.2003.01708.x. PMID: 12941141; PMCID: PMC1783015.
157. Kedersha NL, Miquel MC, Bittner D, Rome LH. Vaults. II. Ribonucleoprotein structures are highly conserved among higher and lower eukaryotes. J Cell Biol. 1990 Apr;110(4):895-901. doi: 10.1083/jcb.110.4.895. PMID: 1691193; PMCID: PMC2116106.
158. Steiner E, Holzmann K, Pirker C, Elbling L, Micksche M, Sutterlüty H, Berger W. The major vault protein is responsive to and interferes with interferon-gamma-mediated STAT1 signals. J Cell Sci. 2006 Feb 1;119(Pt 3):459-69. doi: 10.1242/jcs.02773. Epub 2006 Jan 17. PMID: 16418217.
159. Ben J, Zhang Y, Zhou R, Zhang H, Zhu X, Li X, Zhang H, Li N, Zhou X, Bai H, Yang Q, Li D, Xu Y, Chen Q. Major vault protein regulates class A scavenger receptor-mediated tumor necrosis factor-α synthesis and apoptosis in macrophages. J Biol Chem. 2013 Jul 5;288(27):20076-84. doi: 10.1074/jbc.M112.449538. Epub 2013 May 23. PMID: 23703615; PMCID: PMC3707704.
160. Li C, Gao M, Zha N, Guo G. The prognostic value and immunological role of MVP in pan-cancer study. Aging (Albany NY). 2024 May 6;16(10):8497-8510. doi: 10.18632/aging.205802. Epub 2024 May 6. PMID: 38713157; PMCID: PMC11164508.
161. Otto DJ, Jordan C, Dury B, Dien C, Setty M. Quantifying cell-state densities in single-cell phenotypic landscapes using Mellon. Nat Methods. 2024 Jul;21(7):1185-1195. doi: 10.1038/s41592-024-02302-w. Epub 2024 Jun 18. PMID: 38890426.
162. Wolchok JD, Chiarion-Sileni V, Gonzalez R, Rutkowski P, Grob JJ, Cowey CL, Lao CD, Wagstaff J, Schadendorf D, Ferrucci PF, Smylie M, Dummer R, Hill A, Hogg D, Haanen J, Carlino MS, Bechter O, Maio M, Marquez-Rodas I, Guidoboni M, McArthur G, Lebbé C, Ascierto PA, Long GV, Cebon J, Sosman J, Postow MA, Callahan MK, Walker D, Rollin L, Bhore R, Hodi FS, Larkin J. Overall Survival with Combined Nivolumab and Ipilimumab in Advanced Melanoma. N Engl J Med. 2017 Oct 5;377(14):1345-1356. doi: 10.1056/NEJMoa1709684. Epub 2017 Sep 11. Erratum in: N Engl J Med. 2018 Nov 29;379(22):2185. doi: 10.1056/NEJMx180040. PMID: 28889792; PMCID: PMC5706778.
163. Liu D, Schilling B, Liu D, Sucker A, Livingstone E, Jerby-Arnon L, Zimmer L, Gutzmer R, Satzger I, Loquai C, Grabbe S, Vokes N, Margolis CA, Conway J, He MX, Elmarakeby H, Dietlein F, Miao D, Tracy A, Gogas H, Goldinger SM, Utikal J, Blank CU, Rauschenberg R, von Bubnoff D, Krackhardt A, Weide B, Haferkamp S, Kiecker F, Izar B, Garraway L, Regev A, Flaherty K, Paschen A, Van Allen EM, Schadendorf D. Integrative molecular and clinical modeling of clinical outcomes to PD1 blockade in patients with metastatic melanoma. Nat Med. 2019 Dec;25(12):1916-1927. doi: 10.1038/s41591-019-0654-5. Epub 2019 Dec 2.

Erratum in: Nat Med. 2020 Jul;26(7):1147. doi: 10.1038/s41591-020-0975-4. PMID: 31792460; PMCID: PMC6898788.
164. Gide TN, Quek C, Menzies AM, Tasker AT, Shang P, Holst J, Madore J, Lim SY, Velickovic R, Wongchenko M, Yan Y, Lo S, Carlino MS, Guminski A, Saw RPM, Pang A, McGuire HM, Palendira U, Thompson JF, Rizos H, Silva IPD, Batten M, Scolyer RA, Long GV, Wilmott JS. Distinct Immune Cell Populations Define Response to Anti-PD-1 Monotherapy and Anti-PD-1/Anti-CTLA-4 Combined Therapy. Cancer Cell. 2019 Feb 11;35(2):238-255.e6. doi: 10.1016/j.ccell.2019.01.003. PMID: 30753825.
165. Van Allen EM, Miao D, Schilling B, Shukla SA, Blank C, Zimmer L, Sucker A, Hillen U, Foppen MHG, Goldinger SM, Utikal J, Hassel JC, Weide B, Kaehler KC, Loquai C, Mohr P, Gutzmer R, Dummer R, Gabriel S, Wu CJ, Schadendorf D, Garraway LA. Genomic correlates of response to CTLA-4 blockade in metastatic melanoma. Science. 2015 Oct 9;350(6257):207-211. doi: 10.1126/science.aad0095. Epub 2015 Sep 10. Erratum in: Science. 2015 Nov 13;350(6262):aad8366. doi: 10.1126/science.aad8366. Erratum in: Science. 2016 Apr 15;352(6283):aaf8264. doi: 10.1126/science.aaf8264. PMID: 26359337; PMCID: PMC5054517.
166. Minnie SA, Waltner OG, Ensbey KS, Nemychenkov NS, Schmidt CR, Bhise SS, Legg SRW, Campoy G, Samson LD, Kuns RD, Zhou T, Huck JD, Vuckovic S, Zamora D, Yeh A, Spencer A, Koyama M, Markey KA, Lane SW, Boeckh M, Ring AM, Furlan SN, Hill GR. Depletion of exhausted alloreactive T cells enables targeting of stem-like memory T cells to generate tumor-specific immunity. Sci Immunol. 2022 Oct 21;7(76):eabo3420. doi: 10.1126/sciimmunol.abo3420. Epub 2022 Oct 14. PMID: 36240285; PMCID: PMC10184646.
167. Minnie SA, Waltner OG, Zhang P, Takahashi S, Nemychenkov NS, Ensbey KS, Schmidt CR, Legg SRW, Comstock M, Boiko JR, Nelson E, Bhise SS, Wilkens AB, Koyama M, Dhodapkar MV, Chesi M, Riddell SR, Green DJ, Spencer A, Furlan SN, Hill GR. TIM-3+ CD8 T cells with a terminally exhausted phenotype retain functional capacity in hematological malignancies. Sci Immunol. 2024 Apr 19;9(94):eadg1094. doi: 10.1126/sciimmunol.adg1094. Epub 2024 Apr 19. PMID: 38640253; PMCID: PMC11093588.
168. Miller BC, Sen DR, Al Abosy R, Bi K, Virkud YV, LaFleur MW, Yates KB, Lako A, Felt K, Naik GS, Manos M, Gjini E, Kuchroo JR, Ishizuka JJ, Collier JL, Griffin GK, Maleri S, Comstock DE, Weiss SA, Brown FD, Panda A, Zimmer MD, Manguso RT, Hodi FS, Rodig SJ, Sharpe AH, Haining WN. Subsets of exhausted CD8+ T cells differentially mediate tumor control and respond to checkpoint blockade. Nat Immunol. 2019 Mar;20(3):326-336. doi: 10.1038/s41590-019-0312-6. Epub 2019 Feb 18. Erratum in: Nat Immunol. 2019 Nov;20(11):1556. doi: 10.1038/s41590-019-0528-5. PMID: 30778252; PMCID: PMC6673650.
169. Castellano BM, Thelen AM, Moldavski O, Feltes M, van der Welle RE, Mydock-McGrane L, Jiang X, van Eijkeren RJ, Davis OB, Louie SM, Perera RM, Covey DF, Nomura DK, Ory DS, Zoncu R. Lysosomal cholesterol activates mTORC1 via an SLC38A9-Niemann-Pick C1 signaling complex. Science. 2017 Mar 24;355(6331):1306-1311. doi: 10.1126/science.aag1417. PMID: 28336668; PMCID: PMC5823611.

170. Xiao X, Tang JJ, Peng C, Wang Y, Fu L, Qiu ZP, Xiong Y, Yang LF, Cui HW, He XL, Yin L, Qi W, Wong CC, Zhao Y, Li BL, Qiu WW, Song BL. Cholesterol Modification of Smoothened Is Required for Hedgehog Signaling. Mol Cell. 2017 Apr 6;66(1):154-162.e10. doi: 10.1016/j.molcel.2017.02.015. Epub 2017 Mar 23. PMID: 28344083.
171. Ma X, Bi E, Lu Y, Su P, Huang C, Liu L, Wang Q, Yang M, Kalady MF, Qian J, Zhang A, Gupte AA, Hamilton DJ, Zheng C, Yi Q. Cholesterol Induces CD8+ T Cell Exhaustion in the Tumor Microenvironment. Cell Metab. 2019 Jul 2;30(1):143-156.e5. doi: 10.1016/j.cmet.2019.04.002. Epub 2019 Apr 25. PMID: 31031094; PMCID: PMC7061417.
172. Xu S, Chaudhary O, Rodríguez-Morales P, Sun X, Chen D, Zappasodi R, Xu Z, Pinto AFM, Williams A, Schulze I, Farsakoglu Y, Varanasi SK, Low JS, Tang W, Wang H, McDonald B, Tripple V, Downes M, Evans RM, Abumrad NA, Merghoub T, Wolchok JD, Shokhirev MN, Ho PC, Witztum JL, Emu B, Cui G, Kaech SM. Uptake of oxidized lipids by the scavenger receptor CD36 promotes lipid peroxidation and dysfunction in CD8+ T cells in tumors. Immunity. 2021 Jul 13;54(7):1561-1577.e7. doi: 10.1016/j.immuni.2021.05.003. Epub 2021 Jun 7. PMID: 34102100; PMCID: PMC9273026.
173. Bi K, He MX, Bakouny Z, Kanodia A, Napolitano S, Wu J, Grimaldi G, Braun DA, Cuoco MS, Mayorga A, DelloStritto L, Bouchard G, Steinharter J, Tewari AK, Vokes NI, Shannon E, Sun M, Park J, Chang SL, McGregor BA, Haq R, Denize T, Signoretti S, Guerriero JL, Vigneau S, Rozenblatt-Rosen O, Rotem A, Regev A, Choueiri TK, Van Allen EM. Tumor and immune reprogramming during immunotherapy in advanced renal cell carcinoma. Cancer Cell. 2021 May 10;39(5):649-661.e5. doi: 10.1016/j.ccell.2021.02.015. Epub 2021 Mar 11. PMID: 33711272; PMCID: PMC8115394.
174. Zheng, G. X. Y. et al. (2017). Massively parallel digital transcriptional profiling of single cells. Nature Communications 8: 1-12, doi:10.1038/ncomms14049
175. Hao Y, Stuart T, Kowalski MH, Choudhary S, Hoffman P, Hartman A, Srivastava A, Molla G, Madad S, Fernandez-Granda C, Satija R (2023). “Dictionary learning for integrative, multimodal and scalable single-cell analysis.” Nature Biotechnology. doi:10.1038/s41587-023-01767-y, https://doi.org/10.1038/s41587-023-01767-y.
176. Hao Y, Hao S, Andersen-Nissen E, III WMM, Zheng S, Butler A, Lee MJ, Wilk AJ, Darby C, Zagar M, Hoffman P, Stoeckius M, Papalexi E, Mimitou EP, Jain J, Srivastava A, Stuart T, Fleming LB, Yeung B, Rogers AJ, McElrath JM, Blish CA, Gottardo R, Smibert P, Satija R (2021). “Integrated analysis of multimodal single-cell data.” Cell. doi:10.1016/j.cell.2021.04.048, https://doi.org/10.1016/j.cell.2021.04.048.
177. Stuart T, Butler A, Hoffman P, Hafemeister C, Papalexi E, III WMM, Hao Y, Stoeckius M, Smibert P, Satija R (2019). “Comprehensive Integration of Single-Cell Data.” Cell, 177, 1888-1902. doi:10.1016/j.cell.2019.05.031, https://doi.org/10.1016/j.cell.2019.05.031.
178. Butler A, Hoffman P, Smibert P, Papalexi E, Satija R (2018). “Integrating single-cell transcriptomic data across different conditions, technologies, and species.” Nature Biotechnology, 36, 411-420. doi:10.1038/nbt.4096, https://doi.org/10.1038/nbt.4096.

179. Satija R, Farrell JA, Gennert D, Schier AF, Regev A (2015). “Spatial reconstruction of single-cell gene expression data.” Nature Biotechnology, 33, 495-502. doi:10.1038/nbt.3192, https://doi.org/10.1038/nbt.3192.
180. Grzelak CA, Goddard ET, Lederer EE, Rajaram K, Dai J, Shor RE, Lim AR, Kim J, Beronja S, Funnell APW, Ghajar CM. Elimination of fluorescent protein immunogenicity permits modeling of metastasis in immune-competent settings. Cancer Cell. 2022 Jan 10;40(1):1-2. doi: 10.1016/j.ccell.2021.11.004. Epub 2021 Dec 2. PMID: 34861158; PMCID: PMC9668376.